THE INVERSION

OF TIME-DOMAIN AIRBORNE

ELECTROMAGNETIC DATA

USING THE PLATE MODEL

(c) Pierre B. Keating

A thesis submitted to the Faculty of

Graduate Studies and Research in partial fulfillment

of the requirements of the degree of Ph.D.

Mc GILL UNIVERSITY

Geophysics Laboratory

Departement of Geological Sciences

Montreal, Canada

August 1987

THE INVERSION OF TIME-DOMAIN AIRBORNE E.M. DATA USING THE PLATE MODEL
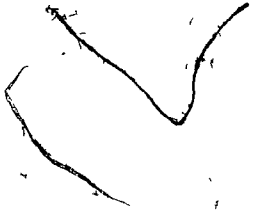
ABSTRACT

Airborne electromagnetic methods were developed in the early 1950's, mostly by Canadian mining exploration companies as a means of economically and successfully searching large areas for conductive massive sulfide mineralisation. As new technologies developed they have become more and more sophisticated. They can detect conductors at depths in excess of 200 m and are routinely used for overburden mapping. The data is digitally recorded and processed. One of the most successful methods is the time domain airborne INPUT[1] system, for numerous mineral deposits were found by this system in the Canadian Shield.

Present interpretation techniques are based on the use of nomograms (i.e. families of pre-computed characteristic responses) and the method is easily amenable to digital processing as it is easy to program and economic to use. For high accuracy interpretation however it is necessary to develop quantitative interpretation techniques that can make full use of all the data available. Inverse theory has been used with great success in all branches of geophysics, but to date in mining exploration it has been used for the interpretation of airborne E.M. data using only the one layer earth model. Use

---

1 Registered trademark of Barringer Research Ltd.

of inverse theory for the plate model has been limited by the high cost of numerically solving the forward problem.

In this thesis we show how to use inverse theory to interpret time domain E.M. data with the rectangular thin plate model by introducing some economies. It is then possible to estimate parameter errors, the correlation matrix and to assess the validity of the model. This is extended to the joint inversion of electromagnetic and aeromagnetic data, a case that often arises in mining problems. It is finally shown that under some assumptions the late time channels can be used to interpret time domain E.M. data in the presence of conductive overburden.

RÉSUMÉ

Le développement des méthodes électromagnétiques aéro-
portées fut réalisé au début des années cinquantes, principa-
lement par des compagnies d'exploration minière canadiennes
dont l'objectif était la recherche de sulfures massifs con-
ducteurs. Avec le développement de nouvelles technologies
celles-ci devinrent de plus en plus sophistiquées. Elles
détectent maintenant des conducteurs à des profondeurs de plus
de 200m et elles sont utilisées de façon routinière pour la
cartographie des morts-terrains. Une des méthodes les plus
fructueuses est le système INPUT qui fonctionne dans le do-
maine du temps. En effet, de nombreux gisements du Bouclier
canadien furent découverts à l'aide de ce système.

Les techniques d'interprétation actuelles sont basées sur
l'utilisation d'abaques (i.e. un ensemble de courbes caracté-
ristiques précalculées). Cette méthode peut facilement être
informatisée et est ainsi économique à utiliser. Pour une
interprétation précise il est néanmoins nécessaire de dévelop-
per des méthodes d'interprétation quantitatives qui utilisent
toutes les données existantes. La théorie de l'inversion a été
utilisée avec beaucoup de succès dans tous les domaines de la
géophysique, en exploration minière elle n'a été utilisée que
pour l'interprétation de levés E.M. aéroportés en utilisant le

modèle d'une terre stratifiée a une seule couche. L'usage du
modèle de la plaque mince pour l'inversion a été limité par
les coûts de la solution du problème direct.

Dans cette thèse nous montrons comment, en introduisant
des économies de calcul, utiliser la théorie de l'inversion
pour interpréter des données E.M. aéroportées dans le domaine
du temps à l'aide du modèle d'une plaque mince rectangulaire.
La méthode est ensuite étendue au cas de l'inversion conjointe
de données E.M. et magnétiques, un cas fréquent en exploration
minière. Nous montrons finalement que si l'on fait certaines
hypothèses, les données des derniers canaux peuvent être
interprétées en présence d'un mort terrain conducteur.

Acknowledgements

TABLE OF CONTENTS

LIST OF FIGURES

LIST OF TABLES

Chapter 1

INTRODUCTION.

1.1 Airborne Electromagnetic Prospecting.

Airborne electromagnetic prospecting came into widespread use in the 1950s. The discovery of seven new orebodies between 1954 and 1956 suffices to explain their subsequent popularity. E.M. methods were first used to detect massive sulfide orebodies, but recently have been extended for structural and overburden mapping. In the coming years we foresee an increase of their use in groundwater and environmental problems.

E.M. methods respond to the electrical properties of the earth, of which conductivity is the most important since it varies over many orders of magnitude, from 10^3 to 10^{-5} S/m. This is the most variable of all the physical properties of rocks and minerals. The other properties, namely permeability and permittivity, are generally assumed to be those of free space; an hypothesis which is most of the time valid in practice.

Since airborne E.M. systems operate at low frequencies (<5kHz) displacement currents are negligible relative to

conduction. currents.. When a conductor is excited by a time varying magnetic field, currents are induced in it and a secondary magnetic field is generated. The response detected by an E.M. receiver is thus the sum of a primary field, usually generated by a transmitter, and a secondary field produced by the conductor. Most systems measure the ratio of the amplitudes of the secondary to the primary field and this ratio is usually expressed in parts per million (ppm). Although some ground E.M. methods such as AFMAG and magnetotelluric use natural atmospheric sources, the majority of them use artificial sources. All airborne methods use a transmitter operating either in the frequency or the time domain.

In the rigid boom configuration the transmitter and the receiver are rigidly mounted relative to one another. This limits the differential movement between the pair of coils and therefore reduces noise due to the effect of variable coil geometry. This is the type of configuration preferred for helicopter-borne E.M. systems. The "bird" containing the transmitter and receiver coils is typically 7m or 8m long and is towed at a height of 30m or 40m above ground. In a frequency domain system the transmitter emits a sinusoidal primary field at three or four frequencies in the 200 to 5000Hz range. Different coil orientations are used to maximize the information. For fixed wing aircraft such as in the Scintrex Tridem system, the transmitter and the receiver are

then housed in special pods attached to the wingtips of the aircraft. Alternatively the nose and the tail can also be used.

In the "towed bird" configuration the transmitter is generally a large current loop attached to the nose, the wingtips and the tail of the aircraft. The receiver is towed at about 70m below and 90m behind the aircraft. This is the preffered geometry for time domain systems. Differential movement between the aircraft and the bird is important and in the frequency domain only the quadrature component of the secondary field can be used, since it is mostly unaffected. Two or more frequencies must then be used to obtain enough diagnostic information. This scheme was used in the Hunting Canso System and the Mc Phar F-400 system.

The first airborne time domain system was introduced by A. Barringer in 1958. The INPUT system, as it is called, uses a half sine pulse of 1 to 2ms of duration of alternating polarity as its primary field. The base frequency is usually 90 or 150Hz. A decaying secondary voltage is measured while the transmitter is off. It is sampled over six non overlapping time windows, called channels. Since the measurements are made while the transmitter is off, the noise is reduced. Further reduction in noise level is obtained by stacking and averaging the measurements over several cycles. Recently a helicopter INPUT system as been introduced. The receiver is then 20m

behind and 70m below the helicopter (Konings, Lazenby and Becker; 1984).

The GEOTEM[2] system, flown by Geoterrex Ltd, consists of an INPUT transmitter and a state of the art digital receiver. It has twelve software selectable time windows. Another system called SWEEPEM has been developed by Shell Mineral and uses a pseudo-random waveform. It operates either in the time domain or the frequency domain. The system has been moth-balled for economic reasons.

1.2 Advantages of Time Domain Systems.

Because of their large geometry and high dipolar moment $(10^5 A/m^2)$ airborne time domain systems can detect deeply buried conductors. They can even locate conductors under thick conductive overburden such as in the Abitibi clay belt. They have a high sensitivity but due to their relatively high altitude of 120m they lack the resolution of helicopter-borne frequency domain E.M. systems. On the other hand this results in better lateral coverage. Between 1980 and 1986, the time domain INPUT system was credited for the discovery of eight commercial orebodies (Northern Miner Magazine, Dec.1986) while none were discovered by frequency domain E.M. systems. It still remains to be seen if this is a matter of chance or technology.

---

2 Registered trademark of Geoterrex Ltd.

1.3 Thesis Objectives and Outline.

The interpretation of airborne E.M. survey data is based upon comparison of known free space model responses and actual data. This is usually done by fitting the anomaly peak response to a set of nomograms to determine the conductance and the depth of the target. The dip of a half-plane or of a plate like conductor can also be found with nomograms.

The objective of this thesis is to use inverse theory to compute the most important physical and geometrical parameters of plate-like conductors and assess the validity of these results. In doing so, the full length of the anomalous profile is used rather than only the peak response, thereby greatly improving the interpretation. Without loss of generality, the discussion will be restricted to time-domain airborne systems.

The use of the plate model in free space, as developed by Annan (1974), is discussed in Chapter 2 and its application in the context of the Canadian Shield is also exposed. The theory of inversion is presented in Chapter 3 and Chapter 4 gives the results of the inversion of synthetic and actual data. It is shown in Chapter 5 that, in some cases, there are some advantages to the joint inversion of E.M. and magnetic data to reduce the error bounds on the parameters. In Chapter 6, it is shown how late time channels can be used to interpret conductive targets in the presence of conductive overburden if

the target conductance is high enough and the overburden not too conductive. Finally the most important conclusions will be reviewed and we will give some suggestions for future work.

Chapter 2

THE PLATE MODEL

2.1 Introduction.

It was decided at the start of this work to use the PLATE program to solve the forward problem. The algorithm was developed by P. Annan (1974) and the last version of the program was written by A.V. Dyck (Dyck, Bloore and Vallée, 1980). The main advantage is that the program is highly interactive and user friendly, it can also simulate most commercial E.M. systems. Before discussing the theory associated with this model, it is justified from a geological and geophysical point of view.

2.2 Geological justification.

A list of the mineral deposits of northwestern Quebec has been published by Avramtchev (1980). This study covers the Quebec part of the Abitibi greenstone belt. Out of a total of 2000 deposits, 307 have an unknown shape, and 92% of the remaining have a shape that can be modeled approximately by a

plate or a half plane. The deposits were classified as follows:

Chimney : it is a tubular orebody more or less vertical. It is generally associated with volcanic intrusives. The ideal geophysical model is a vertical cylinder. There are only 11 such deposits in the study area.

Strata-bound: these deposits are characterised by their continuity. They are usually located at a particular level in sedimentary, metamorphic or magmatic rocks. The are easily modelled by a conducting thin plate. A total of 453 of these are found in the study area.

Dike : these orebodies are associated with intrusive dikes and depending on their extension can be modelled by a half-plane or a plate. They number 99.

Vein : the mineralisation fill the cracks of a fault or a shear zone. They are the most common, 880 in the study area.

Lenticular : these orebodies have the shape of a lens and are modelled by a plate. They number 129.

Stockwerk : this is a very dense assemblage of small and thin veins, in some cases it could be modelled by a sphere. Only 59 are located in the study area.

Mass : these deposits have a more or less spherical shape. They number 62, and a sphere would be a good model.

Most deposits detected by airborne E.M. systems are massive sulfides. Their conductivity is usually caused by pyrrhotite and chalcopyrite, whose respective average conductivities are 10^4S/m and 250S/m (Telford 1976,p450). Pyrite (3S/m) is more abundant and occurs as isolated, closely spaced grains, so that the average response is weak. The conductivity of massive sulfide deposits is generally in the range of 5 to 30S/m. Graphitic conductors are the source of a large number of E.M. anomalies. They usually form long conducting bands of tens and even hundreds of kilometers. It is, nevertheless possible to find some sulfides within the graphitic sediments.

It is obvious that stratabound, lenticular, dike and vein like ore bodies can be modeled by a thin conductive plate or a half plane. For most of them the strike length is much larger than their thickness. However this does not means that they can be considered as inductively thin. According to Lamontagne (1970) a conductor is inductively thin if $\sigma \mu \omega t^2 > 0.67$. Assuming a frequency of 150Hz (base frequency of the INPUT system, $\omega = 2\pi f$) the thickness (t) has to be less than 53m if the conductivity (σ) is 0.2S/m and less than 16m for a conductivity of 2S/m.

2.3 Numerical Development of the PLATE Model.

The inductive response of a rectangular thin plate in free space was solved by Lamontagne and West.(1971). They used

the finite element method, to solve Maxwell's equations.
Annan's solution is based on the concept of equivalent sources
and the mathematical formulation of the plate problem is
discussed in the appendix. The secondary field of a thin plate
excited by an E.M. primary source is considered as being
generated by a set of equivalent sources distributed on the
surface of the plate. This concept has been applied to a
number of different problems by Annan (1974). The same idea
has been used in gravity and magnetic interpretation where the
equivalent layer is commonly used. This concept is a
reflection of the non-uniqueness of the inverse problem in
potential field data.

By applying the equivalent source method the problem of
an inductively thin plate is reduced to a surface integral
equation in terms of unknown surface currents and a known
source field. The equation is solved by a standard finite
element technique : the Galerkin method. This results in a set
of linear equations that are solved in terms of a weighted
eigenvalue problem. The solution is a set of eigenpotentials
that are illustrated in Figure 2.1. They are equivalent to a
set of non interacting current loops and the eigenvalues are
related to the time constant of each current loop. The secon-
dary field outside the conductor is calculated by the Biot-Sa-
vart law. The most interesting aspect of this solution is that
the eigenpotential depends solely on the aspect ratio (depth
extent / strike extent) of the plate. Hence, a number of
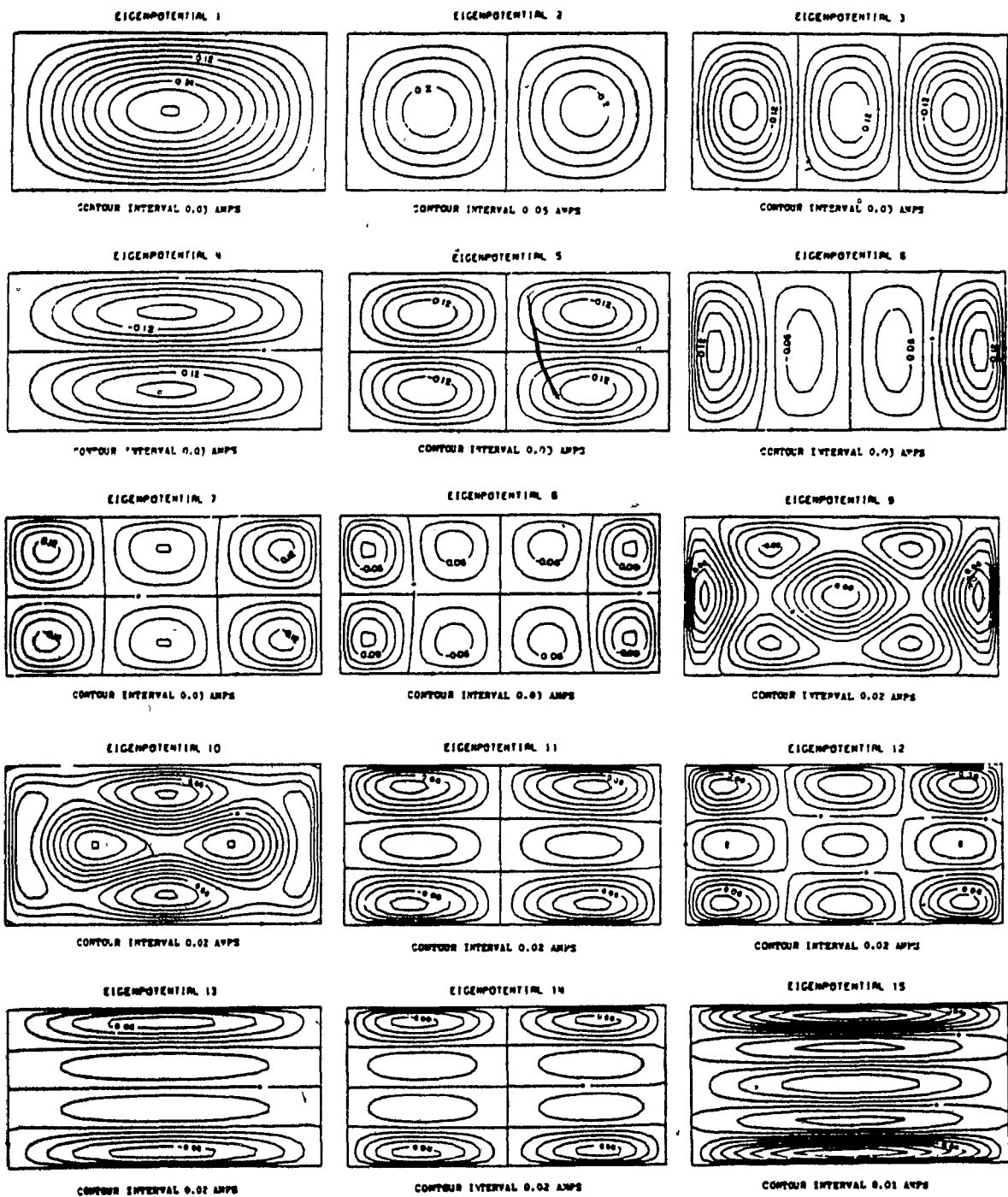
Figure 2.1 Eigenpotential maps (plate whose width/length=0.5) corresponding to 15 eigencurrents (after Annan, 1974).

solutions can be computed and stored for a full range of ratios including most practical cases likely to occur.

There is a strong economic advantage to the use of the PLATE program, particularly if the forward problem has to be solved many times, such as for the case for non-linear inverse problems. Most of the computing effort then goes for the calculation of the primary and secondary field coupling coefficients since the coupling integrals have to be evaluated by numerical quadrature. Any reduction of the CPU time of the numerical integration routines has a direct influence on the CPU time for the inverse solution. There are two direct ways to achieve this goal : a reduction of the number of eigencurrents and a modification of the quadrature routines used in the PLATE program. The standard version of the program uses 15 eigencurrents and a Gaussian quadrature formula with a maximum order of 19. The actual order of the quadrature is determined by the distance between the reference point on the plate (0 ,0 ,0) and the transmitter or the receiver depending on which coupling coefficient is being calculated. Models generated by the standard version will now be called reference models. The response of the airborne INPUT system to a plate having a strike length of 600m and a depth extent of 300m was calculated for different conductances, dip, order of quadrature and number of eigencurrents. The geometry of the plate is shown in Figure 2.2. System integrators were not simulated. Table 2.1 summarises the results for 15 eigencurrents. The
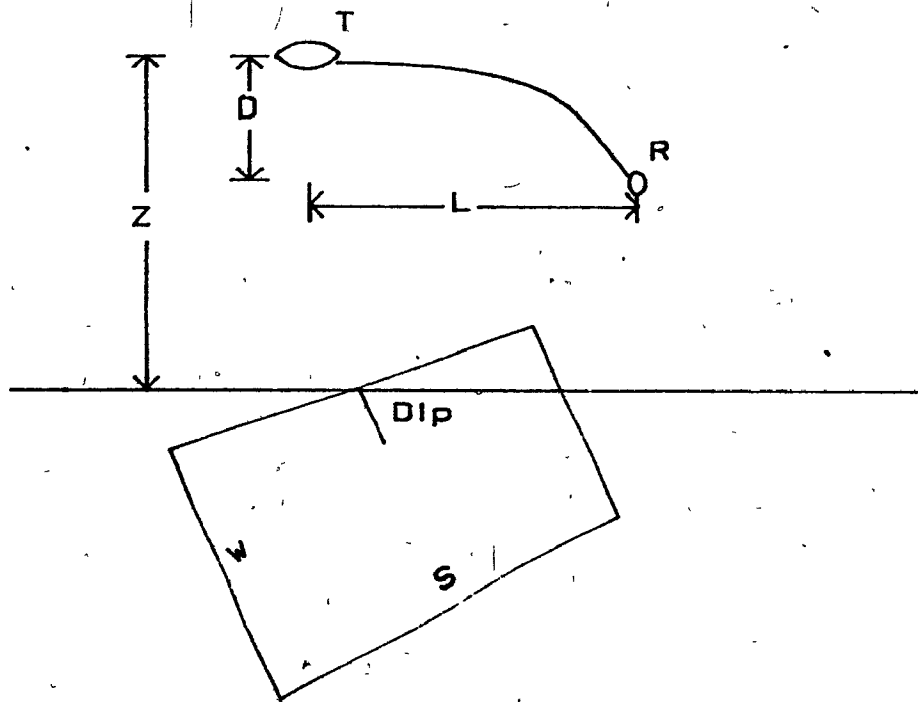
D : Vertical distance T.-R

L : System length

R : Receiver

S : Plate strike length

T : Transmitter

W : Plate width

Z : System height above plate

The strike angle is the angle
between the plate axis and the
flight line.

The profile offset is the distance
between the flight line and the
middle point of the plate upper
edge.

Figure 2.2 Plate geometry.

Table 2.1 : RMS difference between the responses calculated with a 19th and an 8th maximum degree quadrature.

Dip \ Cond.	5	20	50
60°	2.7	9.6	6.2
90°	0.8	3.7	1.8
135°	9.6	22.4	12.8

maximum order of the numerical quadrature was reduced to 8 and the normal magnetic field at the surface of the plate was evaluated on a 400 (20 x 20) point grid rather than the usual 900 points.

The maximum RMS error occurs for a dip of 135° and a conductance of 20S. Profiles of the differences between high and low precision results are shown in Figure 2.3 for different dips and conductances. To study the influence of the number of eigencurrents two nomograms were calculated, one using 15 and the other 10 eigencurrents, their difference is illustrated in Figure 2.4. The plate is vertical and 120m under the transmitter, conductances range from 1 to 100S. When 10 eigencurrents are used, the amplitudes are more and more underestimated as conductance increases. The maximum is reached for a conductance of 50S, channel one is then underestimated by almost 500ppm. The reduction of the order of the quadrature has a minor effect on the exactness of the forward model while a reduction of the number of eigencurrents results in unacceptably large errors.

It is interesting to look at the reduction of the CPU time. The CPU time for the computation of the reference model was normalised and Table 2.2 presents the results. It is obvious that there is a trade-off between precision and speed. Inversion of theoretical models with different noise levels have been attempted for different number of eigencurrents and order of quadrature and they will be presented later.
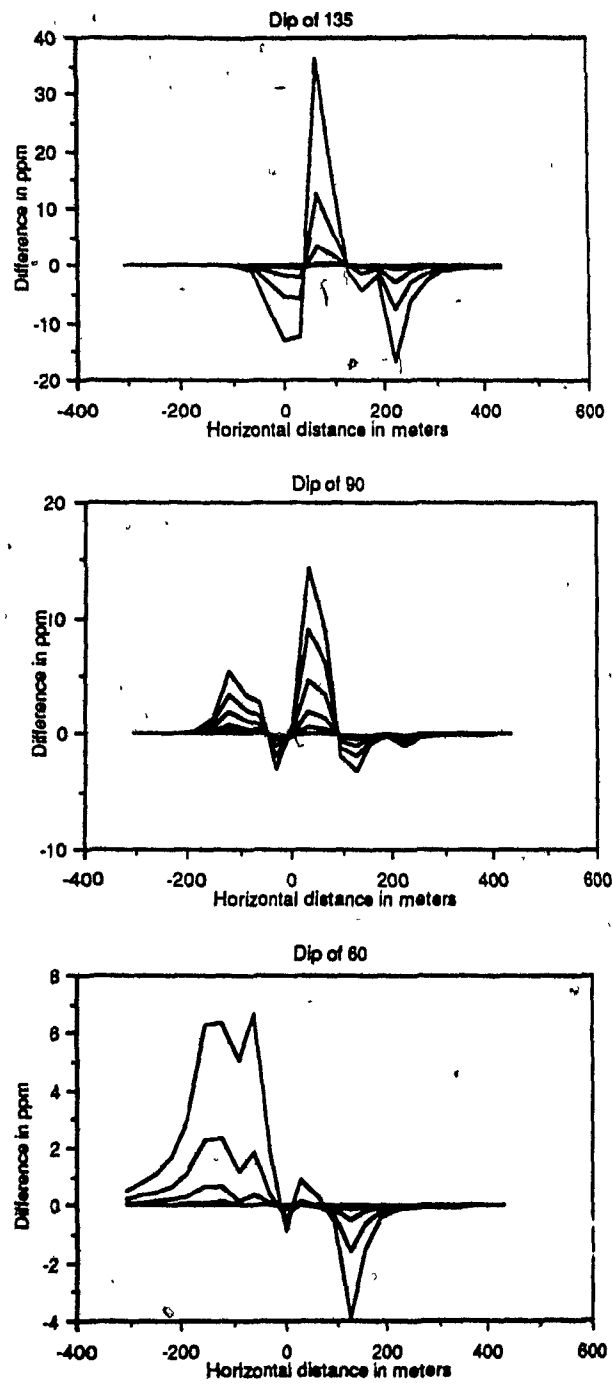
Figure 2.3a Plot of the differences of the responses calculated with a 19th degree and an 8th degree quadrature for the INPUT system and a plate conductance of 5S.
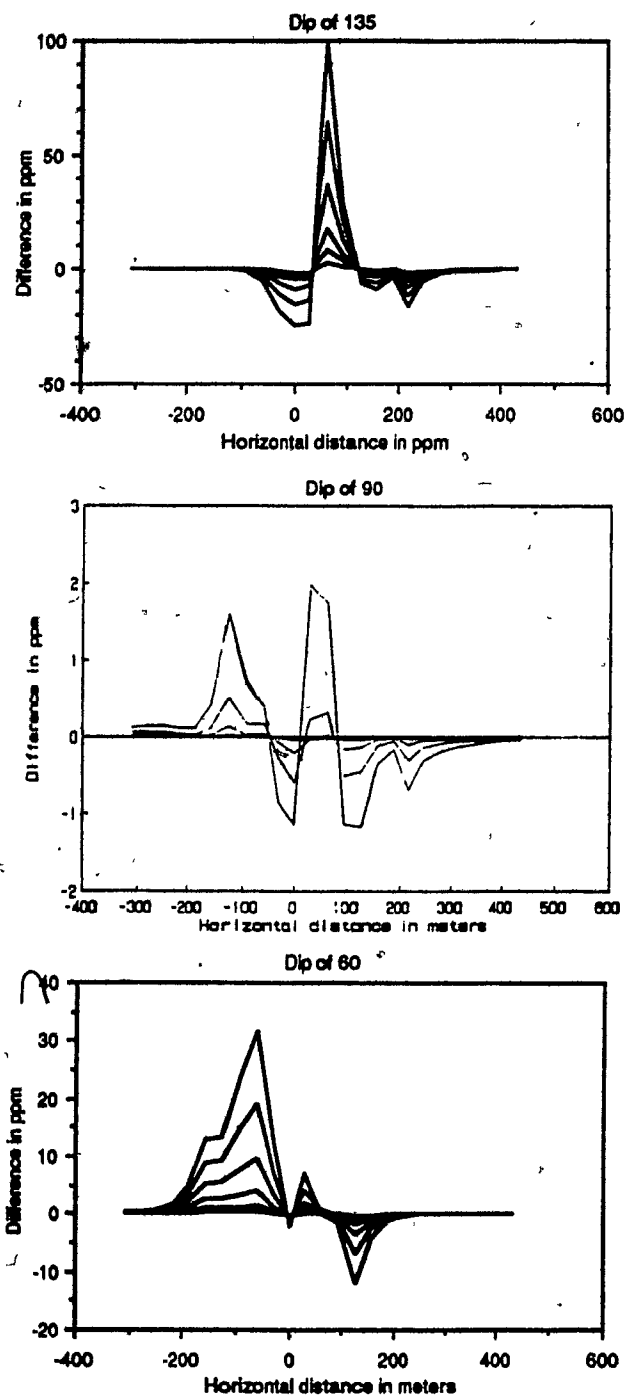
Figure 2.3b Plot of the differences of the responses calculated with a 19th degree and an 8th degree quadrature for the INPUT system and a plate conductance of 20S.
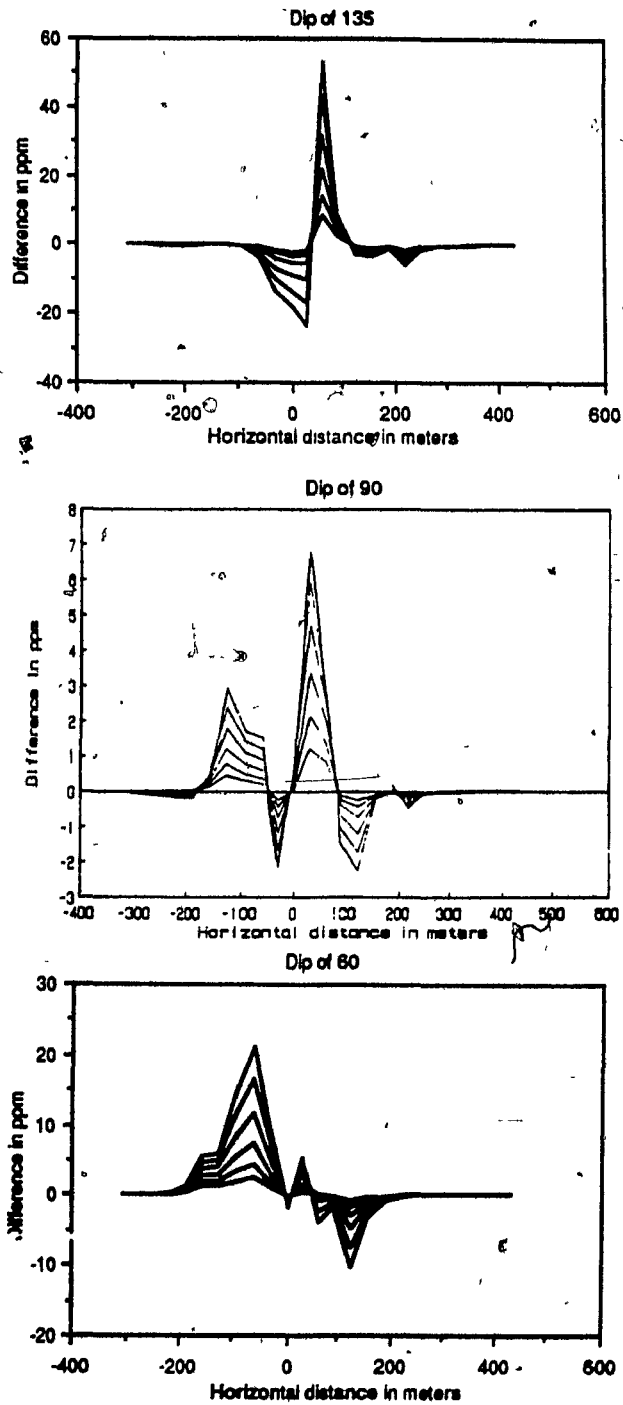
Figure 2.3c Plot of the differences of the responses calculated with a 19th degree and an 8th degree quadrature for the INPUT system and a plate conductance of 50S.
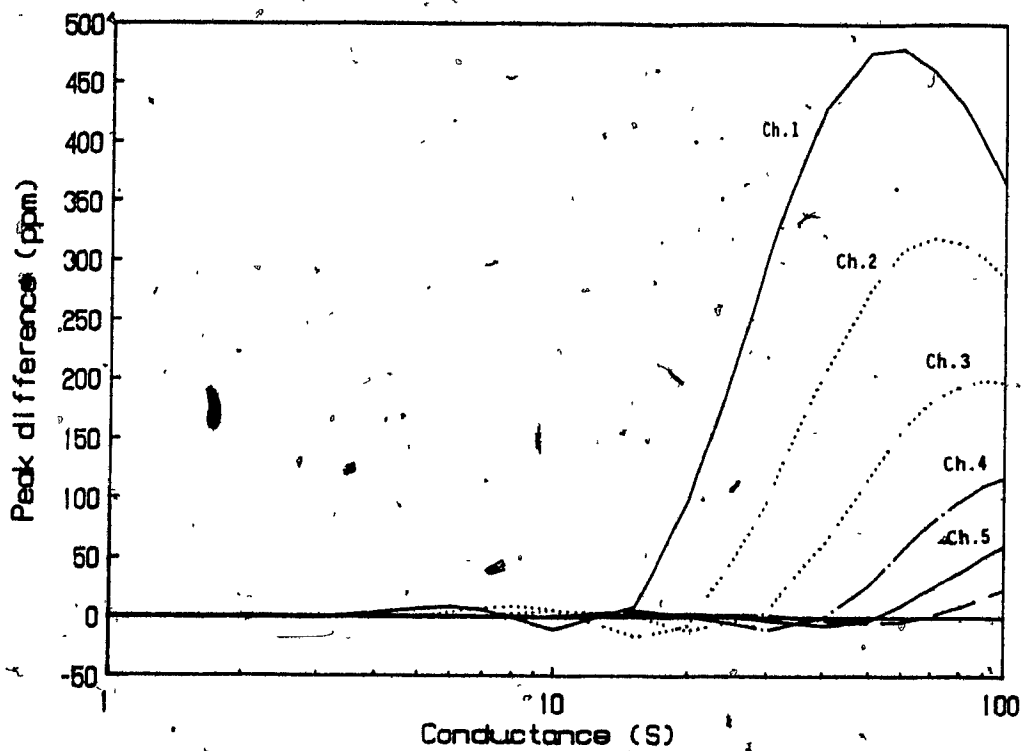
Figure 2.4 Peak differences for channel amplitudes calculated with 10 and 15 eigencurrents for the INPUT system.

Table 2.2 Normalised CPU time for different order of quadrature (N) and number of eigencurrents (M).

M	N	19	11	8
15		1	0.35	0.27
10		0.75	NA	0.26

The Gaussian quadrature used in the PLATE program is probably the type with the highest degree of accuracy. This type of quadrature formula converges to the true value of an integral for almost any conceivable function (Stroud, 1971, p13). Surface integrals such as those in PLATE are usually integrated over one variable with a Gaussian formula and again over the next variable with the same formula. This is known as a product rule; direct rules also exist and they have the following form (Dhatt and Thouzot, 1984, p293):

$$\int_{-1}^{1} f(x,y) \ dx \ dy \ - \ \Sigma \ W_i \ f(x_i,y_i)$$

Where the function $f(x,y)$ is integrated over the x and y variables and the W_i are weighting factors determined by the specific direct rule used. The function is evaluated at r points.

These rules need less function evaluations and are generally faster than product rules. The problem is to find a rule that has the required accuracy. A number of those rules have been studied by Stroud (1971) and their application to finite element problems is discussed by Dhatt and Touzot (1981). A 13 point direct formula of degree 7 taken directly from Stroud (1971) was tested for accuracy and speed. The responses for the same models as those used in Table 2.1 were in error by about 10% at peak amplitude, which is too high.

A Chebychev integration rule was also tested. Since all the weights are equal to unity, it should be faster than a Gaussian rule of the same order. This rule was taken directly from Abramowitz and Stegun (1965) and has the following form:

$$\int_{-1}^{1} f(x) \, dx = (2/n) \sum f(x_i)$$

Where $f(x)$ is the function to be integrated and the x_is the abscissae where the function is evaluated.

This is essentially the summation of n function values at some particular abscissae and it can be easily used in a product rule. Using this rule, the error is about 5% at peak amplitude for the same reference models as previously discussed. Nevertheless there was no substantial reduction of the CPU time when compared with a Gaussian rule of the same order. It is apparent that most of the computing effort is in the evaluation of the kernel of the integral. In fact, the PLATE program evaluates this function on a 30 by 30 mesh over the surface of the plate when computing the coupling coefficients. The function values used by the numerical quadrature are interpolated from this grid. Use of a 20 by 20 mesh results in a reduction of 5% in CPU time while overestimating the peak amplitude by 5ppm, which is negligible .

Some minor modifications of the original FORTRAN code of the PLATE program were also made to make it run faster and more efficiently. Finally, only the parts of the program

pertinent to the inversion algorithm were kept. Needless to say the program is no longer interactive. The inversion program is between three and four times' faster than it would be if the standard version had been used to solve the forward problem.

2.4 Half-Plane Approximation.

A solution has been recently published by Weidelt (1983) for the E.M. response of a dipping half-plane; so it is useful from a computational point of view to be able to approximate the response of this model by the PLATE program. The response of the INPUT system was calculated for a number of plates of varying strike lengths, all with an aspect ratio of 0.5, conductivity thickness products of 5S, 20S and 50S and a dip of 90°. The plates are located at a depth of 120m and 220m and the system is assumed to be flying perpendicular to the strike. System integrators were not simulated. Results are shown in Figure 2.5 for the six channels of the INPUT system. There is a fast increase in the peak amplitudes of all channels with increasing strike length. A total of 15 eigenpotentials and a maximum order of 19 for the Gaussian quadrature were used for these tests. Although in theory, the simulation of a real half-plane would required an infinite number of eigenpotentials a finite number is sufficient for a good approximation. No test have been made to simulate the response of the GEOTEM system to a half-plane since in would
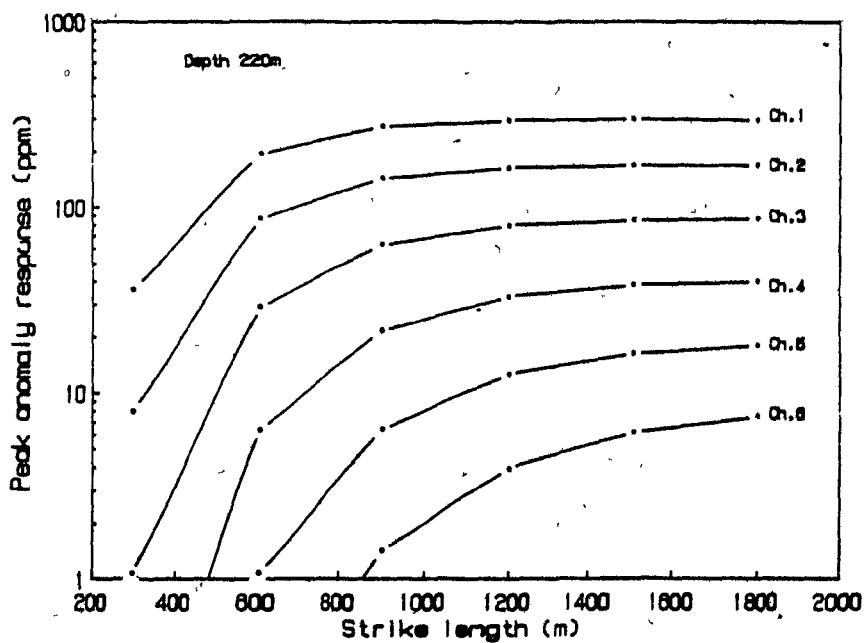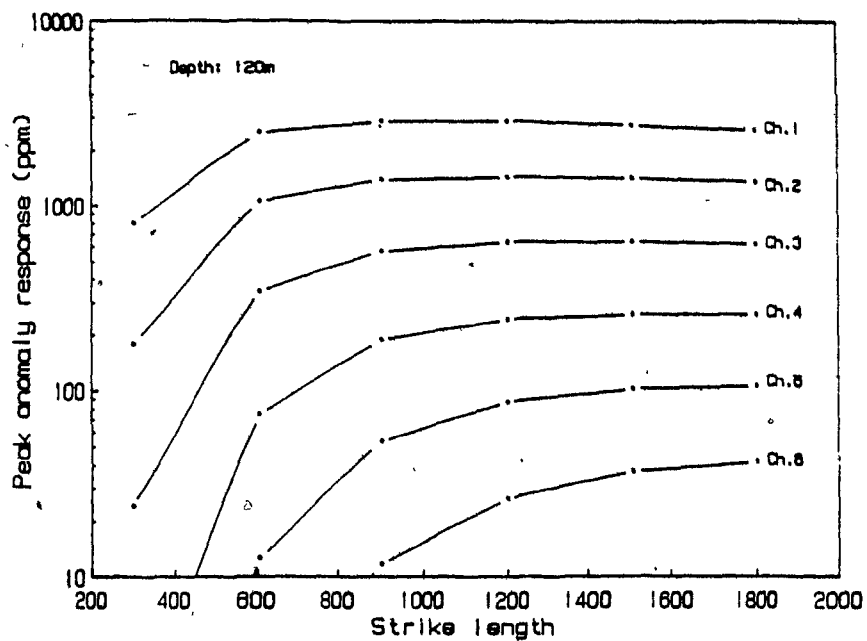
Figure 2.5a INPUT system peak response for a vertical plate with a conductance of 5S as a function of the strike length for depths of 120m and 220m.
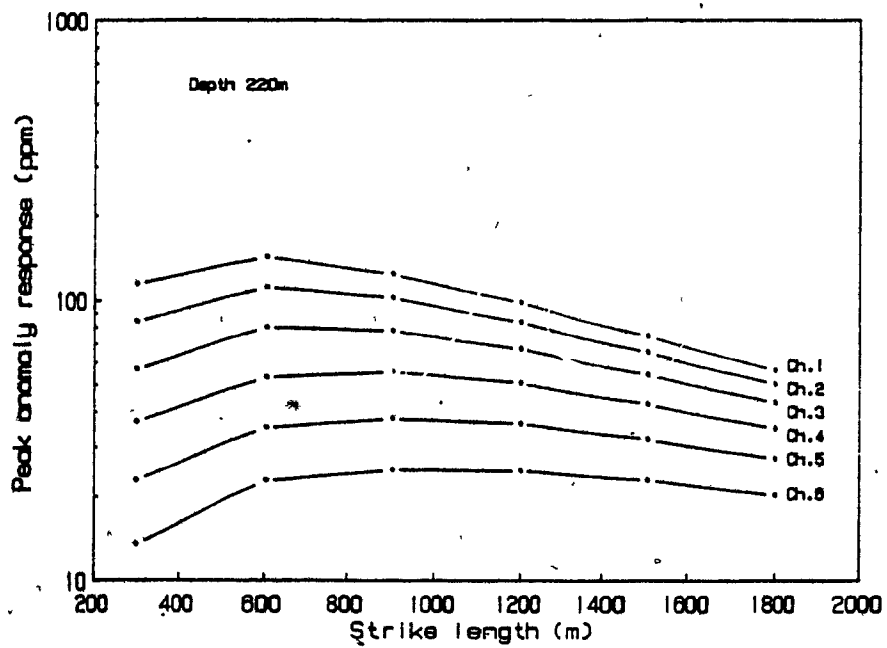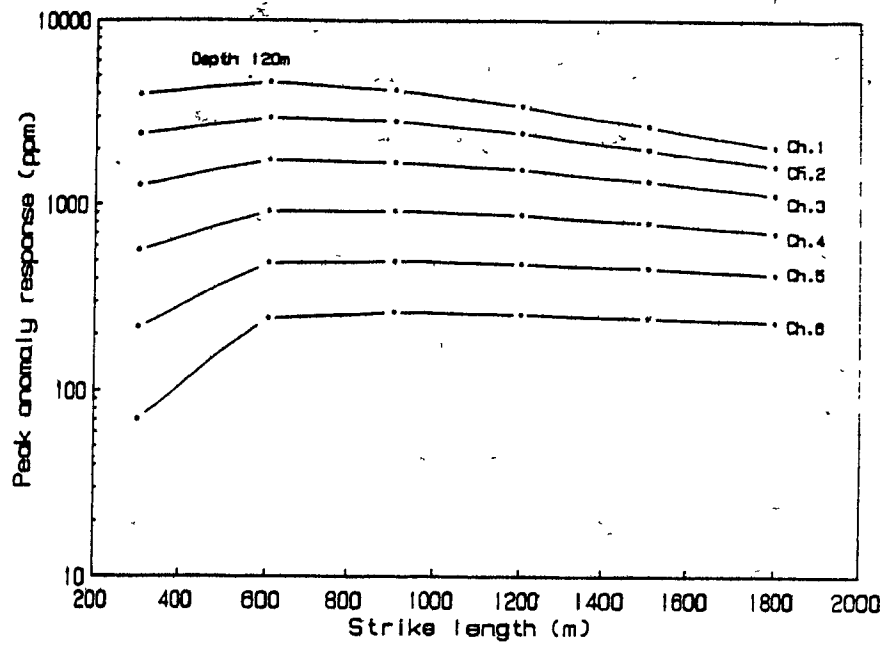
Figure 2.5b INPUT system peak response for a vertical plate with a conductance of 20S as a function of the strike length for depths of 120m and 220m.
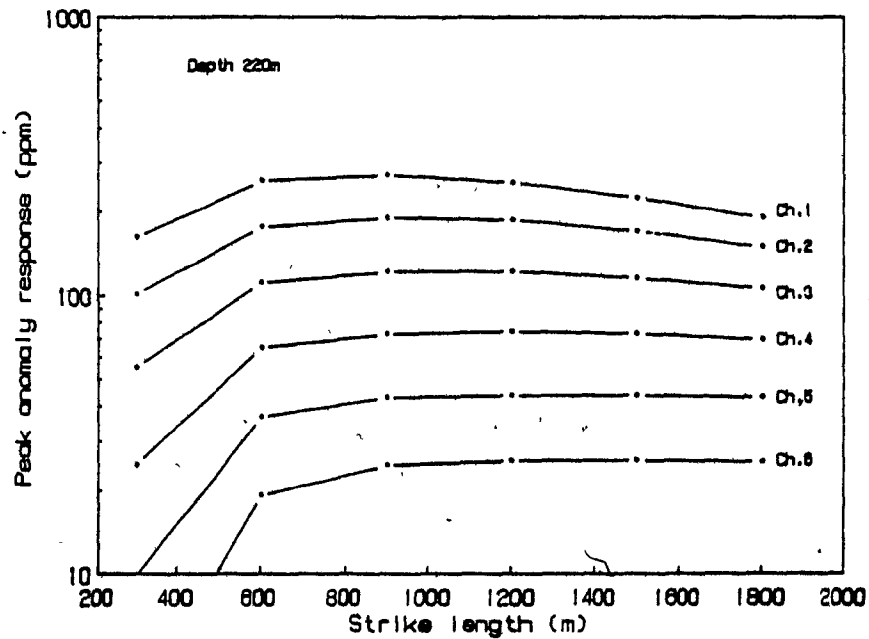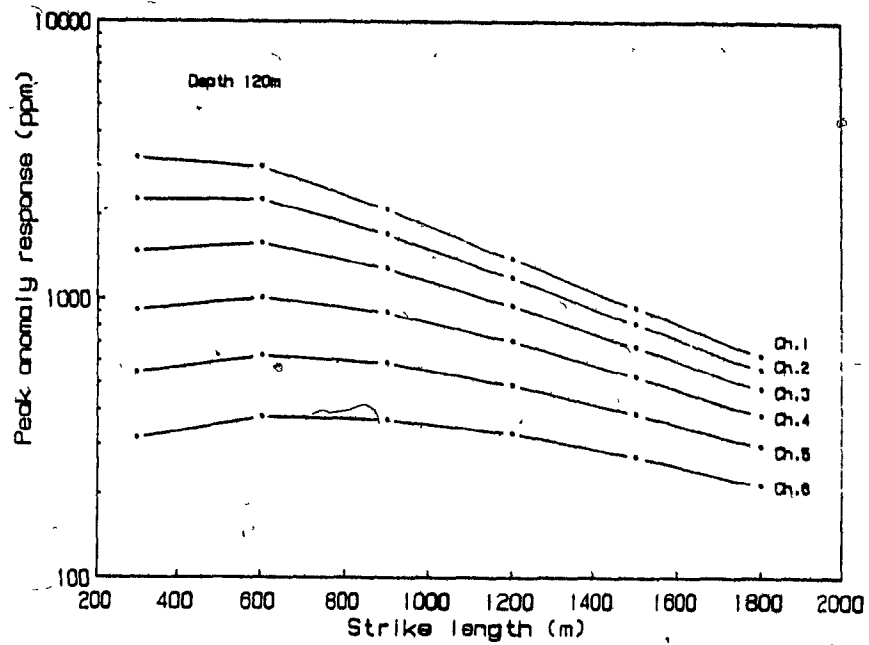
Figure 2.5c INPUT system peak response for a vertical plate with a conductance of 50S as a function of the strike length for depths of 120m and 220m.

be very similar. The differences would be due to different time windows and would be similar to those observed for the INPUT system.

A plate can be considered to be infinite when the maximum amplitude stabilises with increasing plate size (Hanneson and West, 1984). This criteria was also used by Palacky (1975) when he used analog modeling to study the INPUT system response to a half-plane. His "half-plane" sheet corresponded to a plate of a strike length of 1183m and width of 592m. It was then found that an increase of the sheet size would not affect the anomaly amplitude except for conductances less than 5.6S. For a plate located 120m under the transmitter, it is observed in Figure 2.5 that when the conductivity thickness product is 5S, the plate has to be about 1800m of strike length to be considered infinite. It need be only 600m when the conductance is 20S or 50S. The observed decrease of the amplitude with increasing strike length is most likely due to the fact that more than 15 eigencurrents should be used to model a real half-plane. The conclusions are the same if the plate is located 220m under the transmitter. The choice of the plate size, when modelling a half-plane , should therefore be made a function of the expected conductance of a particular target. In inverse problems the plate strike length is measured directly on the anomaly map. It is the common practice to use a 600m strike length to model a half-plane. If

a low conductance is suspected, a longer strike length of the order of 900m should be used.

2.5 Some Particular Considerations.

When simulating the response of any real airborne system it is essential to take into account some properties of the electronics used in the receiver. All airborne E.M. systems use some form of filtering or averaging to reduce the high frequency noise. The receiver can be modeled as a low pass filter that has two main effects on an anomaly, first a modification of its shape and amplitude, symmetric anomalies become asymmetric, secondly, the position of the maximum is delayed along the flight line, this is the effect of the phase response of the filter.

That problem has been studied by Jensen and Becker (1979) who designed digital filters to reduce the anomaly distortion and correct for the spatial phase-shift. The effect of a 1.1 sec. time constant is illustrated in Figure 2.6 for the response of the INPUT system. When solving the forward problem, it is easy to simulate those effects by convolving the actual system response of the receiver with the theoretical anomaly obtained from the PLATE program. It is essential to include that procedure as part of the solution of the forward problem in any inversion scheme.
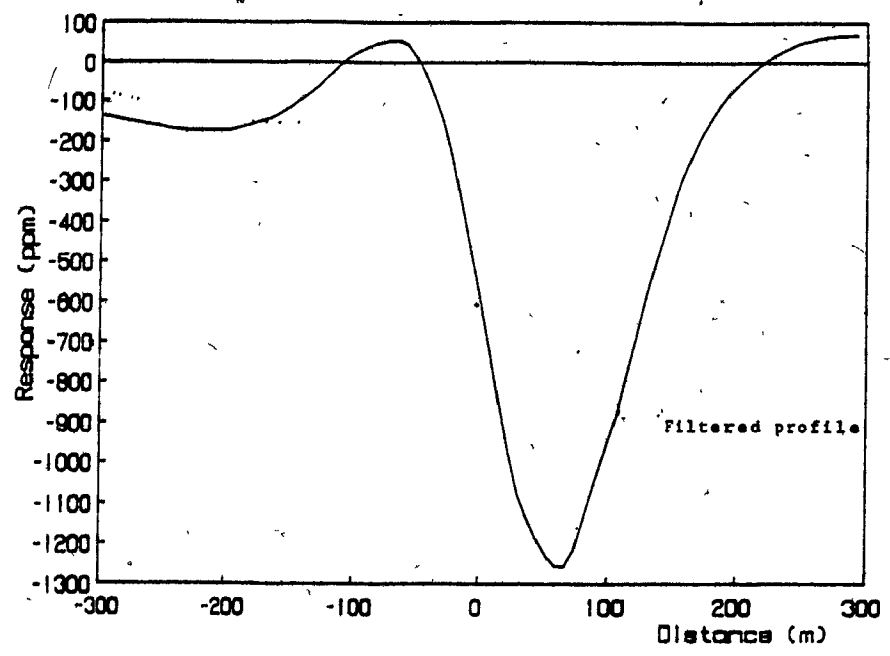
Figure 2.6 Effect of system integrators on channel two of a typical anomaly.

Chapter 3

THEORY OF INVERSION

3.1 General considerations.

It is important to understand what is meant by such words as inversion and interpretation in the context of geoscience. Interpretation is the process by which the geophysicist translate physical observations into geology, taking into account known geological constraints. It is obvious that an interpretation can easily be subjective, being often an art more than a science, and is largely based on experience. On the other hand inversion is a mathematical technique to translate the data, the geophysical observations, into a model and provide an estimate of the parameters and their uniqueness. This is related to the solution of the forward problem, that is the computation of theoretical observations assuming a known model. In principle once the forward problem is solved it should be easy to solve the inverse problem but in practice this is generally not the case. A point not very often discussed, is the choice of the model itself. In general, most inverse problems have an infinite number of solutions as demonstrated in potential field theory. This subject

is discussed by Grant and West (1965, p.214-216) for the gravity and magnetic data. For E.M. soundings, Fullagar (1984) demonstrates that for a one dimension conductivity profile, given an infinite number of arbitrary accurate measurements, there is a unique solution. The solution is however unique only because a specific model (i.e. one dimensional variation of conductivity) has been chosen. Thus, the choice of the model is a critical part of any geophysical inversion. Unfortunately there is no general rule to select the right model. This is still largely based on experience and intuition. Inversion theory is however of great help to assess the validity of any proposed model.

For a long time, most geophysical interpretation was done with the help of nomograms, which is really a form of manual curve fitting procedure. It was the first method used for the interpretation of gravity and magnetic data. A good example is the set of nomograms proposed by Koulomzine and al. (1970) for the interpretation of magnetic data. It was also used by Gosh (1972) and Palacky (1972) for the interpretation of E.M. surveys. Figure 3.1 is an illustration of the nomogram published by Palacky (1972) for the interpretation of INPUT survey data. The model is the infinite half-plane and the data was obtained from analog scale models. These curves can easily be digitized and used with a computer program to automatise this type of inversion. An example of this type of work is given by DeMoully and Becker (1984) who interpreted INPUT data in terms
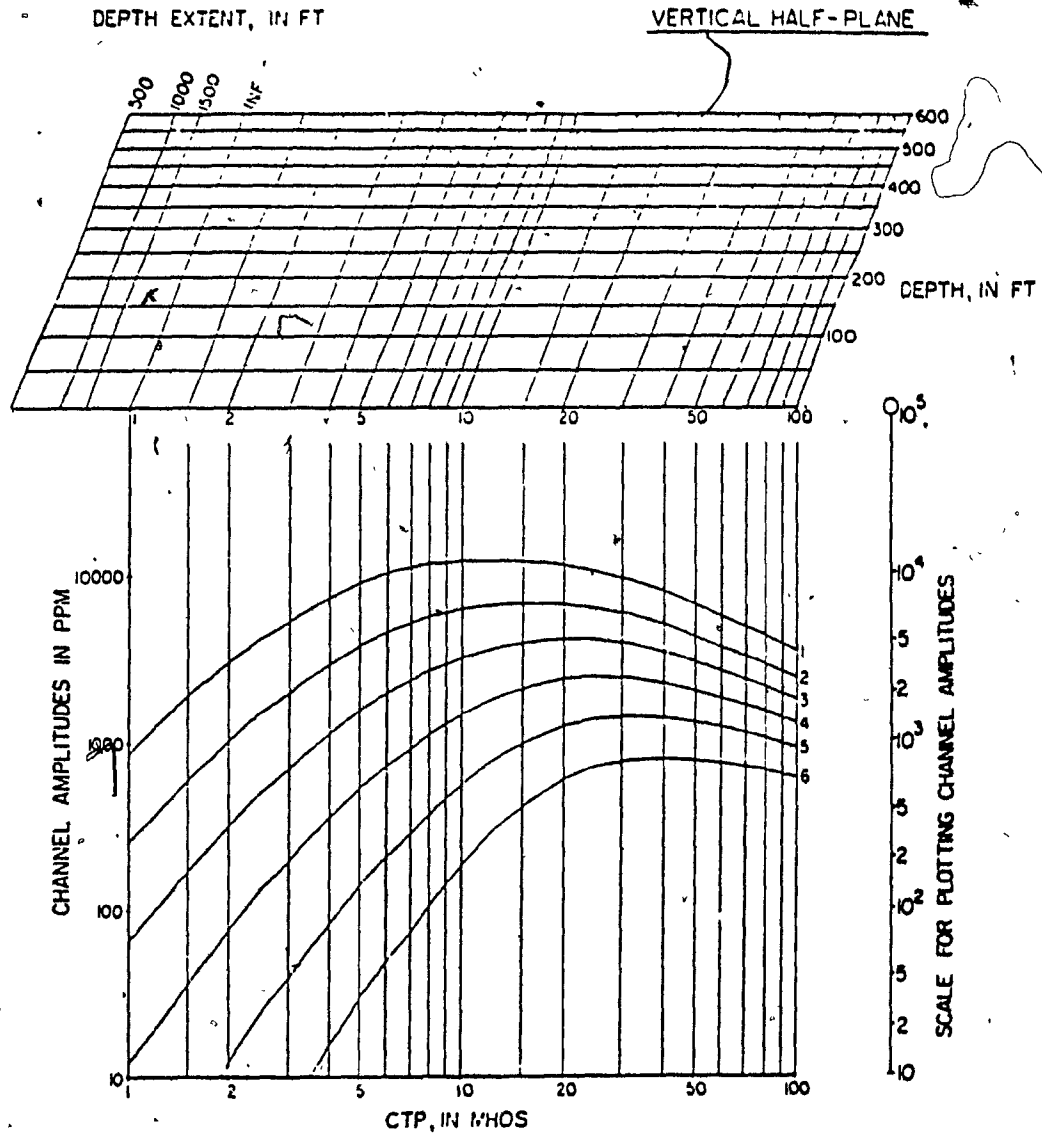
Figure 3.1 Nomogram for the estimation of conductance, depth and depth extent of a conductor. The peak anomaly amplitudes have to be plotted on a transparent paper using the scale on the right hand side when the data points have to be translated to fit the respective curves. The position of the 10^5ppm mark will indicate conductance and depth. (after Palacky, 1972)

of a one layer earth.

Very few inverse problems are amenable to a direct solution. For magnetic field data and a thick dike model, such a solution has been published by Rao et al (1973). It is based on the numerical evaluation of the horizontal gradient of the magnetic anomaly. The same idea can be applied to vertical magnetic gradient data. Because this is a new result we provide an outline below.

3.2 Exact Inverse Solution for Magnetised Dike.

The vertical magnetic gradient of a thick dike is given by:

$$G(x) = 2 \ J \ b \ c \ \text{Sin} \ \theta \ [\ \text{Sin} \ A(\frac{X - D - T}{Z^2+(X-D-T)^2} - \frac{X - D + T}{Z^2+(X-D+T)^2})$$

$$- \text{Cos} \ A(\frac{2Z}{Z^2+(X-D+T)^2} - \frac{2 \ Z}{Z^2+(X-D-T)^2})] \qquad (3.1)$$

where : J : intensity of magnetization

    b = Sin i / Sin p

    c = Sin I / Sin l

    I : ambient field inclination (i=I for perfect induc-
    tion)

    a : ambient field declination

    α : $\gamma + \lambda - \theta$

    γ = Arctan (Tan I / Cos A)

    λ = Arctan (Tan i / Cos a)

θ : dip

T : dike half-width

T : depth to top of dike

D : location of the center of the dike

Rearranging the equation gives :

$$X^4 G + C_1 X^3 G + C_2 X^2 G + C_3 X\ G + C_4 G + C_5 X^2 + C_6 X + C_7 = 0 \quad (3.2)$$

where $C_1 = -4\ D$

$C_2 = 2Z^2 + 6D^2 - 2\ T^2$

$C_3 = 4D\ (\ T^2 - Z^2 - D^2\ )$

$C_4 = (\ Z^2 + D^2 + T^2\ )^2 - 4D^2 T^2$

$C_5 = -\ A\ T$

$C_6 = 2\ T\ (\ A\ D + B\ Z\ )$

$C_7 = -\ A\ T\ D^2 + A\ T\ Z^2 + A\ T^3 - 2\ B\ T\ Z\ D$

The previous equation generates as many equations as there are observations and they can be solved for the C_i by standard techniques. The dike parameters are then given by:

$$D = -\ C_1\ /\ 4 \quad (3.3)$$

$$T^2 = Z^2 + 3\ D^2 - C_2\ /\ 2 \quad (3.4)$$

$$4Z^4 + 2Z^2(6D^2 - C^2) + 2D^2(2D^2 - C_2) + C_2^2/4 - C_4 = 0 \quad (3.5)$$

Equation 3.5 is solved for Z, after rejecting negative and complex roots. It is then trivial to solve for T. It can also be deduced that:

$$A = -C_5\ /\ T \quad (3.6)$$

$$B = -\ (\ 2\ T\ A\ Z + C_6)\ /\ 2\ T\ Z \quad (3.7)$$

It follows that:

$$\theta = Arctan\ (\ A\ /\ B\ ) \quad (3.8)$$

This is a very attractive direct solution. As a matter of fact, for theoretical data, it is always possible to recover the original model with a high degree of accuracy. The interesting point is that when a realistic noise level is added to the data, the solution becomes unstable unlike the case shown by Rao et al (1973). This is an example of the non-uniqueness of such a solution when real measurements contaminated by noise are inverted.

Two different classes of problems arise in inverse theory: linear and non-linear problems, depending on the type of equation describing the forward problem. Non-linear problems are generally linearized through an expansion in a Taylor series. It follows that most of the discussion on inversion will be centered on the linearised inverse problem, after an introduction to the linear problem.

3.3 Linear Inversion.

A simple linear problem is the fitting of a straight line to a set of data. If there are only two observations, the solution is unique; in most cases there are many observations and a least squares fit is computed. It is worthwhile to describe the standard least squares fit, since it is at the origin of most of the discussion.

Consider n data points y_i taken at x_i , that are to be fitted by a straight line. An obvious solution, is to minimise

the distance between the desired line and the data points. If the distance is measured along the y axis, and if the equation of that line is $y = ax + b$ then:

$d^2_i = (y_i - a - bx_i)^2$ is the square distance

This problem is formulated as :

$$y = A \ m \tag{3.9}$$

where A is the system matrix and m the model (in this case : (a, b).

The least squares solution is :

$$m = (A^tA)^{-1}A^ty \tag{3.10}$$

Which is unique provide A^tA is non singular.

The problem of fitting a parabola to a set of data points is then simply :

$$y_i = a + bx_i + cx_i^2 \tag{3.11}$$

so again we write:

$$y = A \ m \tag{3.12}$$

where :

$$m = (a,b,c)^t \quad and \quad m = (A^tA)^{-1}A^ty \tag{3.13}$$

This equation is linear in the unknown coefficients, but not in x_i. A more interesting problem is the fitting of an exponential decay curve of the form :

$$y = A \ e^{-bx},$$

Although this is obviously a very non linear problem, it is nevertheless possible to take the logarithm of both sides of the equation to obtain :

$$ln \ (y/A) = - b \ x$$

This is the previous problem of fitting a straight line. The disadvantage is that the solution will be biased, and y cannot be negative. Very few non linear problem have such an easy solution.

3.4 Linearised Inversion.

A very good description of linearised inversion is given by Jackson (1972) and an example of its application to DC resistivity soundings interpretation is found in Inman (1972). Our use of linearised inversion closely follows that of Jackson and the same notation is used. Suppose a set of equations such that the observations y_i (i=1,...n) are related to the parameters x_j (j=1,...m) in the following way:

$$y_i = f_i(x_j) \tag{3.14}$$

where $f_i(x_j)$ is a non linear function of x_j.

If this function is analytic, it can be expanded in a Taylor series about some initial value x_j^o :

$$f_i(x_j) = f_i(x_j^o) + \frac{\partial f_i}{\partial x_j}\bigg|_{x_j^o}(x_j - x_j^o) + \frac{\partial^2 f_i}{\partial x_j^2}\bigg|_{x_j^o}(x_j - x_j^o)^2 + \ldots \tag{3.15}$$

If it can be assumed that second and higher order terms are small and if y_i is defined as:

$$y_i = f_i(x_j^o) + \Delta y_j \tag{3.16}$$

then:

$$\Delta y_i = \frac{\partial f_i}{\partial x_j}\bigg|_{x_j^o} \Delta x_j \tag{3.17}$$

This equation can be expressed in matrix notation as:

$$y = A x \tag{3.18}$$

where A is the n x m matrix with elements A is the matrix of the partial derivatives of the non linear equation describing the forward problem. It is also called the Jacobian and, sometimes, the sensitivity matrix. The solution is:

$$x = H y \quad \text{where H is the generalised inverse of A.} \tag{3.19}$$

Non linearity is then taken into account by using an iterative procedure of the form:

$$x_{k+1} = x_k + H (y_{obs} - y_k) \tag{3.20}$$

The starting values x_0 have to be guessed or chosen near the global minimum of the error function to ensure convergence. Different criteria exist to stop the iteration. The simplest one is to check the RMS error against some arbitrary value, usually the estimated noise level of the data. A chi-squared test can also be used, one could also use the rate of convergence of the iteration process.

The computation of H is a central problem in inverse theory. In general A is non-square and there is, depending on the minimisation criteria, an infinite number of inverses. Jackson (1972) identifies the following properties of a "good" inverse:

- $S = A H \simeq I_n$, the n x n identity matrix; this is a measure of how well the model fits the data;

- $R = H A \simeq I_m$, this is a measure of the uniqueness of the solution;

- the parameter variance should be small

Backus and Gilbert (1968) and Wiggins (1972) give physical interpretations of the product AH and HA ,the resolution and information density matrices. Different ways exists to solve the problem and Menke (1984), mentions that the same general solutions can be obtained from three different viewpoints:

1- The classical least squares solution can be generalised to include the undetermined case (n<m).

2- The generalised inverse of Backus and Gilbert.

3- The maximum likehood method, or the statistical approach.

The first two viewpoints will be described with the solution of the E.M. inversion problem in mind. The third one cannot be used to solve our E.M. problem, since it requires some statistical knowledge about the expected solution.

3.5 The Classical Least Squares.

As seen before, linear least squares is the minimisation of the distance between the observed and the predicted data. This was illustrated by the fitting of a straight line. The choice of the square length as the criteria of goodness of fit is determined by the assumption of a Gaussian distribution of errors. One might as well choose the absolute value of the distance or any other norm. A norm l of order k is defined as $l_k = (y_i - f_i)^k$ were y_i are the data values and f_i the calculated

values. As shown by Menke (1984, sec. 3.2) different norms produce different fits. Least squares have nevertheless become the standard method for solving that class of problems because it leads to a linear set of corrective equations.

3.6 Generalised Inverses.

In the standard least squares approach the emphasis was on solution simplicity and the minimisation of the prediction error. The solution had the form:

$$x = H\ y \qquad\qquad (3.21)$$

In the generalised inverses approach the /emphasis is now placed on the study of the matrix H (or equivalently A), the generalised inverse. For the overdetermined least squares problem it is equal to $(A^tA)^{-1}A^t$ and for the undetermined case it is : $A^t(AA^t)^{-1}$. It is evident that in general H is not a square matrix. Assuming that H exists, we will now study its properties. If $R = I_m$, then all the model parameters are uniquely determined. They are then said to be perfectly resolved. Such is the case for overdetermined problems. For the underdetermined case $R \neq I$, and the rows of R give an indication of how well each parameter is resolved from its neighbors.

Then $S = I_n$ for the underdetermined problem and $S \neq I_n$ for the overdetermined case. This matrix is interpreted as a measure of the independance or the resolution of the data. Each row of the matrix is interpreted as a window averaging

neighboring data points (see Wiggins 1972). Thus, the closeness of a resolution matrix to the identity matrix is a measure of how well the parameters or the data are resolved.

Ideally, one would like the resolution matrices to be as close as possible to the identity matrix and the parameter variance to be minimal. It is then useful to define the following measures:

$$\text{spread} \; (S) - | \; S - I \; |^2 \qquad (3.22)$$

$$\text{spread} \; (R) - | \; R - I \; |^2 \qquad (3.23)$$

Both are called the Dirichlet spread functions.

One can also define a unit covariance matrix, (cov(x)) which is a function of the covariance of the data. It is generally assumed that the data errors are uncorrelated and the data values possess only the same variance s^2. This statistical assumption is generally difficult to establish. These three matrices (R, S, cov(x)) can be used to design a generalised inverse. It is also useful to define a measure of the "size" of the covariance matrix as :

$$\text{size} \; (\text{cov} \; y) - \Sigma \; (\text{var} \; y) \qquad (3.24)$$

One can use the previous criteria to find the generalised inverse for the overdetermined case. It is already known that the parameter resolution matrix is the unit matrix; in that case, it then remains to minimise the spread of S . As shown by Menke , the generalised inverse is then :

$$H^{-1} - (A^t A)^{-1} A^t \qquad (3.25)$$

a result already obtained from least squares theory. An analogous result is obtained for the underdetermined case. One may questioned the usefulness of this concept since it gives the same results as the least squares method. The answer lies in the generality of the approach. It is now possible to minimise a weighted sum of the spreads and the covariance size. This is formulated as :

$$Min \ \{\alpha_1 spread \ (\ S \ ) \ + \alpha_2 spread \ (\ R \ ) \ + \alpha_3 size \ (\ cov \ )\}$$

The α's being the weighting factor. This leads to the following equation (Menke p.70):

$$\alpha_1(\ A^tA \ )A^t+H(\alpha_2AA^t+\alpha_3[cov]) \ - \ (\alpha_1+\alpha_2) \ A^t \qquad (3.27)$$

Unfortunately there is no known explicit solution for H. It is nevertheless possible to find special solutions by selecting the values of the α's. If $\alpha_1 - 1$ and $\alpha_2 - \alpha_3 - 0$, the least squares solution is obtained ; if $\alpha_1 - \alpha_3 - 0$ and $\alpha_2 - 1$ the minimum length solution is now obtained. The most interesting case is when $\alpha_1 - 1$, $\alpha_2 - 0$ and $\alpha_3 - \epsilon^2$ an arbitrary positive constant. The generalised inverse is then:

$$H^{-1} - (A^tA + \lambda^2 I \ )^{-1}A^t \qquad (3.28)$$

This is the damped least squares solution. It is then interpreted as the minimisation of the weighted sum of the data resolution spread and the covariance size. This is also known as the Marquardt (1970) or ridge regression method. The eigenvalues of $(A^tA+\epsilon^2I)$ are $\lambda^2_i+\epsilon^2$. Thus, the effect of the introduction of ϵ^2 is to augment the size of the eigenvalues and therefore to reduce the influence of the small eigenvalues

on the solution. The effect of small eigenvalues is discussed in Section 3.4 and the method has been generalised by Jupp and Vozoff (1975). Menke (1984, p71) notes that resolution matrices can have negative off-diagonal elements and, thus, may cause interpretation difficulties if the rows are interpreted to be localized averages. An analogous interpretation can be given to the elements of the rows of an information matrix.

Backus and Gilbert (1967) define a different spread function to select resolution matrices that have their largest elements concentrated along the main diagonal. This approach has been used by Fullagar and Oldenburg .(1984) for the inversion of horizontal loop E.M. frequency soundings. The Backus and Gilbert spread function is simply:

$$\text{spread} (R) = \Sigma \; \Sigma \; w(i,j) \; [\; R_{ij} - I_{ij} \;]^2 \qquad (3.29)$$

$$\text{spread} (S) = \Sigma \; \Sigma \; w(i,j) \; [\; S_{ij} - I_{ij} \;]^2 \qquad (3.30)$$

where $w(i,j)$ is a weighting factor designed to maximise the delta likeness of the resolution matrices. A convenient weighting factor is :

$$w(i,j) = (i-j)^2$$

This factor implies a linear ordering.

This is particularly helpful when the data have some special ordering. Two actual examples should help to clarify this point. Consider, first, an underdetermined case. Assume we have n DC resistivity data that we would like to interpret in terms of m layers, where m is larger than n. The data

resolution matrix is then perfect, and it is only natural to select a parameter resolution matrix whose rows can be interpreted as localised averages of neighboring earth layers. Consider now the overdetermined case of the interpretation of a magnetic profile in terms of the parameters of an infinite thick dike. Then, the parameter resolution matrix is perfect and again it is natural to select a data resolution matrix whose rows can be interpreted as localised averages of neighboring data points.

3.7 The Singular Value Decomposition.

The singular value decomposition of a matrix is a very powerful tool for the study of least squares problems. A complete description is given in Lawson and Hanson (1974), and Menke (1984) explains its use in geophysical inverse problems. Some very good examples of its use are given by Wiggins (1972) and Jupp and Vozoff (1975). Although it has been used mostly in the solution of underdetermined problems it can be also applied to the inversion of overdetermined geophysical problems.

Lanczos (1958) introduced the singular value decomposition (later noted SVD) of a matrix. Any matrix A can be decomposed in the product of three matrices (Jackson, 1972):

$$A = U \Lambda V^t \qquad (3.31)$$

If A is m x n, then U is an n x n orthogonal matrix and V is an m x m orthogonal matrix; Λ is an n x m diagonal matrix, whose diagonal elements are greater than or equal to zero. By convention the singular values are ordered in decreasing order. Note that the singular values are the square eigenvalues of the matrix ($A^t A$).

If p of these values are non null, the matrix is of rank p. The generalised inverse is simply given by:

$$A^{-1} = V \Lambda^{-1} U^t \qquad (3.32)$$

If one or more singular values are zero, the matrix Λ can be partitioned in a square matrix Λ_p of the p non zero singular values and three zero submatrices.

$$\Lambda = \begin{bmatrix} \Lambda_p & 0 \\ & \\ 0 & 0 \end{bmatrix} \qquad (3.33)$$

The SVD then becomes:

$$A = U_p \Lambda_p V_p{}^t \qquad (3.34)$$

U_p and V_p are the first p columns of U and V, the other portions of these matrices are noted U_0 and V_0. Therefore A contains no information about the subspaces spanned by these matrices. A null singular value means that a linear combination of the unknowns is not represented in the system. In other words some of the equations are linearly dependent; some information is absent for the problem. Therefore small singular values are associated with weakly represented linear combination of the unknowns. This is often due to the fact

that real data cannot be obtained with absolute accuracy but is always contaminated by some amount of noise. This was well illustrated in Section 3.1 where a direct solution for the inversion of vertical gradient total magnetic field due to a thick dike was developed. The solution became unstable when a realistic noise level was added to the synthetic data. This was directly caused by the presence of a small singular value.

The "natural" generalised inverse was introduced by Lanczos (1961) and is defined as:

$$H = V_p \Lambda_p^{-1} U_p^t \qquad\qquad (3.35)$$

The parameter resolution matrix is then simply:

$$R_p = H A = V_p \Lambda_p^{-1} U_p^t U_p \Lambda_p V_p^t = V_p V_p^t \qquad (3.36)$$

When the matrix is full rank, the model resolution matrix is the identity matrix and the parameters are perfectly resolved. This is often the case for overdetermined problems.

Similarly the data resolution matrix, or information matrix is:

$$S_p = U_p U_p^t \qquad\qquad (3.37)$$

This will be equal to the identity matrix only if U_p spans the complete data space, then $p = n$. This is generally the case for overdetermined problems.

The data resolution matrix indicates how well the observed data are predicted by the inverse. Combining equation 3.19 and 3.20 we find that the predicted data are related to the observed data by:

$$y_{pre} = A H y_{obs} \qquad\qquad (3.38)$$

The rows of S are then interpreted as kernels averaging the observed data. When the data have a natural ordering the predicted value is then an average of neighboring observed values. A sharp maximum centered about the main diagonal indicates that the data are well resolved, while a broad maximum is indicative of poorly resolved data.

Inspection of the data resolution matrix can be difficult, especially when the matrix is large. Jackson (1972) suggested the use of the vector:

$$s_k = \Sigma \ (S_{ki} \cdot \delta_{ki})^2 \tag{3.39}$$

as a measure of the independence of the kth data point. Crossley (1982) suggested the use of a relative information vector $s_k' = 1/2 \ (1 - s_k)$. The limits are 0, no information, and 1 for an entirely independent data point. If S is orthonormalised, its diagonal elements then give the relative information content of each data point. They are given by:

$$S_{kk}' = S_{kk} / (\ \Sigma \ S_{kl}^2)^{1/2} \ . \tag{3.40}$$

Menke (1986) notes that the diagonal elements of S are often called the importance of the data. The difference between this definition and the previous one is in the normalization of S.

Assuming uncorrelated data with a uniform variance (s^2), the covariance of the model parameters is given by:

$$[cov \ y] = s_p^2 V_p \Lambda_p^{-2} V_p^t \tag{3.41}$$

The variance s^2 is estimated as:

$$s^2 = (Ax - y) / (m - n) \tag{3.42}$$

The diagonal elements of the parameter covariance matrix are the parameter variances and their square root give their estimated standard error. This is very sensitive to the smallest singular values because of the terms $1/\lambda^2$ in Λ^{-2}.

The determination of p, the rank of the matrix is in principle very well defined, however in practical problems, the singular values are likely to be very small rather than identically zero. Observing that Λ^{-1} is built from the reciprocal of the singular values, it is clear that a very small value can destabilise the generalised inverse. Various strategies can be used to avoid that problem. One can assume that the matrix is full rank and then replace the reciprocal of the singular values by $1/(\epsilon^2 + \lambda_i^2)$. This has almost no effect on the larger values while reducing the influence of the smaller ones. This is often called a damped least squares.

A more general strategy has been developed by Jupp and Vozoff (1975), they introduced a diagonal damping matrix used to modifify the generalised inverse as follow:

$$A^{-1} = V \, T \, \Lambda^{-1} U^t \qquad (3.43)$$

Where the p index has been dropped for convenience. The elements of T are:

$$t_i = s_i^{2n}/(\lambda_i^{2n} + \epsilon^{2n}) \qquad (3.44)$$

For n = 1, this is equivalent to the standard damping solution of Section 3.3.2. By doing this, the variance of the estimated parameters is greatly reduced, and some a priori knowledge of the parameters' variance is therefore assumed. Recall that it

can also be interpreted as the minimisation of the weighted sum of the data resolution spread and the covariance size. In practice the choice of the damping factor ϵ^2 depends on the problem being considered (see Jupp and Vozoff; 1975).

3.8 Inversion and SVD.

When a matrix is well conditioned or well behaved, it is convenient to compute its inverse by standard techniques, such as Gaussian elimination. On the other hand, if the matrix has a large condition number (ratio of the largest to the smallest singular value), or is nearly singular, one should rather use a singular value decomposition (SVD). It is then possible to identify the source of the near singularity and modify the inverse by damping or deleting small singular values. Therefore, it is suggested to first use a SVD when a new type of problem is solved for the first time. For example, the partial derivative matrix needed in the inversion of the INPUT E.M. system is well behaved as its condition number is about 5, and no singular value is much smaller than the others. If, one now considers the joint inversion of an INPUT anomaly and a magnetic anomaly, a case studied in Chapter 5, the condition number can be as high as 300 and at least one of the singular values is much smaller than the others. Note that the SVD is computed after scaling the partial derivative matrix where the Euclidian length of each column was normalised to unity.

In our opinion, the strategy should be to use a SVD to evaluate the difficulty of a new problem. The only disadvantage of the SVD is that it takes more time to compute than a Gaussian elimination. This is insignificant in a problem such as E.M. inversion where most of the CPU time is spent for the solution of the forward problem. In this work we used the program published by Lawson and Hanson (1974) which is based on the algorithm of Golub and Reinsch (1970). A faster program has been published by Chan (1985) and could be very useful when the number of rows of the matrix to be decomposed is much greater than the number of columns.

3.9 Inversion of Airborne Time Domain E.M. Data.

Most of the previous work in E.M. inversion has been concerned with the layered earth model (Ward and al. 1974, Jupp and Vozoff 1975, Fullagar 1984). The inversion of E.M. data was studied by Paterson (1982) and his program is used by some helicopter-borne E.M. contractors to interpret the conductivity and the thickness of the overburden. The inversion is based on a SVD of the parameter partial derivative matrix. Results seem to be excellent. To our knowledge only one 3D case has been solved to date, and it is the inversion of transient E.M. data from a spherical conductor (Lee 1984). He uses the program developed by Jupp and Vozoff (1975) which is based on SVD. A very useful model in the context of the Cana-

dian shield is the thin plate model and by extension the infinite half-plane. As seen before, most orebodies can be related to lenticular or tabular bodies. This explains the popularity of this model since the first days of airborne E.M. surveys.

One of the most used systems is the airborne INPUT system developed by Barringer (1962). More recently a similar system called GEOTEM was introduced by Geoterrex in 1985. Both systems use the same transmitter waveform : a semi-sinusoidal pulse of alternating polarity. The secondary transient is measured during the off time. The primary and secondary fields are illustrated in Figure 3.2. The number of channels varies from six to twelve depending on the receiver used. Unfortunately the INPUT system suffers from a drift in zero levels. This is corrected by using the calibrations done in flight and assuming a linear drift. The GEOTEM system is almost drift free due to its digital receiver (Thomson; 1986).

Thefore the inversion of INPUT data has to include the zero levels as unknowns. The other parameters are the dip, the depth, the conductance and the location of the plate along the profile. The strike angle and the length of the conductor are usually easily deduced from the anomaly map.

As seen before, Annan's solution involves a fair amount of numerical integration and so numerical differentiation has to be used for the computation of the partial derivatives.

Primary field at transmitter

Time on — Time off

Total voltage at receiver

Volts

1 2 3 4 5 6

Decaying secondary voltage
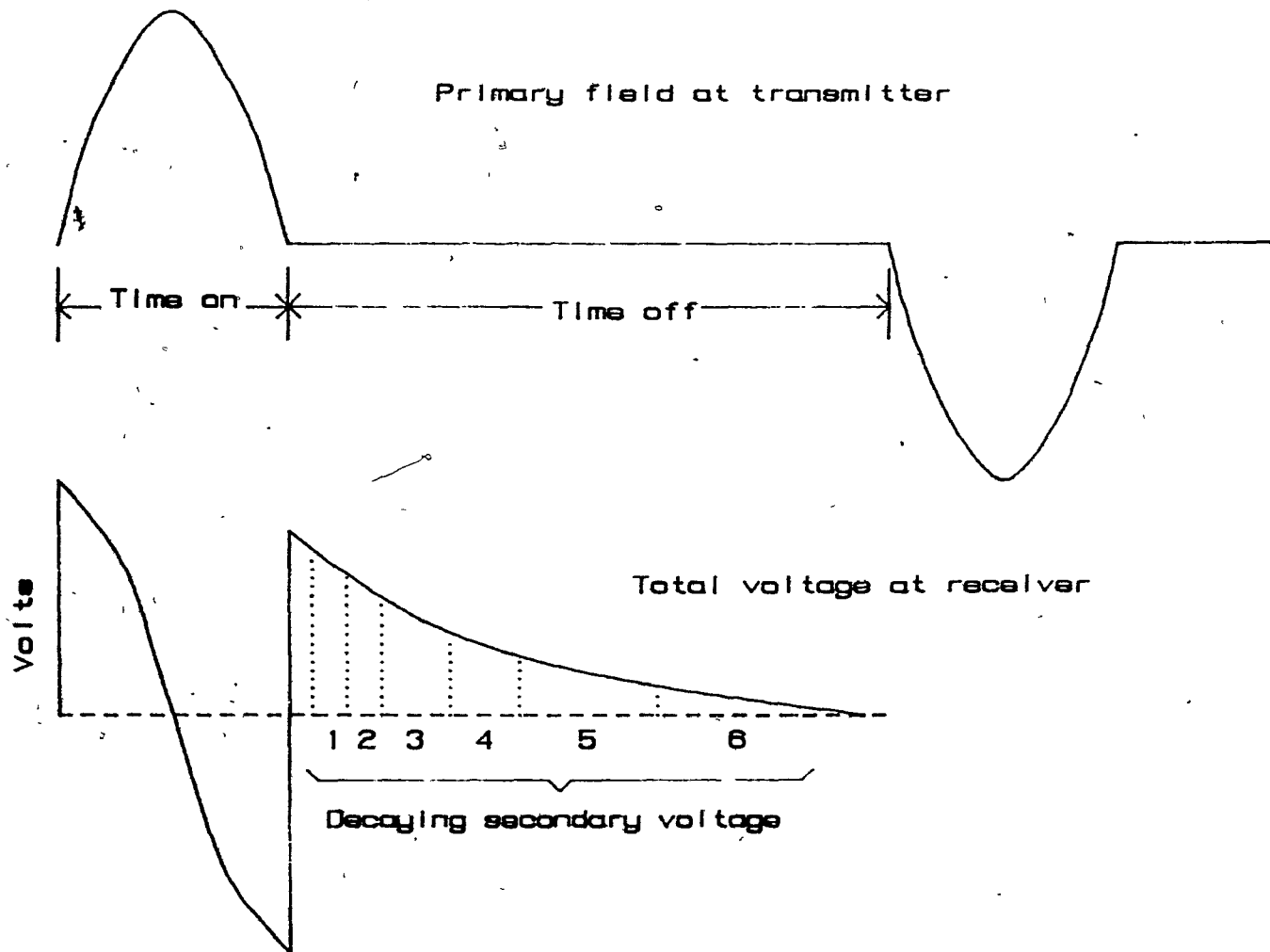
Figure 3.2 INPUT primary and secondary fields.

Some of these are trivial and the computational effort is thereby greatly reduced. The partial derivatives involving the zero levels are equal to one, since they are not involved in the computation of the system response to a conductor. They can be seen as a different DC shift for each channel. The partial derivative involving the conductivity thickness product is also easily calculated, since it is introduced into the computation of the response after the numerical integration. The partial derivatives involving the other parameters have to be evaluated numerically. A very simple forward difference formula is used and has been shown to give excellent results. The partial derivatives are approximated as follows:

$$\frac{\partial f}{\partial x} = \frac{f(x + \Delta x) - f(x)}{\Delta x} \qquad (3.45)$$

In general Δx is of the order of 0.1% of x For the dip Δx is fixed to 1° and for the reference x_0 to 1m. This helps to avoid numerical problems when small values of those parameters are involved. Numerical tests have shown that decreasing x below 0.1% does not improve the estimation of the partial derivatives.

3.10 Structure of the Inversion Program.

The structure of the program itself is fairly simple, the forward response is computed with a set of routines directly taken from the PLATE program while the partial derivatives matrix is calculated by numerical differentiation as shown in the previous section. The SVD routine comes from Lawson and Hanson (1974). In the case of non convergence the singular values are damped as proposed by Jupp and Vozoff (1975). The damping factor is taken as the pth singular value, the smallest one. If the problem still does not converge, then the (p-1) singular value is used. This procedure can be repeated up to the largest singular value. If it is then impossible to obtain convergence, the problem should be restarted with a new initial model.

Damping was not used for the inversion of the INPUT data tested in this work. However it was used a few times in the joint inversion of magnetic and INPUT data and for the inversion of INPUT data using only the late time channels. It was commonly used for the inversion of magnetic data of the actual data profiles interpreted in Chapter 5. This could indicate that the E.M. inversion problem is more linear than the magnetic inversion problem. On the other hand this could be because it is easier to find a "good" initial model for the E.M. problem.

The iteration process is stopped when the RMS error is smaller than the assumed noise level of the data or when the maximum number of iterations has been attained. Parameter errors are estimated by equation 3.42. The correlation matrix, the singular values and the singular vectors are also estimated. The residuals, that is the difference between the observed and calculated data, are listed for each channel. Finally, a linear regression is calculated for each channel between the observed and calculated data. We then obtained the correlation, the error of fit and a Student's t test for each channel.

The program is very versatile, all parameters that can influence the inversion results are variable. The order of the numerical quadrature and the dimensions of the grid used to interpolate the magnetic field over the plate can be modified for each problem. Different plate width to length ratios can be used by assigning different files prior to running the program. The pulse repetition rate, its length and the time gates of each channel are variable. The program flow chart is illustrated in Figure 3.2.
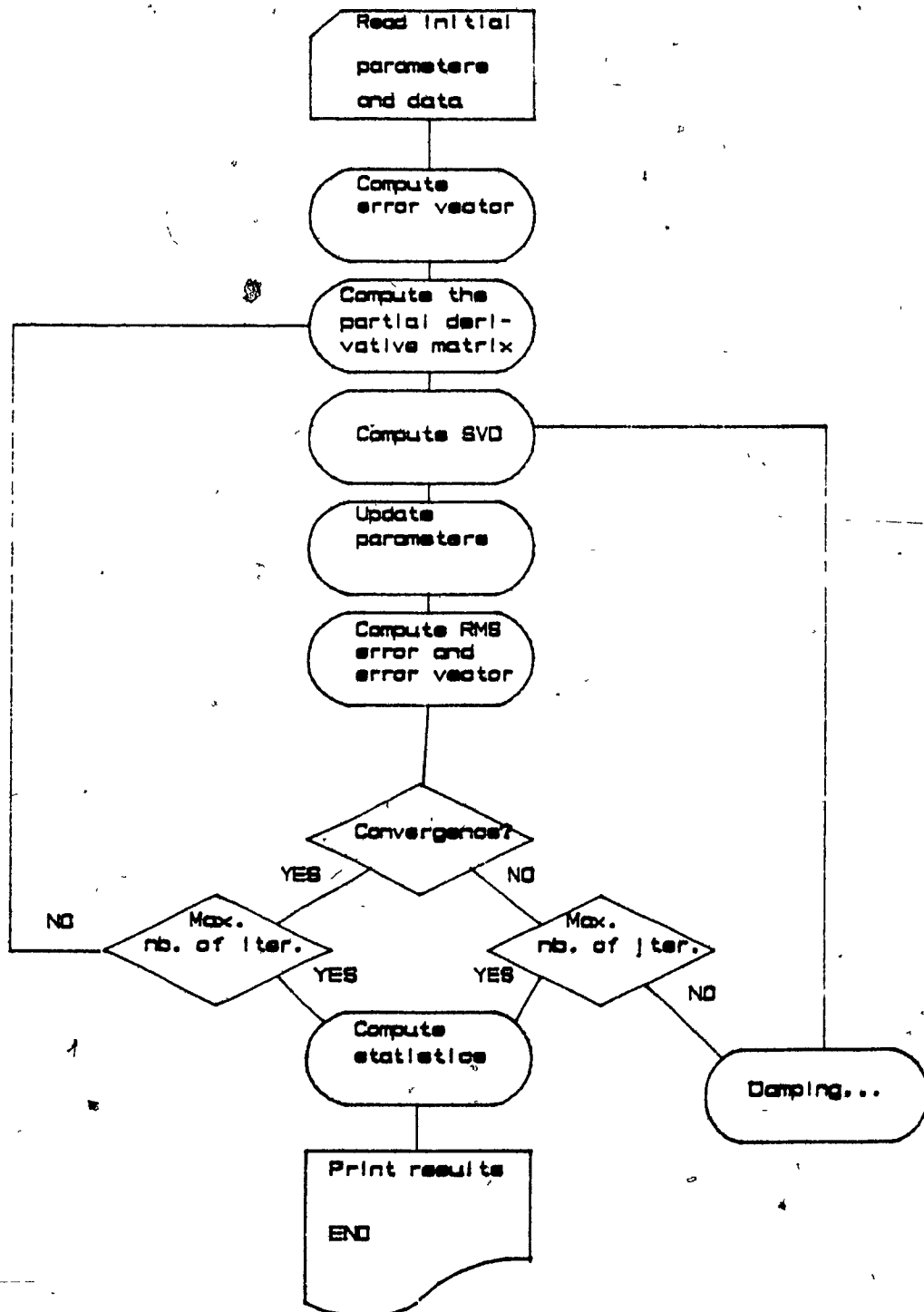
Figure 3.3 Inversion program flow chart

Chapter 4

SYNTHETIC AND ACTUAL DATA INVERSION

4.1 Synthetic Data Inversion

4.1.1 Noise Free Synthetic Profiles

A set of theoretical profiles was calculated to investigate the quality and the limits of the inversion algorithm. The plate model characteristics used to compute the profiles are listed in Table 4.1 and some typical profiles are illustrated in Figure 4.1. The digital filter used to simulate the real system integrators has a time constant of 1.1sec. The speed of the aircraft was assumed to be 200km/h and the profiles were sampled at a distance equivalent to a sampling interval of 0.5sec. The INPUT system time specifications used for these simulations are listed in Table 4.2.

The first case investigated is a vertical plate with a conductivity of 5S, it simulates a weak conductor located 150m under the transmitter or 30m below the ground surface. Although the profile was generated with the highest precision available with the PLATE program, 15 eigencurrents and a Gaussian quadrature of the 19th degree, the inversions were computed with a Gaussian quadrature of the 8th degree. The RMS

Table 4.1   Parameters of the plates used to generate the theoretical profiles.

Depth	:	120m and 150m
Strike length	:	600m and 900m
Dip	:	60°, 90° and 135°
Strike angle	:	90°
Plunge	:	0°
Conductance	:	5S, 15S and 50S

Table 4.2 INPUT system specifications used to compute the synthetic profiles.

Pulse width   :   1.0msec

Base frequency: 149Hz

Time gate limits:

    Channel 1: 0.240-0.404msec

    Channel 2: 0.404-0.568msec

    Channel 3: 0.568-0.896msec

    Channel 4: 0.896-1.224msec

    Channel 5: 1.224-1.716msec

    Channel 6: 1.716-2.208msec

Transmitter-receiver horizontal distance: 93m

                      vertical distance : 69m
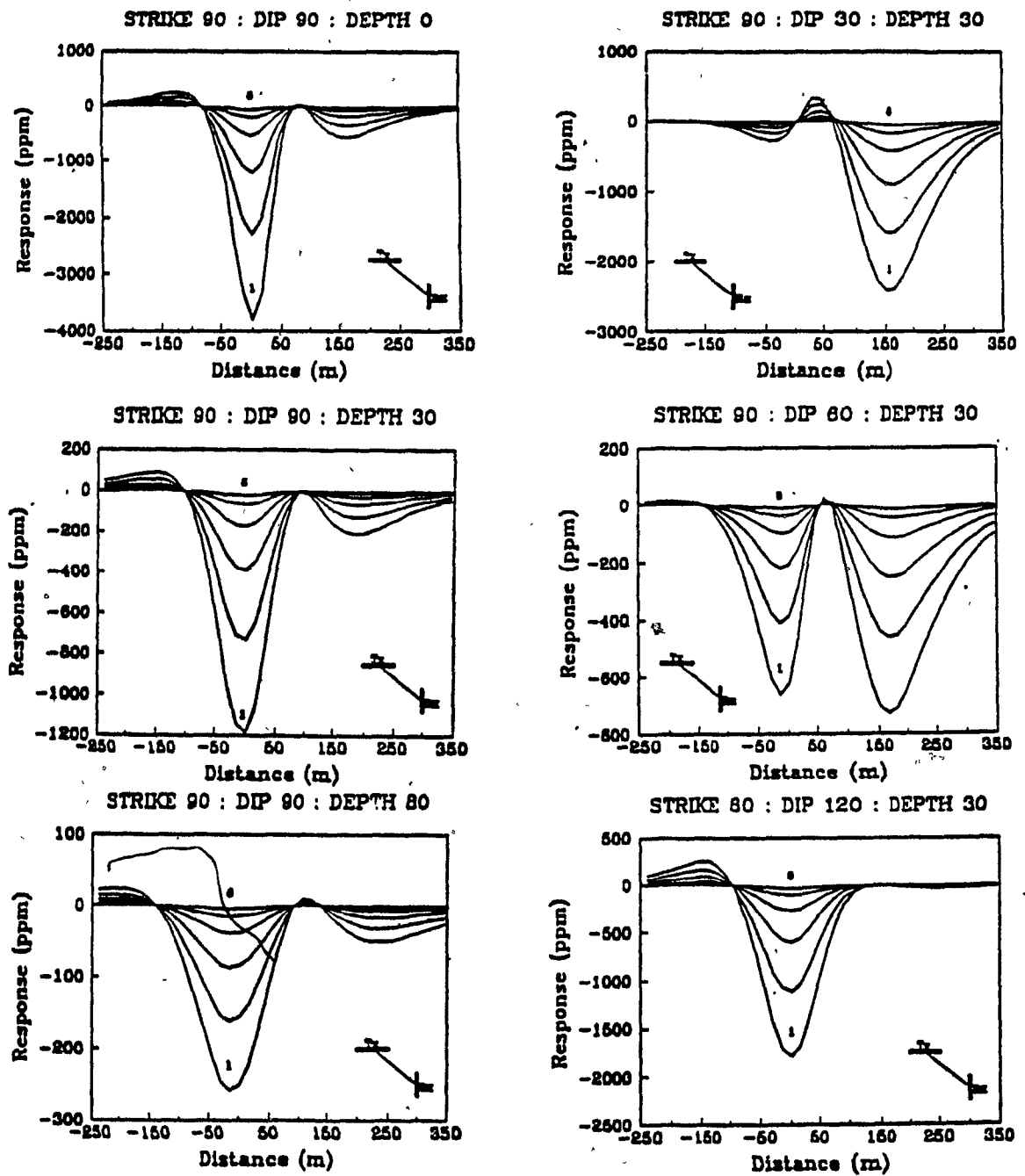
Figure 4.1 Noise free synthetic profiles calculated for plates
of various dips, depths and conductances (after Ferneyhough;
1985).

error of the starting model is 335ppm and is down to 0.3ppm
after 4 iterations, resulting in an almost perfect fit. The
evolution of the RMS error is listed in Table 4.3. For that
case the convergence of the inversion is fast and the results
are listed in Table 4.4.

The same profile, filtered to simulate real system
integrators, was inverted and the results are also listed in
Table 4.4. The model was fully recovered and the filtering
process has no negative effects on the results. This
demonstrates that in this case, a noise free actual profile
can be interpreted without any problem if the filter is taken
into account in the inversion algorithm. Of particular
interest is the fact that the exact location of the conductor
is easily found. This is often a problem when actual data are
interpreted with nomograms, and of consequence when the target
is likely to be drilled.

The correlation matrix indicates that most parameters are
uncorrelated (see Table 4.5), except the conductance and the
depth. This is a result that could be expected since these
parameters are linked together in the Palacky nomogram (see
Figure 3.1). These parameters can be "de-correlated" if the
partial derivative matrix is weighted by the reciprocal of the
amplitudes of the responses. This has the effect of giving an
equal influence (weight) to each data point, thus reducing the
influence of the peak of the anomaly.

Table 4.3 Reduction of the RMS error with the number of iteration.

Iteration number	RMS error (ppm)
0	335.3
1	74.1
2	25.5
3	3.8
4	0.3

Table 4.4 Results of the inversion of a noise free synthetic profile in the presence (filtered) and absence of system integrators.

Parameter		Starting model	Inversion unfiltered model	Inversion filtered	True model
Cond.(S)		10	5.0	5.0	5.0
Depth (m)		125	149.7	149.7	150.0
Dip		75	89.9	90.0	90.0
Ch zero	1	100	0.1	-0.7	0.0
(ppm)	2	70	0.0	-0.8	0.0
	3	30	0.0	-0.5	0.0
	4	10	0.0	-0.2	0.0
	5	3	0.0	0.1	0.0
	6	0	0.0	0.1	0.0
Reference (m)		65	48.5	48.4	48.75
RMS error		--	0.3	0.7	---

Table 4.5 Correlation matrix from the inversion of a noise free synthetic profile.

Cond.	Depth	Dip	E.M. zero levels						Ref.
			Ch.1	Ch.2	Ch.3	Ch.4	Ch.5	Ch.6	
1.00	0.86	-0.12	0.06	-0.39	-0.45	-0.31	-0.15	-0.05	-0.15
	1.00	0.31	0.35	-0.19	-0.32	-0.25	-0.12	-0.04	-0.27
		1.00	0.37	0.22	0.12	0.06	0.02	0.01	-0.19
			1.00	0.16	0.05	0.01	0.00	0.00	-0.21
				1.00	0.21	0.14	0.06	0.02	-0.04
					1.00	0.15	0.07	0.02	0.02
						1.00	0.05	0.02	0.03
							1.00	0.01	0.02
								1.00	0.01
									1.00

By this scheme, the correlation between the conductance and the depth is reduced from 0.86 to 0.44: unfortunately the location of the plate and most of the zero levels are now correlated as shown in Table 4.6. This type of weighting increases the influence of the flanks of the anomaly and is particularly sensitive to small values, close to zero. This problem could be overcome by adding a constant to each channel; these constants would then be included in the zero levels of each channel and should be subtracted from the inversion results to get the actual zero levels.

Plots of the singular values associated with the previous problems are shown in Figure 4.2. The most obvious characteristic is the presence of a step made of six almost equal singular values associated with the zero levels of the INPUT system. This indicates that the zero levels equally influence the inversion. The last four singular values are significantly reduced if the amplitude weighting strategy is used, resulting in a higher condition number. Thus one should be very careful when using that type of weighting.

The parameter singular vectors are plotted in Figure 4.3. Each one is a combination of the model parameters and their influence on the calculated response is proportional to the magnitude of the singular value associated with each one of them. However, in the inversion, parameter corrections are very sensitive to very small singular values. Therefore parameter singular vectors associated with small singular

Table 4.6 Correlation matrix from the inversion of a noise free synthetic profile when the data are weighted by their amplitude.

Cond.	Depth	Dip	Ch.1	Ch.2	Ch.3	Ch.4	Ch.5	Ch.6	Ref.
1.00	0.44	0.01	-0.02	-0.06	-0.08	0.02	-0.01	-0.04	0.02
	1.00	-0.26	-0.18	-0.50	0.03	0.16	0.02	-0.02	-0.09
		1.00	0.35	0.41	0.26	0.09	0.07	0.07	0.27
			1.00	0.48	0.35	0.25	0.18	0.17	-0.27
				1.00	0.61	0.45	0.36	0.33	-0.64
					1.00	0.50	0.34	0.29	-0.62
						1.00	0.29	0.25	-0.58
							1.00	0.17	-0.40
								1.00	-0.35
									1.00

E.M. zero levels: Ch.1–Ch.6

Figure 4.2 Singular value spectra from the inversion of synthetic anomalies with different weightings.
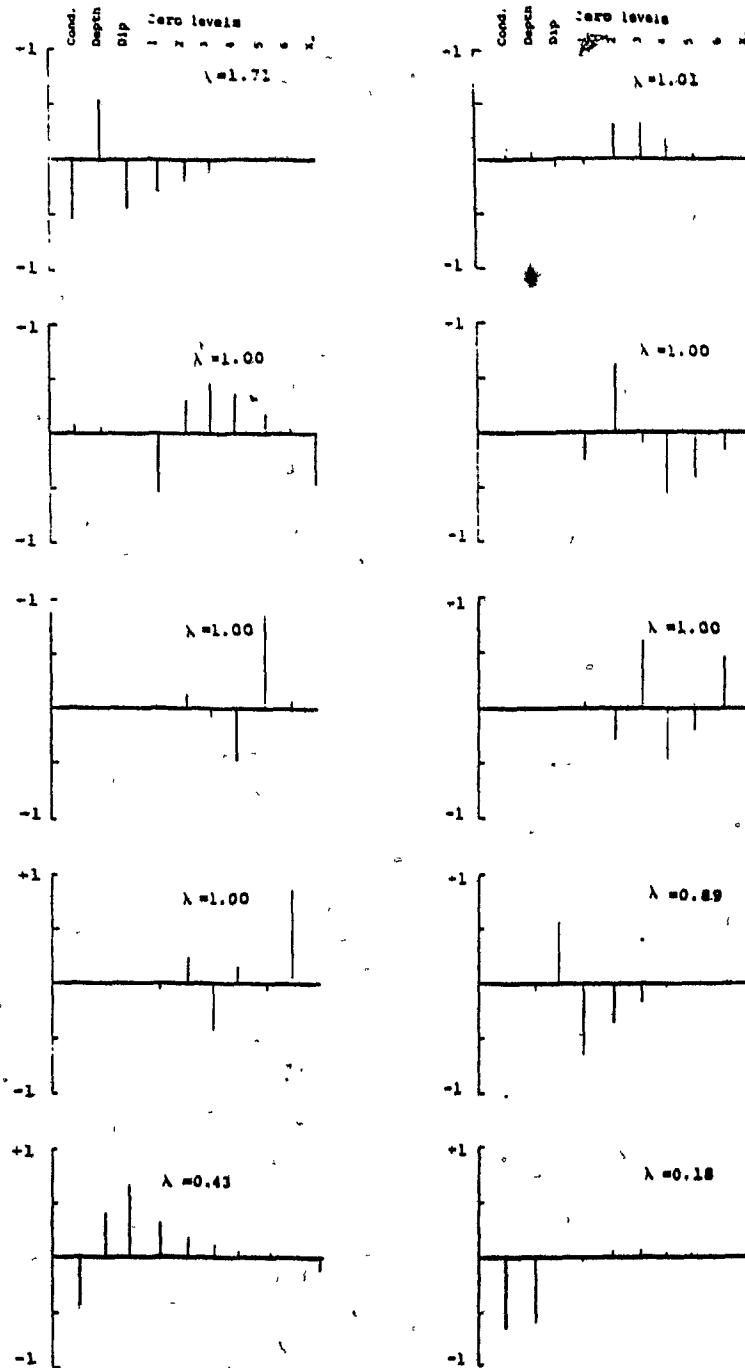
Figure 4.3 Singular values and parameter singular vectors from the inversion of a noise free synthetic anomaly. System integrators were simulated.

values that have little influence on the calculated response but greatly influence parameter corrections during the inversion. These parameter combinations correspond to highly correlated parameters.

The first parameter singular vector is mostly influenced by the conductance, the depth and the dip. The second one has a very strong component corresponding to the location of the plate. The third has components mostly associated with the zero levels of the first and third channel and the location of the plate. The next four singular parameters and values are associated with the zero levels, while the eight and ninth are also influenced by the dip. The strongest components of the last singular vector, associated with the smallest singular value, correspond to the conductance and the depth. Such parameter groupings cannot be found by inspecting the correlation matrix, one has to look at the singular vectors to gain a better insight into the problem of the grouping of the parameters.

Inversion tests were also performed for other dips and conductances. They converge to the correct results in most cases including the filtered profiles. The 60° dip case is highly typical of the INPUT system since the profile is characterised by two peaks; the second one being right over the conductor if the profile is unfiltered (no system integrators). For a dip of more than 135°, however there is only one peak and the inversion does not always easily

converge when the profile is filtered to simulate the actual field situation. If the starting model is the same as the one used for the unfiltered case the inversion sometimes stops in a local minimum. The global minimum is reached only if the starting model is relatively close to the theoretical one. In the case of a "close" initial model with an RMS error of 202ppm, the error is down to 4 ppm after only three iterations. The inversion results from each iteration are given in Tables 4.7 and 4.8 for both cases: when system integrators are simulated and when they are not.

Another filtered synthetic profile was calculated from the same model geometry, the only difference being that the conductance was fixed at 20S. The inversion converged to a RMS error of 4.7ppm in four iterations from an initial RMS error of 535.5ppm. The results are listed in Table 4.9.

4.1.2 Influence of the Strike Angle and the Strike Length.

Some parameters such as the length of the plate and the angle between the plate and the profile were not included in the inversion for practical considerations. They would neces-sitate the joint inversion of three or four profiles and the cost could then be prohibitive. In most cases the strike length of the plate is easily deduced from the anomaly map and it is unlikely that one could err by more than 200 m.The

Table 4.7 Inversion of a noise free synthetic profile. System integrators were not simulated.

Iter.	Cond. (S)	Depth (m)	Dip (deg.)	E.M. zero levels (ppm)						Ref. (m)	Error (ppm)
0	10	125	90	20	10	10	10	3	0	62	193
1	3	137	117	183	101	43	15	9	7	59	191
2	5	161	139	22	7	6	6	4	1	40	55
3	5	150	136	-4	-2	0	0	0	0	46	5
Model	5	150	135	0	0	0	0	0	0	46.5	

Table 4.8 Inversion of a noise free synthetic profile. System integrators were simulated.

Iter.	Cond. (S)	Depth (m)	Dip (deg.)	E.M. zero levels (ppm)						Ref. (m)	Error (ppm)
0	7	125	120	0	0	0	0	0	0	62	202
1	5	140	127	20	7	1	1	2	2	53	23
2	5	149	134	9	4	2	1	0	0	47	4
3	5	150	135	3	2	1	0	0	0	47	2
4	5	150	135	3	1	1	0	0	0	47	2
Model	5	150	135	0	0	0	0	0	0	46.5	

Table 4.9 Inversion of a noise free synthetic profile. System integrators were simulated.

Iter.	Cond. (S)	Depth (m)	Dip (deg.)	E.M. zero levels (ppm)						Ref. (m)	Error (ppm)
0	10	125	45	100	70	30	10	3	0	62	535
1	11	108	81	3	67	77	64	46	31	42	254
2	18	127	101	102	47	25	13	8	6	40	96
3	20	143	129	89	66	47	31	20	12	44	60
4	20	150	134	10	8	6	4	3	2	46	5
Model	20	150	135	0	0	0	0	0	0	46.5	

strike angle is also easily read from the same map and should be accurate to +/- 10°.

A synthetic profile due to a conducting vertical plate of 900 m strike length with a 90° strike angle was inverted assuming erroneous strike lengths and strike angles. The results are shown in Tables 4.10 and 4.11.

It should be noted that for the case where the strike angle is 130°, the solution diverges after the first iteration. One could interpret these results as the inversion of profiles contaminated by a biased source of noise although it is then difficult to interpret the error of fit as due to errors in a strike length or strike angle merely from the inversion results. However on the positive side, it is very unlikely that these variables could be misjudged by an experienced interpreter.

The singular value spectra associated with these different cases are shown in Figure 4.4. It can be seen that the general shape of the singular value spectrum is not affected by erroneous strike angles and lengths. They are similar to the spectrum of profiles contaminated by noise as shown in Figure 4.2.

Table 4.10. Results of the inversion of a 900m plate when various strike lengths are used.

Parameter	Inversion results		
	S=600m	S=900m	S=1200m
Conductance (S)	8.8	5.0	17.2
Depth (m)	163.1	149.5	170.4
Dip (degree)	94.4	90.3	96.3
Zero levels			
Ch. 1 (ppm)	29.1	0.8	41.7
2	16.4	0.2	27.6
3	5.7	0.1	9.8
4	2.7	0.0	-0.2
5	1.5	0.0	-0.8
6	0.6	0.0	-0.9
Reference (m)	64.9	48.8	48.4
RMS error (ppm)	45.5	2.9	63.1

Table 4.11 Results of the inversion of a plate when erroneous strike angles are used. The true strike is 90°.

Parameter	Inversion results		
Strike angle	110°	120°	130°
Conductance (S)	4.8	4.6	4.2
Depth (m)	141.4	131.2	113.3
Dip (degree)	89.9	89.4	80.8
Zero levels			
Ch. 1 (ppm)	-4.8	-14.1	-197.4
2	-3.3	-8.4	-74.9
3	-0.7	-1.7	-51.9
4	-0.1	-0.3	-8.4
5	0.0	0.0	-0.4
6	0.0	0.0	1.1
Reference (m)	48.1	47.2	68.7
Error(ppm)	23.2	52.4	106.1
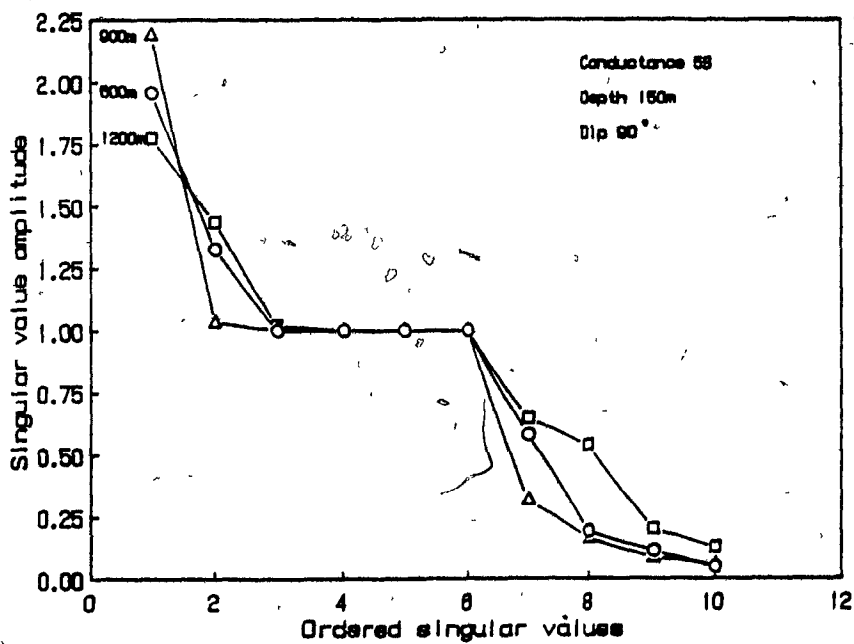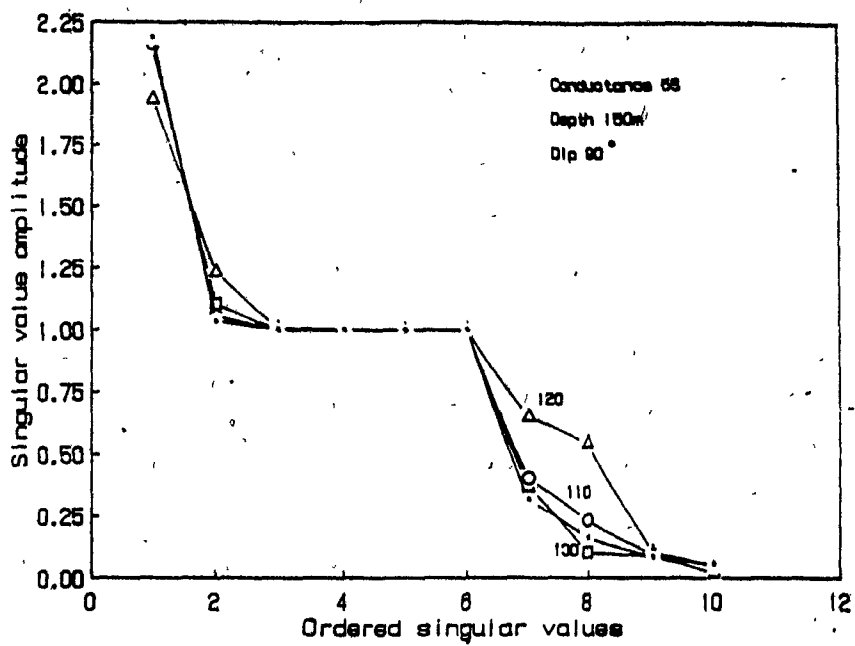
Figure 4.4 Effect of erronous strike angles and strike lengths on the singular value spectra.

4.2 Inversion of Synthetic Profiles With Noise.

4.2.1 Noise Characteristics.

Noise free actual data does not of course exist, and this is why any inversion algorithm has to be tested with different noise levels to estimate its reliability. The current practice is to add white Gaussian noise of various levels to the syntetic profiles before their inversion. A time domain E.M. system is subjected to different sources of noise. Annan (1983) studied the problem of bird motion. The bird containing the receiver has a natural period in the 1 to 20sec range depending on its construction. The exact location of the bird is a function of the airspeed of the airplane, and tables of its location vs airspeed are available from the contractors using these systems.

Another source of noise is E.M. noise. Sferics are caused by lightning discharges and show up as impulses, in the northern hemisphere they are mostly active in summer time. They are easily detected because of their impulsive character. Electronic noise is reduced to a minimum in modern receivers and can be minimised by applying standard filtering techniques to the digital data recorded in flight.

A third source is "geologic" noise, usually defined by the geophysicist as everything a geologist would recognise but which cannot be modelled geophysically. It is generally the response of conductive overburden (if any); graphitic bands,

faults or shear zones carrying groundwater will also conceal the target response. The final response will then be the result of a convolution involving all these variables. This convolutional noise cannot be removed by standard filtering techniques. The ideal solution would be to include these new parameters in a global inversion scheme.

Aliasing or insufficient data sampling is potentially a source of noise, but an anti-aliasing filter is included in the receiver instrumentation. Depending on the type of analog to digital converter used, it is possible that the quantization error has some effect on the noise level. It is important to be aware of these sources of noise when inverting actual data; some can be minimised by careful preprocessing of the data. Finally let's recall that noise is additive, it does not cancel.

An actual survey line was used to study the noise character of such a type of system. Part of line 470 (about 8km) of the Waconichi area airborne INPUT survey published by Le Ministère de l'Énergie et des Ressources (1979) is flown over non conductive granitic rocks. The E.M. channels do not show any correlation with the topography indicating that they are diagnostic of the zero levels of the system. Thus it can be assumed that the data recorded on each channel is composed exclusively of noise components.

The current practice is to visually estimate the noise levels from the analog records as the peak to peak amplitude

of the observed signal. A more objective determination is to compute the standard deviation of the signal on each channel. The calculated levels of noise for the six channels are given in Table 4.12. Visually, the noise levels are about twice these figures. The noise amplitude diminishes for the late channels due to their longer time windows and to the fact that late times more or less correspond to low E.M. frequencies which are less likely to be contaminated by noise. Experience shows that many surveys have a more important noise level, a noise level of 50ppm is reasonable while a noise level of 100 ppm is quite possible.

It was therefore decided to test the inversion both at the 50ppm and 100ppm noise level. The synthetic "white noise" generator is allowed to simulate the variation of noise levels with channel number. Channel 1 and 2 have the same noise level, it is then divided by a factor of 2 for channels 3 and 4, and by 3 for the last two channels. The random number generator used by the white noise routine was taken from Forsythe et al. (1977).

It is useful to define the signal to noise ratio S/N as the ratio of the peak anomaly amplitude to the average noise level. This will permit an easy comparison of the effect of noise levels on differents type of anomalies.

Table 4.12 Observed noise levels on a section (8km) of line
470 flown over a highly resistive area for the Waconichi INPUT
survey.

Channel	Noise in ppm	Length of window (μsec)
1	35	164
2	34	164
3	14	328
4	10	328
5	4	492
6	4	492

4.2.2 The Effects of Noise.

A 50ppm white Gaussian noise was added to the models. The initial values were the same as for noise free data inversion tests and it was always possible to recover the theoretical models. The only problematic case was the one of a 135° dipping plate with a conductance of 5S; the starting model had to be closer than for the other cases. This was expected, since the same problem arose for the noise-free synthetic profile when system integrators were simulated. An interesting point is that an unfiltered profile is easier to interpret; the initial model has to be closer to the global minimum for the inversion of a profile filtered with a time constant of 1.1 second that simulates the system integrators. Therefore there is some advantage in the use of a receiver that does a minimum of filtering to the original data. The inversion itself takes care of the noise, since the difference between the actual data and the calculated model is minimised in the least squares sense. The effect of a filter is to destroy the high frequency content of the data and some useful information can then be lost. Even if those conclusions were obtained for a case corresponding to a low signal to noise ratio for the late channels, such cases are very likely to occur in the interpretation of real survey data. For all the tested cases the RMS error of fit is about the same as the noise level after only three or four iterations.

The same inversion tests were performed at the 100ppm noise level. The results are essentially the same and confirm that the inversion is robust and stable. The inversion program includes a statistical analysis of the fit of the observed and calculated data for each channel. The residuals are also listed. They essentially consist of white noise and a typical case is illustrated in Figure 4.5.

When the data are weighted by the reciprocal of their variances the results are the same as without any weighting, this is most likely because the weights differ by only a factor of three between the first and the last channel.

4.2.3 Analysis of the Information Matrix.

A typical INPUT anomaly profile sampled at a 0.5sec. interval has between 60 and 150 readings for the six channels. Thus, the data information matrix is at least 60x60 and typically 100x100. The easiest way to analyze such a matrix is by displaying the information density vectors and the importance of the data as discussed in Section 3.7. The information vectors associated with the last iteration of the inversion of a synthetic profile (Figure 4.6) due to a 20S conducting plate (dip: 135°; depth:150m) and contaminated by a 100ppm white noise are illustrated in Figure 4.7; Figure 4.8 shows the importance of each data point. The information vectors and the data importance are ordered and presented in the same way as
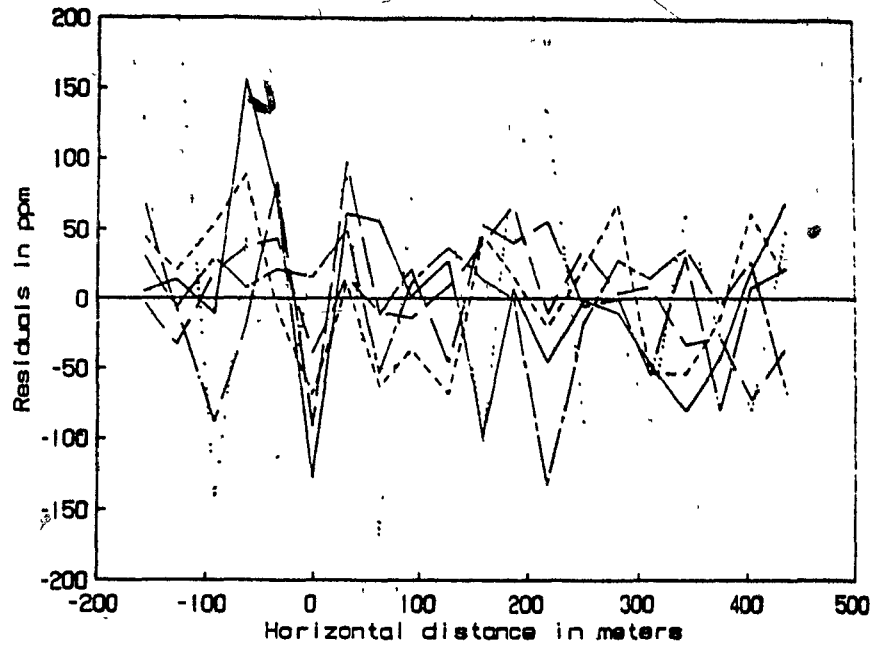
Figure 4.5 Residuals from the inversion of a synthetic profile contaminated by a white noise of 100ppm.
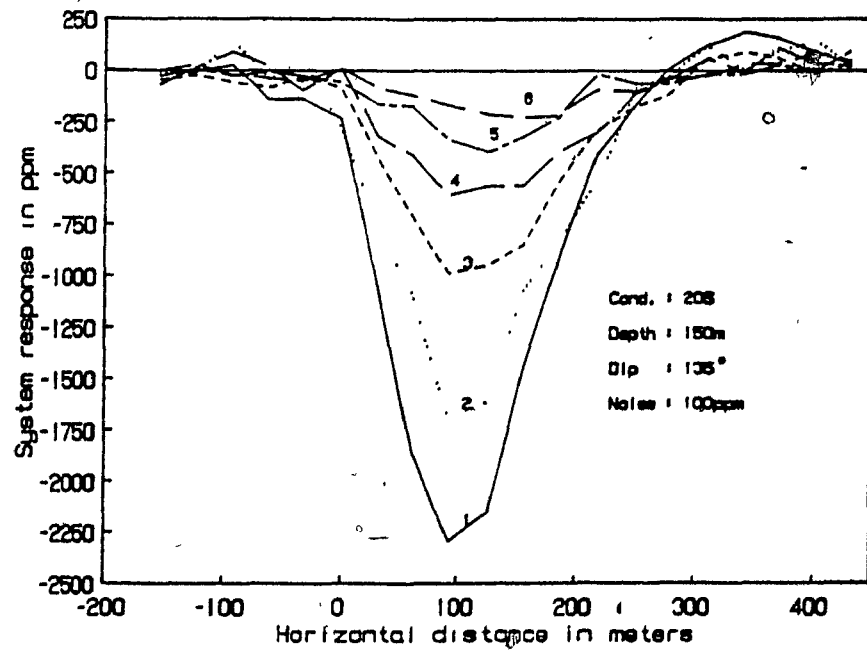
Figure 4.6 INPUT anomaly contaminated by a noise of 100ppm.
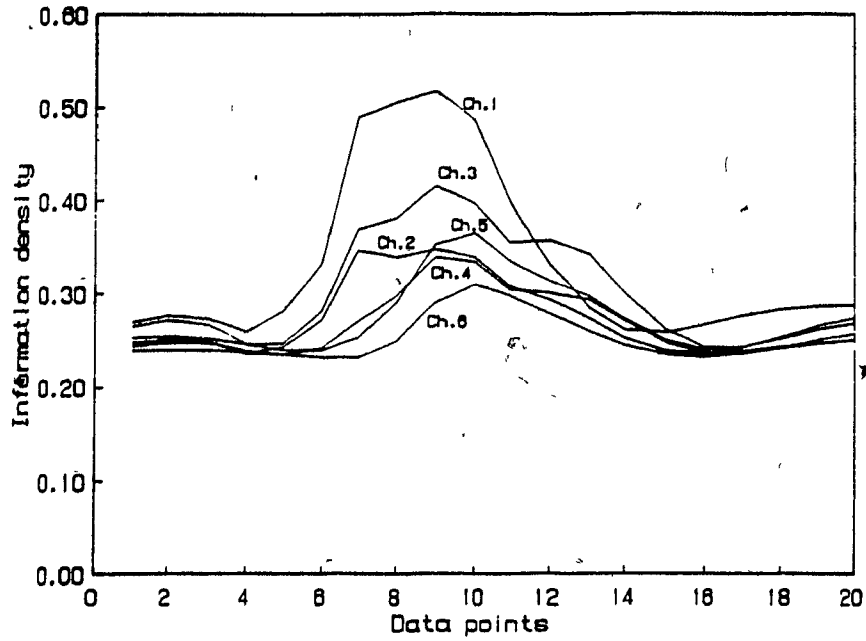
Figure 4.7 Information density profiles resulting from the inversion of the anomaly of Figure 4.6.
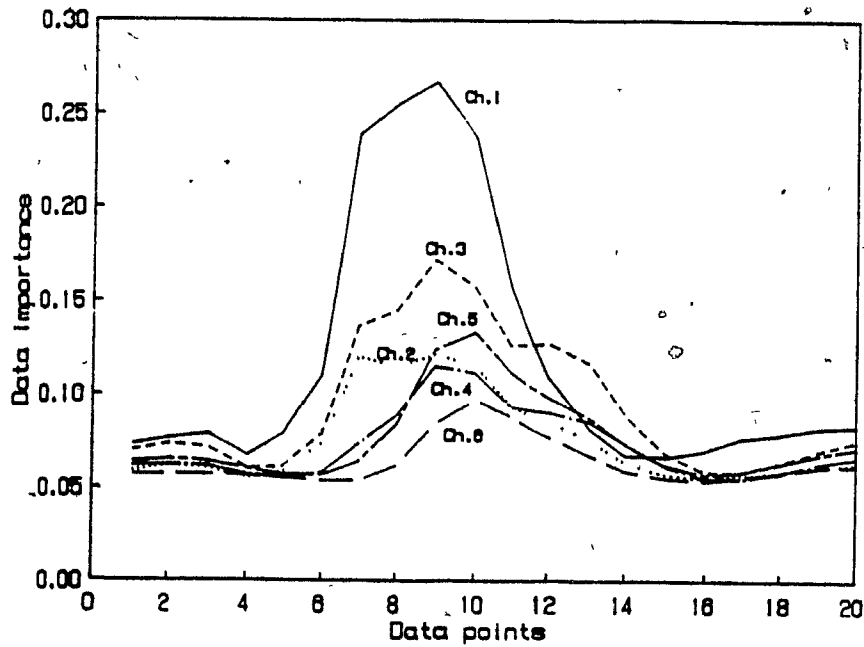
Figure 4.8 Data importance profile resulting from the inversion of the anomaly of Figure 4.6.

an anomaly profile. Each curve in the figure corresponds to one particular channel. It is then evident that both are similar to the data profile. There are nevertheless some subtle differences. The data importance decays faster, relative to the channel number, than the information vector. This is because the information vectors are orthonormalised and give the relative information density. On the other hand, the data importance is simply the diagonal of the information matrix.

We remark that the information profiles are not ordered with increasing channel number as the E.M. channel amplitudes. Channel one has the highest information content and channel six has the lowest. The second highest channel is three, followed by channels five, two and four. The same is observed for the data importance vectors. Information vectors are a measure of how close the information density matrix is to the unit matrix. Low values mean that the value of a data point is predicted by some kind of averaging of neighboring points. A value close to one would mean that a data point almost predicts itself. The preceding results should not be interpreted as a way to rank the importance of the E.M. channels, but rather as an indication of the content of independent information in each data point.

The reordering of the information density profiles is an effect of the weighting of the E.M. channels by their noise channels. Figure 4.9 shows the information density profiles
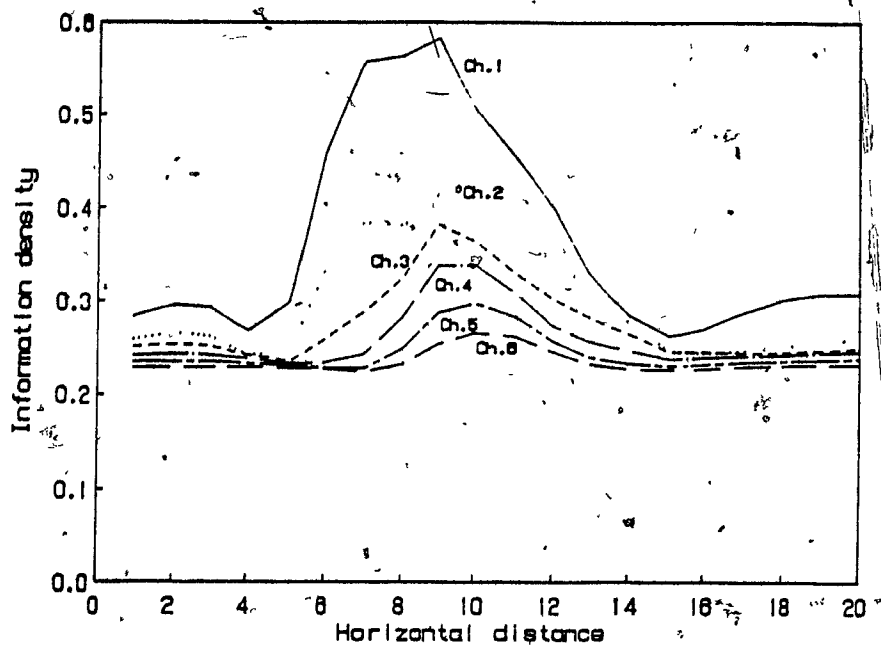
Figure 4.9 Information density profiles from the inversion of the anomaly of Figure 4.6 without weighting.

resulting from the inversion of the same anomaly, but without weighting. The profiles are then ordered with increasing channel number.

The same unfiltered anomaly (no system integrators) was interpreted; the data were weighted by their noise levels. The information and data importance profiles are shown in Figures 4.10 and 4.11. Their amplitude is larger than for the filtered profiles indicating that the system integrators reduce the information content of each data point and that the average value of neighboring data is less important than for an unfiltered profile. Their ordering is the same as when system integrators are simulated.

4.3 Acceleration of the Inversion.

Considering the results of a number of inversions, one realises that the singular values do not change very much from one iteration to the next one. This is usually an indication that the partial derivative matrix of the problem does not vary significantly. The evolution of the singular value spectrum as a function of the number of iterations is illustrated in Figure 4.12 for different inversion cases. For noise free data there is almost no variation of the singular values. This suggest the possibility of not updating this matrix in the iteration process. This has been previously used by Pilkington and Crossley (1986) in a different problem. In many inverse problems it is possible to improve efficiency
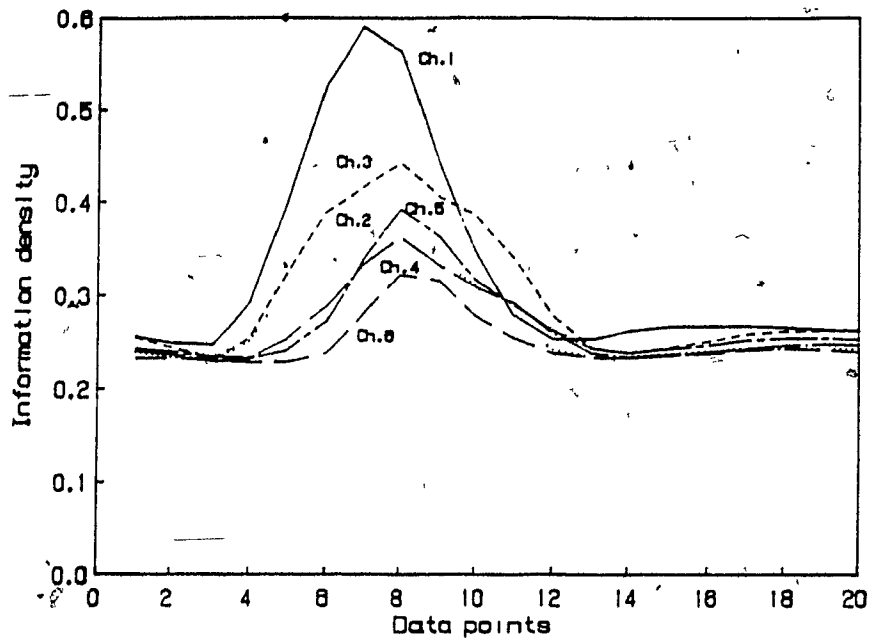
Figure 4.10 Information vectors from the inversion of an anomaly without system integrators.
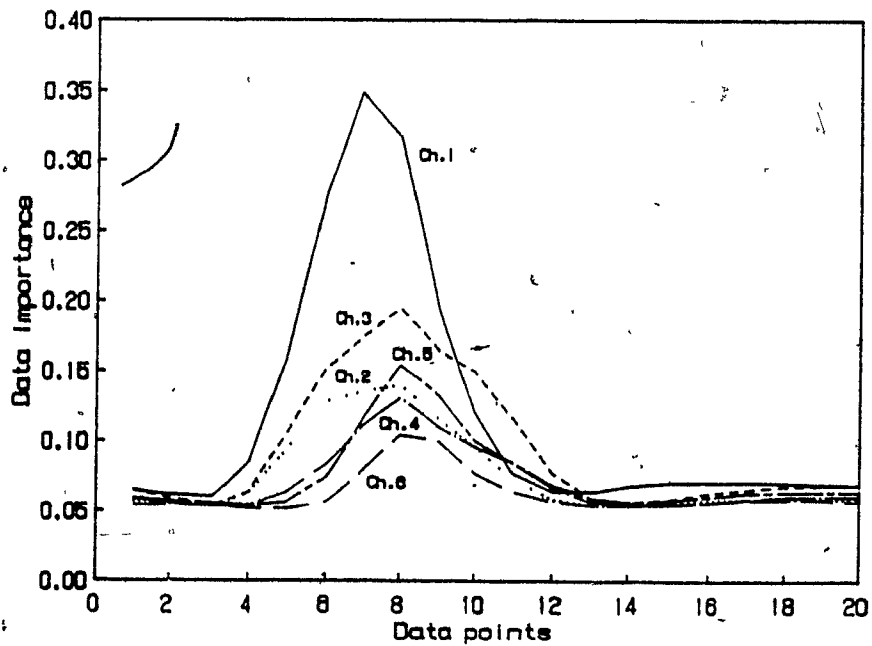
Figure 4.11 Data importance vectors from an anomaly without system integrators.
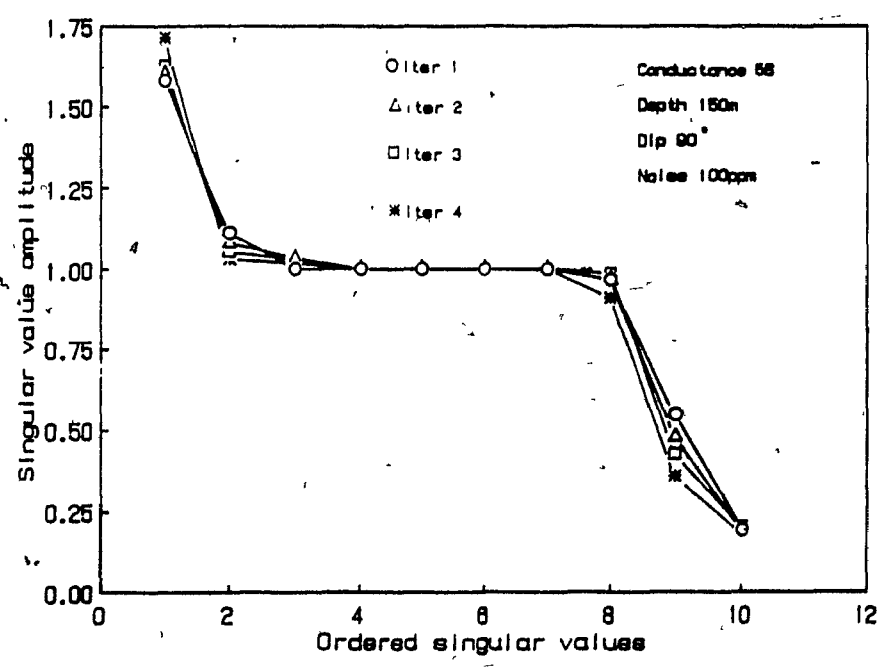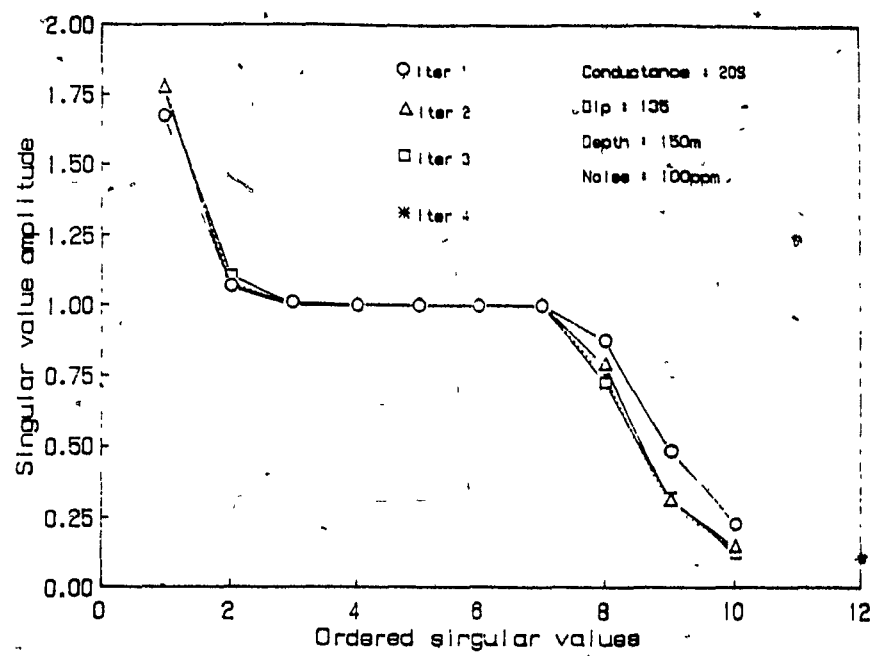
Figure 4.12 Evolution of various singular value spectra for different inversions as a function of the number of iterations.

by updating the partial derivative matrix only every nth iteration. Tests made with noise free data indicate that the same precision can be obtained when the partial derivative matrix is updated every two iterations rather than every one. The inversion is then about twice as fast. Unfortunately the inversion does not converge when a noise level of 50ppm is added to the synthetic profiles. Since higher noise levels are most likely for actual data, this approach is now impractical.

4.4 Inversion of Actual Data.

4.4.1 The Richardson Test Site.

Actual data from an INPUT survey flown in 1977 by Questor Surveys Ltd for the Quebec government (DP-749; 1979) were used to test the inversion program. The selected area is north of lake Waconichi in the Richardson township, 25km north east of Chibougamau (Que.); it has been used as a test site for different geophysical and geochemical methods (Bazinet and Sabourin; 1987) in a study of regional INPUT conductors. This graphitic conductor is at the contact of the Blondeau (felsic tuff) and the Gilman (basalt) formations. It has been drilled at four different locations in 1984 to help interpret the geophysical and geochemical surveys done in the area.

The results of the interpretation of a UTEM and a horizontal loop (Geonics, EM-17) E.M. survey are given by

Bazinet and Sabourin (1987,op. cit.). The survey lines are perpendicular to the conductor axis and their spacing is 125m. The HLEM survey was interpreted for the width, the depth, the dip and the conductance of the conductor. This type of survey is highly sensitive to dip but cannot resolve closely spaced thin conductors. Generally the conductor is dipping south and is subvertical in a few places. Its conductance ranges from 2S to 80S, and its width from 1m to 160m. The interpreted depth is generally indicated as smaller than 7m and is 20m at the most. The smallest depth resolved by this system is 7m.

UTEM (Lamontagne, 1975) is a time domain system using a fixed transmitter consisting of a large current loop, typically 500m x 500m. The receiver measures the vertical magnetic field and is moved along the survey lines outside the transmitter loop. Only the conductance and the depth of the conductor were interpreted. The interpreted depths from this survey are greater than those obtained from the HLEM and INPUT surveys. UTEM is a large geometry system and therefore induces currents deeply into the ground. This results in grater interpreted depth than for the HLEM. Lowering the frequency has the same effect.

Drilling results indicate that the conductor corresponds to a transition zone between the Gilman and the Blondeau Formation. The top of the Gilman includes many veins of pyrrotine and magnetite. Felsic tuffs containing some massive sulfides lenses are found at the base of the Blondeau. Black

graphitic shales are also present. This conducting zone is easily detected by the INPUT and UTEM surveys. The HLEM survey accurately locates the conductor and is diagnostic of its dip and thickness.

The geology and the location of the INPUT anomalies are shown in Figure 4.13. The HLEM interpretation map and the drill hole locations are shown in Figure 4.14.

4.4.2 Line 4615

Anomalies A and B on flight line 4611 are characteristics of a south dipping conductor since the line was flown in the north direction. Anomaly C on line 4615 is located about 50m east of anomaly A and is illustrated in Figure 4.15. The plane was flying south and there is only one peak. The radar altimeter indicates a height of about 118m above ground. A qualitative interpretation of the anomaly map indicates that the conductor is cut by faults, most of them already mapped on the geological compilation map published with the survey results. That section of the conductor dips south and is about 600m long.

The initial model was a 600m vertical plate with a conductance of 10S and 125m below the plane. The system integrators had a time constant of 1.1sec. and the sampling interval was 0.5sec. corresponding to about 30m on the ground. The initial RMS error was 398ppm and the final RMS residual

(V₆ : ANDESITE ; V₇ : BASALTE ; ● : COUSSINEE ; V₉ : TUF ; 3G : GABBRO ; S₁ : CONGLOMERAT ; S₂ : ARKOSE ,
S₄ : ARGILITE ; ◆ : ANOMALIE DE 6 CANAUX ; ◈ : ANOMALIE DE 5 CANAUX ; ◈ : ANOMALIE DE 4 CANAUX ;
◈ : ANOMALIE DE 3 CANAUX).
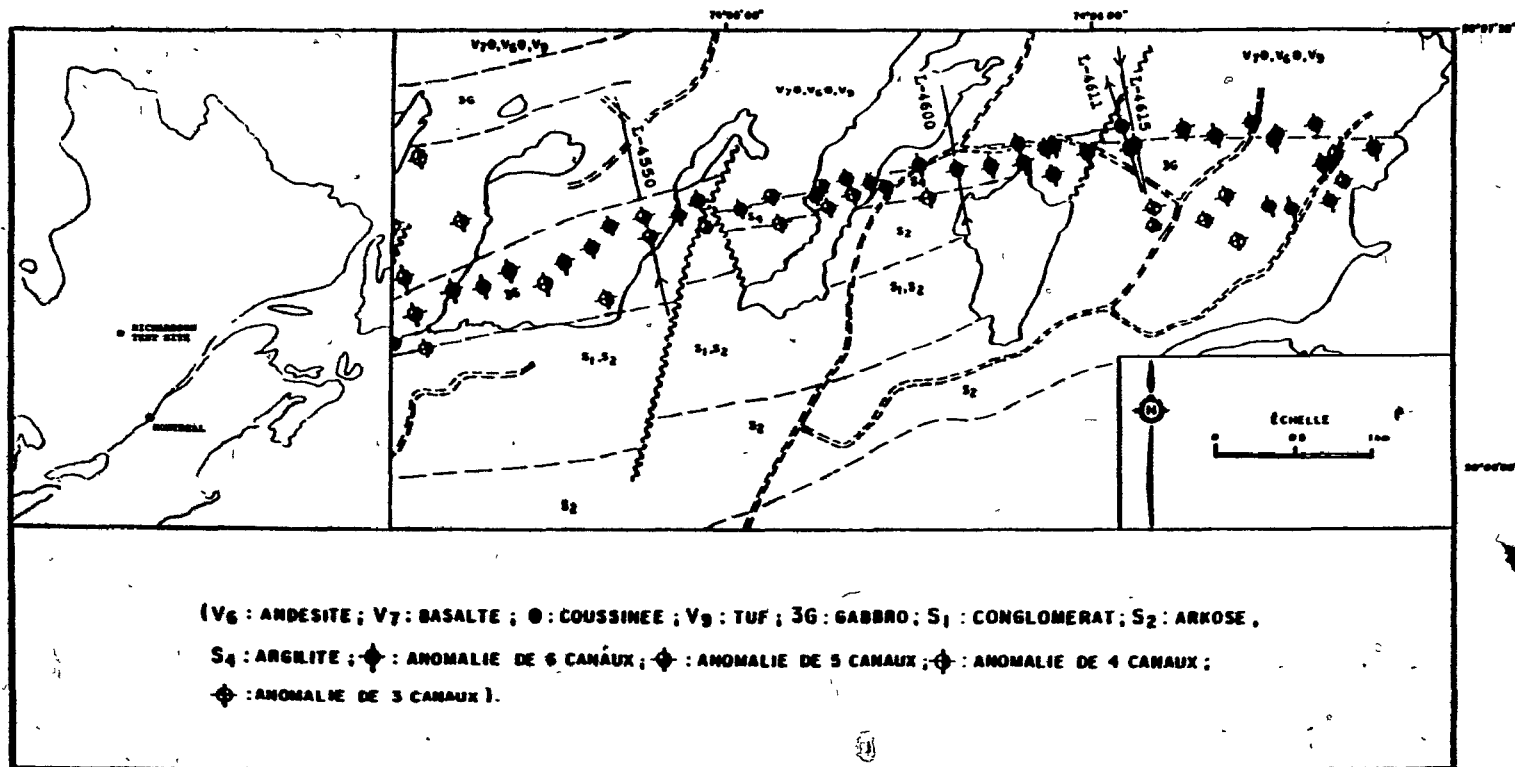
Figure 4.13 Geology and INPUT anomalies of the Richardson test site.

(after Bazinet and Sabourin, 1987)

91
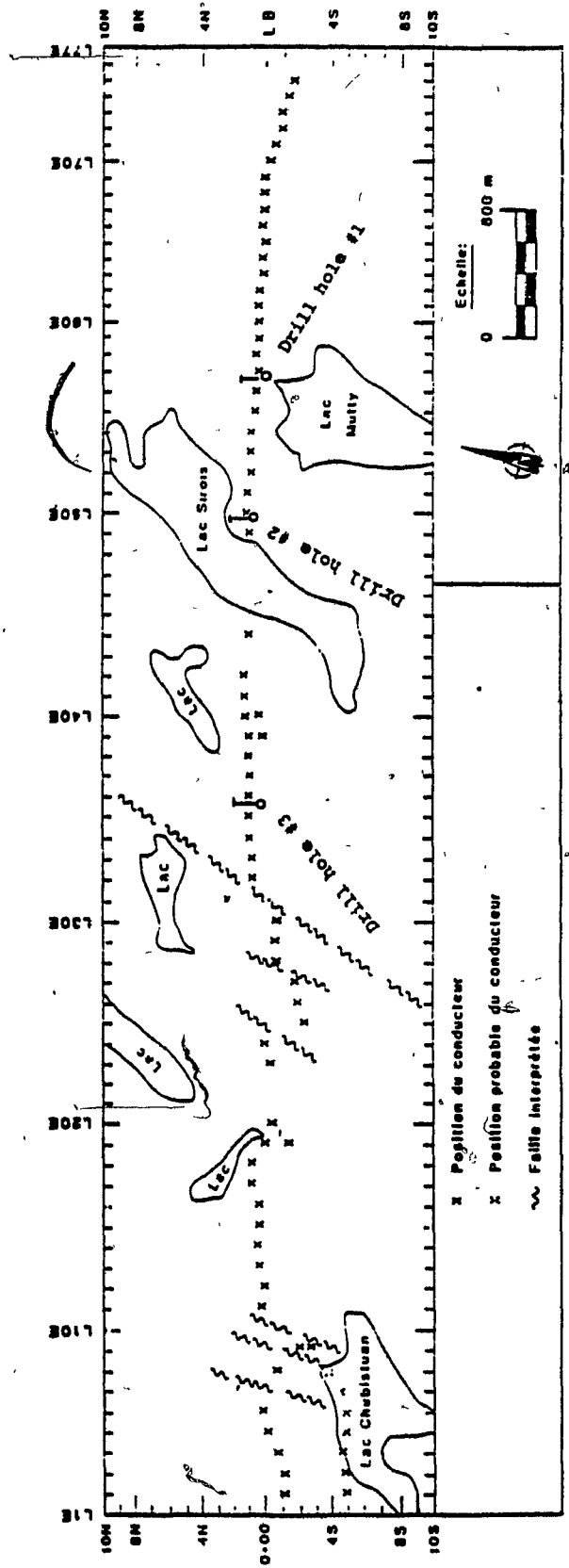
Figure 4.14 HLEM interpretation map (after Bazinet and Sabourin, 1987).
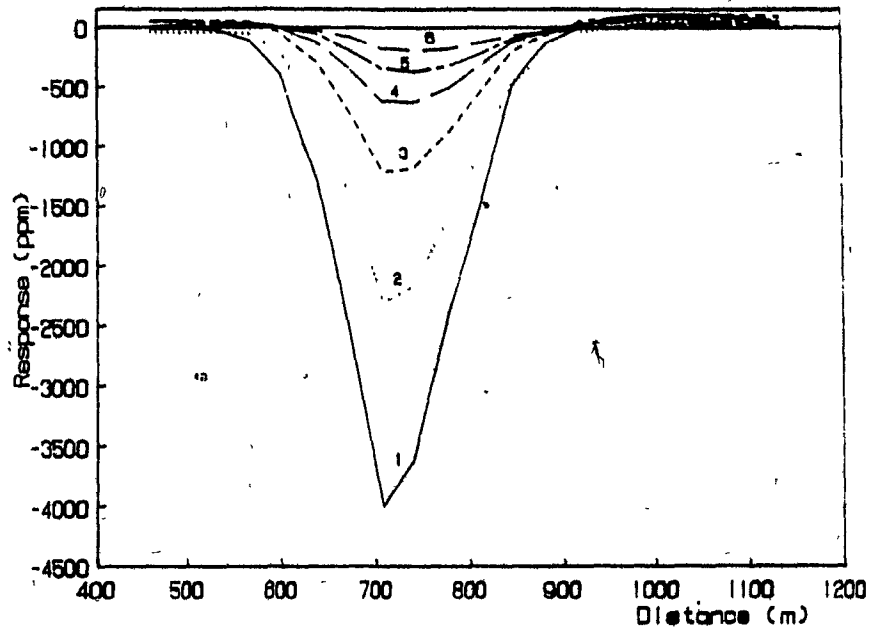
Figure 4.15 INPUT anomaly C from line 4615 of the Waconichi survey.

error was 56ppm after three iterations. The assumed noise levels were 100ppm for channels 1 and 2, 50ppm for channels 3 and 4 and 33ppm for the last two channels. Each channel was weighted by its noise level for the inversion. The results of the inversion of anomaly "C" are listed in Table 4.13. The correlation matrix shows a maximum correlation of 0.97 between the depth and the dip and no other significant correlation is observed.

Inspection of the residuals shown in Figure 4.16 indicates that channel one has the poorest fit. The presence of a slightly conductive overburden sometime explains this but in this area, it mostly consists of sand, gravel and till. The information density profile (Figure 4.17) associated with the first channel has an amplitude that is about twice that of channel two. Both maxima are located at the same position along the profile. The information vectors maxima associated with the late channels are shifted down along the profile indicating that the flanks of the anomaly are more important to the inversion than the peak amplitude. There is also a shift of the maxima of the late channel responses, but less important than for the information profiles. The shift of the response is usually indicative of the dip of the conductor, and is confirmed by the inversion results.

The singular values and the parameter singular vectors are presented in Figure 4.18. The first parameter singular vector has two strong components: the depth and the dip. This

Table 4.13 Results of the inversion of anomaly C from line 4615.

```
        Conductance :   14.4S   +/- 0.5S

        Depth       : 132.4m   +/- 1.9m

        Dip         : 130.7°  i.e. 49.3° South  +/- 1.9°

        Reference   : 657.5m   +/- 1m

        Zero levels

              Ch 1  :   94.7ppm  +/- 23.7ppm

              Ch 2  :   44.8ppm  +/- 22.1ppm

              Ch 3  :  +61.7ppm  +/- 11.3ppm

              Ch 4  : -39.2ppm   +/- 11.2ppm

              Ch 5  :    0.4ppm  +/-  7.6ppm

              Ch 6  : - 8.7ppm   +/-  7.3ppm

        RMS Error

              Ch 1  :   89.8ppm

              Ch 2  :   36.2ppm

              Ch 3  :   25.8ppm

              Ch 4  :   19.6ppm

              Ch 5  :   19.9ppm

              Ch 6  :   16.4ppm

        Average flight altitude: 114m
```

Correlation matrix

Cond.	Depth	Dip	Ch.1	Ch.2	Ch.3	Ch.4	Ch.5	Ch.6	Ref.
1.00	-0.22	-0.27	0.24	0.06	-0.12	-0.22	-0.31	-0.24	0.51
	1.00	0.97	0.05	-0.01	-0.05	-0.02	0.00	0.02	-0.45
		1.00	-0.04	-0.07	-0.11	-0.05	-0.01	0.02	-0.47
			1.00	0.10	0.06	-0.01	-0.04	-0.04	0.01
				1.00	0.07	0.03	0.01	0.00	0.04
					1.00	0.08	0.08	0.05	-0.03
						1.00	0.09	0.06	-0.08
							1.00	0.08	-0.13
								1.00	-0.11
									1.00

E.M. zero levels
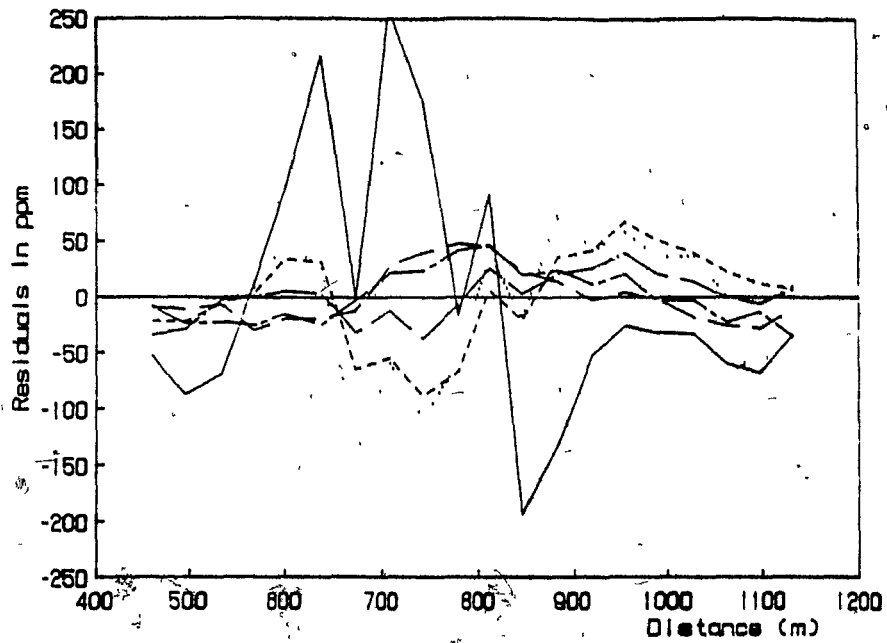
Figure 4.16 Residuals from the inversion of anomaly C from line 4615.
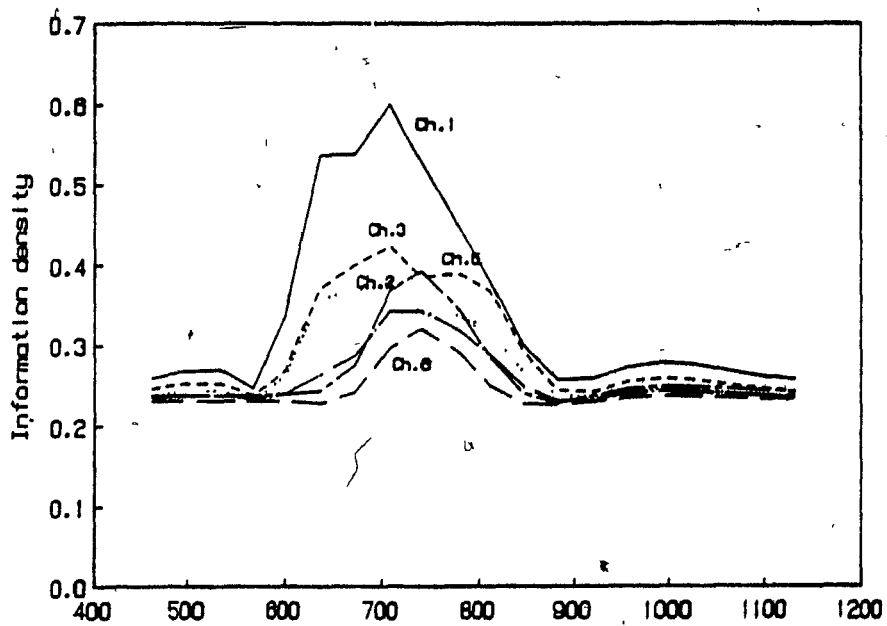
Figure 4.17 Information density profiles from the inversion of anomaly C of line 4615.
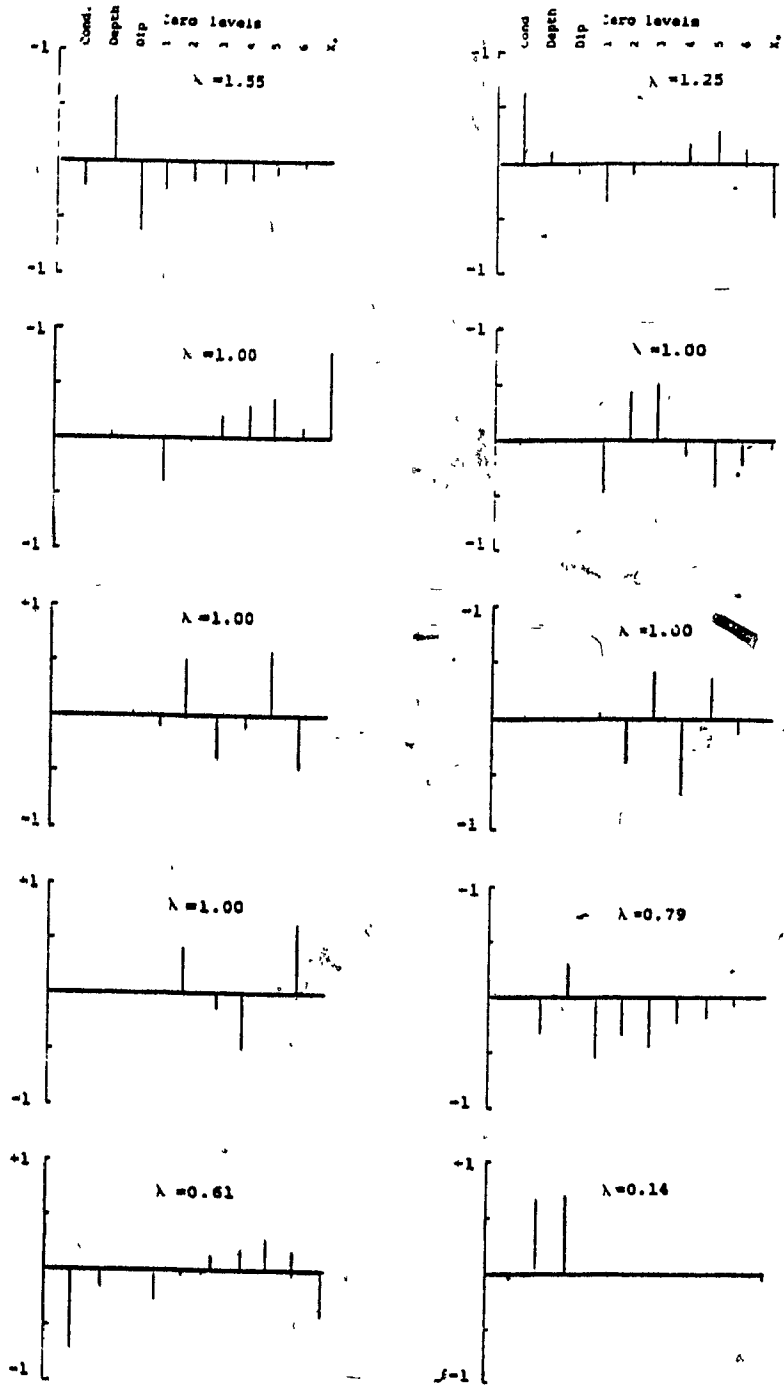
Figure 4.18 Parameter singular vectors for anomaly C line 4615.

indicates that if the depth is increased and the dip decreased, the response will be drastically modified, yielding a poor fit. A decrease in depth and increase in dip would have the same effect. The second singular vector is more complex: four parameters influence the response: the conductance, the plate reference and the zero levels of channel 1 and 5. There are five equal singular values (3, 4, 5, 6, 7) corresponding to parameter combinations that equally influence the inversion. Four of the associated parameter singular vectors have components that correspond to the E.M. zero levels while the third singular vector has its strongest component corresponding to the plate reference. The smallest singular value is significantly smaller than the next to smallest (0.14 vs 0.61). It correspond to a high correlation (0.97) of the depth and the dip. If both parameters are simultaneously increased or decreased, there is little modification of the response.

The UTEM survey indicates that the conductance of the conductor is 17S and its depth 25m. However the HLEM survey gives a depth of less than 7m, a thickness of 15m and a south dip.

A drill hole is located about 250m West of this anomaly and the overburden is 8m thick. The conductor is explained by bands of sulfide rich black graphitic shales of the Blondeau formation. Their thickness is 17m. These observations confirm the inversion results.

4.4.3 Line 4600

Two other anomalies caused by the same conductor were also used to test the inversion. Anomaly E on line 4600 (see Figure 4.19) is about 800m west of anomaly C on line 4615. The initial model was a vertical plate 125m below the transmitter with a conductance of 10S. A 900m strike- length plate was used to simulate a half plane. The initial RMS error was 227ppm, it was down to 55ppm after seven iterations. The final model has a conductance of 7S and a depth of 190m. The detailed results are given in Table 4.14. The calculated dip is 150° and since the line was flown from the south to the north, it indicates that the conductor has a dip of 30° North.

The UTEM survey indicates a depth to the conductor of 35m and a conductance of 15S, while the HLEM survey indicates a depth of less than 7m and a conductance of 55S. The interpreted width of the conductor is 70m and it is subvertical. Clearly, the inversion results do not agree with these interpretations. The depth would be overestimated and the conductance underestimated. The dip calculated from the inversion is 30° North, while all the dips from this area, in the geology map, are about 60° South. If, as indicated by the HLEM survey, the conductor is 70m thick, then it cannot be considered as inductively thin and therefore the thin plate model could be inadequate.
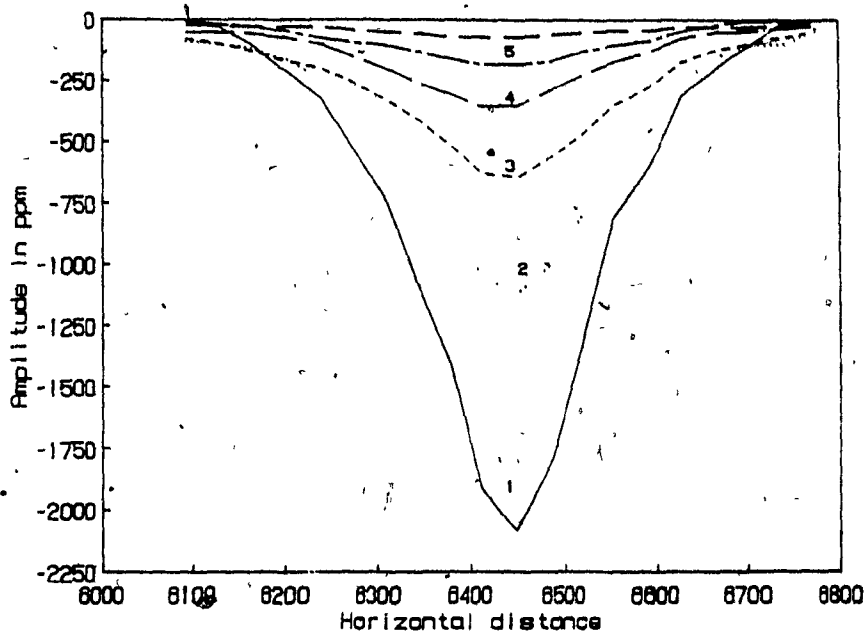
Figure 4.19 INPUT anomaly E on line 4600 of the Waconichi survey.

Table 4.14 Results of the inversion of anomaly E of line 4600.

Conductance :   6.8S   +/- 0.5S

Depth   : 190.4m +/- 5.7m

Dip   : 149.8°   i.e. 30.2° South   +/- 3.4°

Reference   : 6335.4m +/- 3.3m

Zero levels

      Ch 1   : 262.6ppm +/- 25.7ppm

      Ch 2   : 177.2ppm +/- 22.7ppm

      Ch 3   : 149.3ppm +/- 11.9ppm

      Ch 4   : '92.5ppm +/- 11.3ppm

      Ch 5   : 59.5ppm +/- 7.5ppm

      Ch 6   : 101.3ppm +/- 7.2ppm

RMS Error

      Ch 1   : 100.2ppm

      Ch 2   : 40.4ppm

      Ch 3   : 30.1ppm

      Ch 4   : 35.7ppm

      Ch 5   : 20.8ppm

      Ch 6   : 27.4ppm

Average flight altitude: 112m

Correlation matrix

Cond.	Depth	Dip	E.M. zero levels						Ref.
			Ch.1	Ch.2	Ch.3	Ch.4	Ch.5	Ch.6	
1.00	-0.14	-0.31	0.32	0.05	-0.21	-0.29	-0.33	-0.19	0.56
	1.00	0.96	-0.20	-0.19	-0.22	-0.09	-0.04	-0.01	-0.59
		1.00	-0.35	-0.26	-0.24	-0.07	0.00	0.02	-0.66
			1.00	0.19	0.12	0.00	-0.05	-0.04	0.28
				1.00	0.14	0.06	0.03	0.01	0.14
					1.00	0.15	0.12	0.06	0.02
						1.00	0.12	0.07	-0.09
							1.00	0.07	-0.14
								1.00	-0.09
									1.00

The anomaly is 200m east of drill hole #2 where the overburden thickness is 6m. The Blondeau formation containing the conductor is 7m thick. The residuals are illustrated in Figure 4.20. The maximum errors of fit occur on the peak and leading flank of the first channel. The information density profiles are plotted in Figure 4.21.

The singular values and the parameter singular vectors are illustrated in Figure 4.22. The two strong components of the parameter singular vectors associated with the smallest singular values correspond to a high correlation of the depth and the dip of the conductor. The small singular value is an indication that the estimation of these parameter is sensitive to noise and that their standard errors are conservative.

Line 4550

Anomalies M and N on line 4550 (see Figure 4.23) are likely to be caused by the same conductor, the first one being indicative of a dipping conductor. It is about 1.6km west of the previously interpreted anomaly. A dip of 50° was used for the initial model. Conductance was assumed to be 10S and the depth 125m. This initial model has a RMS error of 210ppm. The final model was obtained after four iterations, but for the last two iteration the RMS error changed by only 2ppm while the parameters remained almost fixed. The final model has a conductance of 19.3S, a depth of 134m and a dip of 46°. The
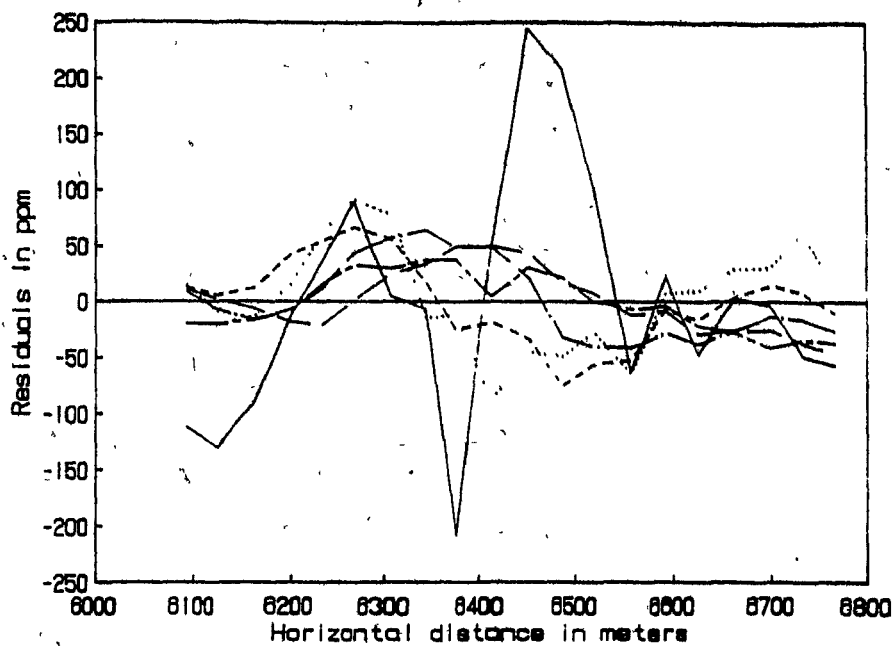
Figure 4.20 Residuals from the inversion of anomaly E, line 4600.
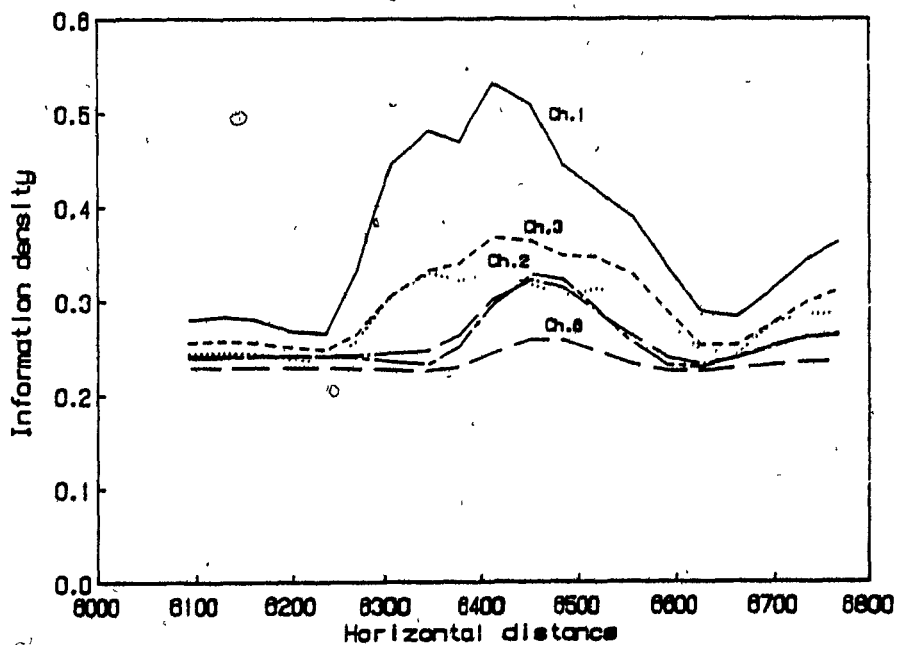
Figure 4.21 Information vectors from anomaly E, line 4600.
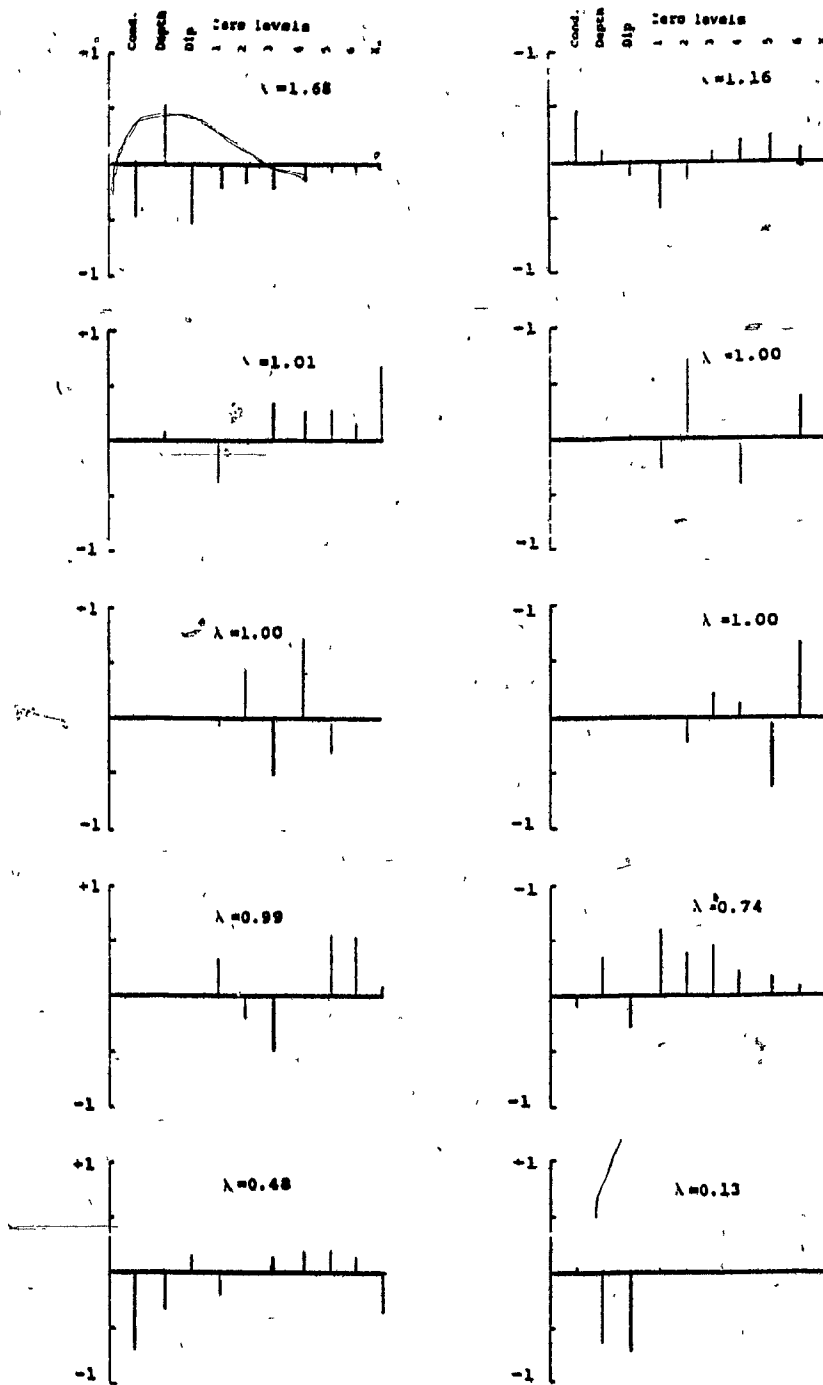
Figure 4.22 Singular values and parameter singular vectors from the inversion of anomaly E on line 4600.
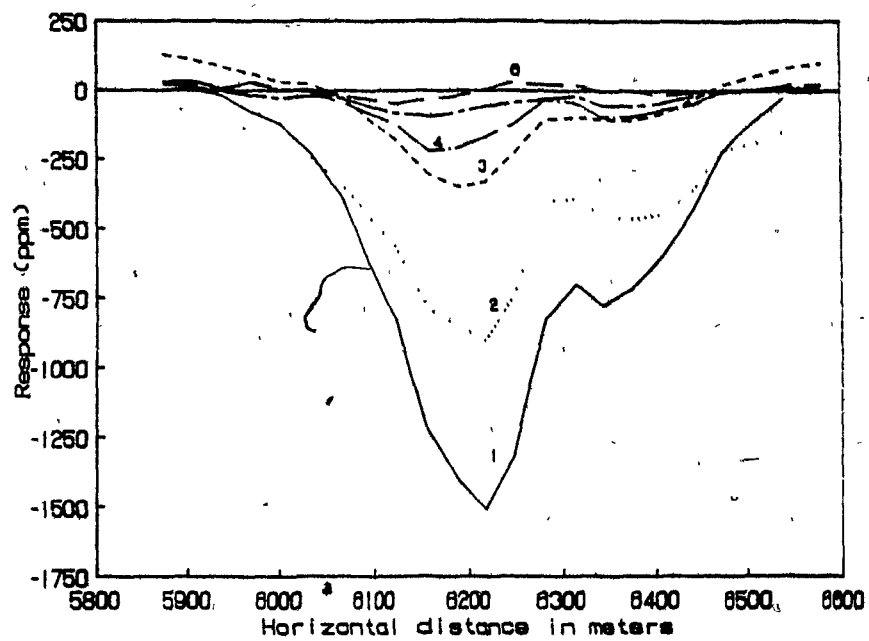
Figure 4.23 Anomalies M and N, line 4550 of the Waconichi INPUT survey.

detailed results are listed in Table 4.15. The residuals from the inversion are illustrated in Figure 4.24 and, as in the previous cases, channel one has the poorest fit. For this channel the error is systematically positive before the second peak and negative after this peak. The trailing flank of the second peak is overestimated by the inversion for the first five E.M. channels.

The parameter singular vectors and the singular values are presented in Figure 4.25. Most parameter singular vectors show complex groupings of their components. The first one shows a combination of the conductance, the depth and the dip offsetting the zero levels of the first five INPUT channels. The second one is mostly influenced by the depth and the plate reference. The third one is dominated by the reference of the plate and the zero levels. The smallest singular value is associated with a parameter singular value that has three almost equal components: the conductance, the depth and the zero level of the first channel. This indicates that an increase or decrease of these three parameters has little influence on the response. Such complex relations cannot be detected from the correlation matrix.

The interpretation of the UTEM survey indicates a conductance of 26S and a depth of 50m. On the other hand, the HLEM survey indicates a conductance of 14S and a depth of 10m. The interpreted dip is south and the conductor thickness is 10m.

Table 4.15 Results of the inversion of anomalies M and N of line 4550.

        Conductance :   19.3S   +/- 1.3S

        Depth   : 133.8m   +/- 1.2m

        Dip   : 46.3°   +/- 0.7°

        Reference   : 6329m   +/- 3m

        Zero levels

                Ch 1   : -76.8ppm   +/- 34.4ppm

                Ch 2   : -54.8ppm   +/- 25.6ppm

                Ch 3   : -227.3ppm   +/- 12.7ppm

                Ch 4   : -112.7ppm   +/- 11.0ppm

                Ch 5   : -64.1ppm   +/-   7.4ppm

                Ch 6   : -53.3ppm   +/-   7.2ppm

        RMS Error

                Ch 1   : 106.2ppm

                Ch 2   : 40.8ppm

                Ch 3   : 40.1ppm

                Ch 4   : 27.8ppm

                Ch 5   : 14.2ppm

                Ch 6   : 11.2ppm

        Average flight altitude: 112m

Correlation matrix

Cond. Depth Dip 'E.M. zero levels   Ref.

			Ch.1	Ch.2	Ch.3	Ch.4	Ch.5	Ch.6	
1.00	0.26	-0.26	0.67	0.43	0.25	-0.04	-0.04	-0.24	-0.67
	1.00	-0.52	0.52	0.43	0.46	0.24	0.14	0.04	0.00
		1.00	-0.14	-0.06	0.04	0.10	0.15	0.12	0.08
			1.00	0.47	0.40	0.12	-0.02	-0.09	-0.39
				1.00	0.33	0.13	0.03	-0.03	-0.24
					1.00	0.18	0.11	0.03	-0.11
						1.00	0.12	0.07	0.06
							1.00	0.10	0.17
								1.00	0.17
									1.00
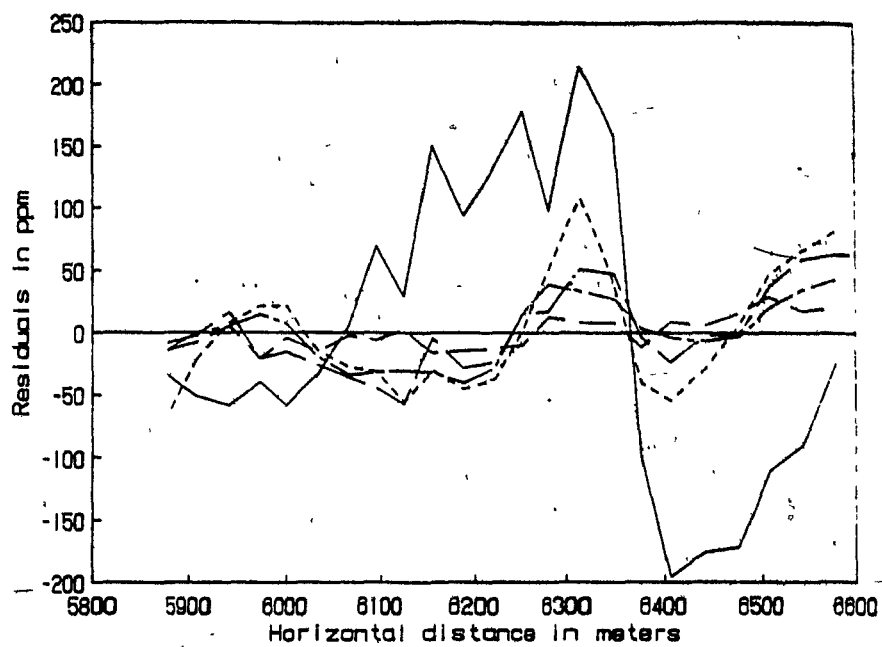
Figure 4.24 Residuals from the inversion of anomalies M and N, line 4550 of the Waconichi INPUT survey.
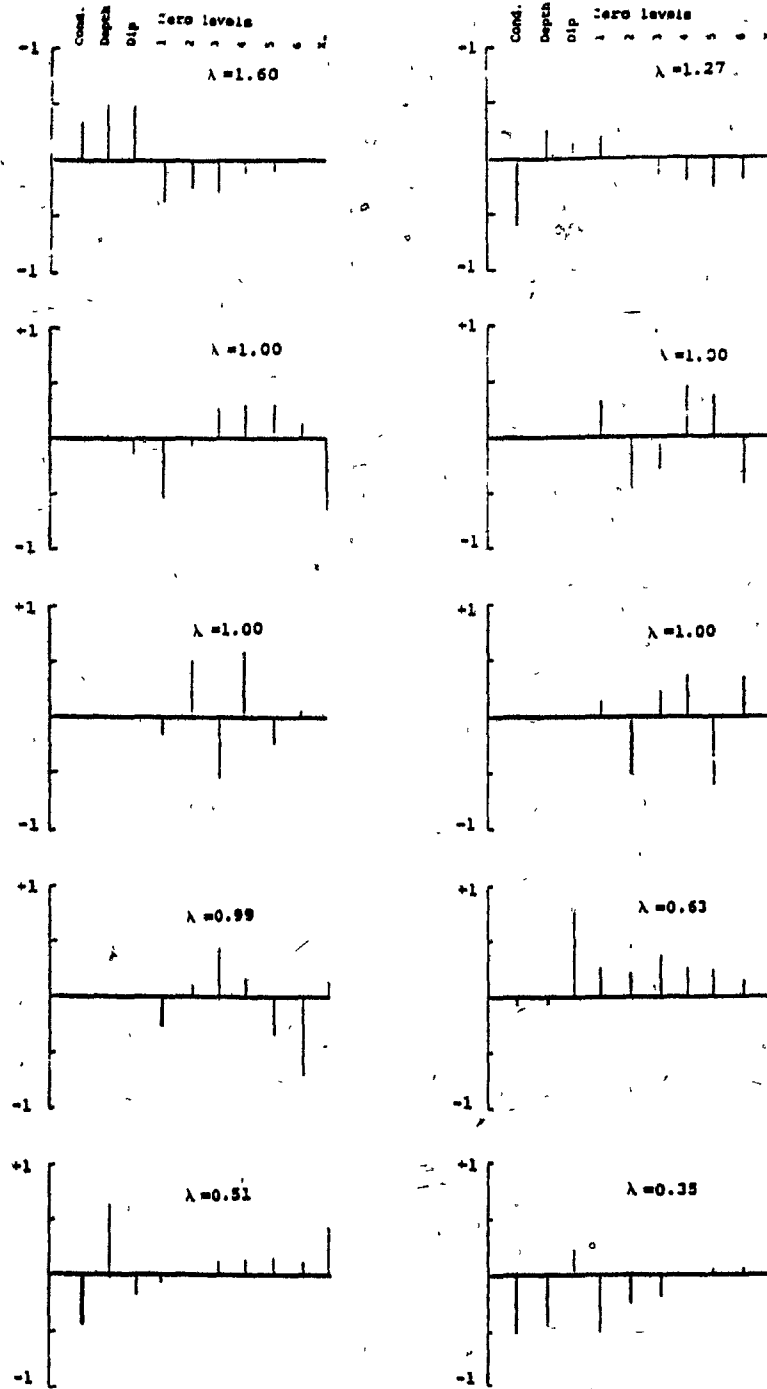
Figure 4.25 Parameter singular vectors from anomaly M and N, line 4550.

Drill hole #3 is coincident with this anomaly. The overburden thickness is 20m and this agrees with the calculated depth of 21m below the surface for the conductor. From the drilling results the thickness of the Blondeau formation is 36m. Bazinet and Sabourin (1987, op. cit.) concluded that the dip of the conductor in locally vertical after comparing the HLEM and the drill hole results. However, the surface geology indicate dips of about 60°in this area. These geological observations confirm our interpretation of the INPUT anomaly. It could be argued that the minor peak observed on the INPUT profile is indicative of a second conductor rather than of a dip effect. This is highly unlikely since no other conductor has been detected by the HLEM or the UTEM surveys.

All three anomalies are caused by the same conductor which is known to be mostly graphitic with some associated sulfides. It also outcrops in a few places. A high conductance and a depth below the transmitter of about 120m should be expected. Obviously anomaly E on line 4600 does not give the expected results, the conductance is too low and the depth too great. The interpretations of the other two anomalies agree with the geology and the interpretation of the ground geophysics.

Chapter 5

JOINT INVERSION OF E.M. AND MAGNETIC DATA

5.1 Introduction.

It is the current practice in mining geophysics to note in the compilation maps the presence and the amplitude of any magnetic anomaly associated with an E.M. anomaly. This is called a magnetic correlation. Inspection of a number of INPUT anomalies that led to the discovery of commercial orebodies shows that many of them are indeed located on the flanks of magnetic anomalies. Figure 5.1 is a taken from Questor's commercial publicity and illustrates this.

Massive sulfide deposits do not have any specific magnetic responses. Some have a direct magnetic association while others have no response at all. Some have flanking magnetic anomalies close to the sulfide body. These anomalies are usually due to the presence of pyrrhotite and magnetite in the volcanic rocks associated with deposits.

It was therefore believed useful to develop an algorithm for the joint inversion of E.M. and magnetic anomalies. A reasonable assumption is that they both have the same dip and the same depth. It can sometimes be assumed that the conductor

South Bay (Selco)

Mattabi (Mattagami/Abitibi)

West Zone (Chibex)

Lyon Lake (Mattagami)

Magusi River (Iso/Copperfields)

Reed Lake (Freeport/Beth Canada)

Lemoine Mines (Patino)

Brouillan Twp. (Selco/Picklands Mather)

Embury Lake (Granges AB)

Dawn Lake (Asamera et al)

Creek (Mattagami)

Boundary (Mattagami)

E.M. CHANNELS

MAGNETOMETER

ALTIMETER

Detour River (Amoco Canada)

Pelican River (Noranda)

Figure 5.1 Various anomalies illustrating the presense of an associated magnetic anomaly.

is located close to the flank of a magnetic thick dike. The model is illustrated in Figure 5.2. This joint inversion problem is different from the one studied by Vozoff and Jupp (1975) although the same theory can be used. They simultaneously interpreted MT and DC resistivity data, then the geometry and the physical parameters are the same for both data sets. In our case only two parameters are common: the dip and the depth.

A thick dike of infinite extension is used to model the magnetic anomaly; other models such as a prism could have been used but the dike is the most commonly used model for this kind of problem. The forward solution is easy to compute and an inversion program is easily written since the parameter derivatives can be computed analytically.

5.2 The Joint Inversion Problem.

Although the inversion algorithm is identical to the one developed previously, the two data sets have to be properly combined and the weighting of their relative influence is then very important. It is natural to use the reciprocal of the noise levels of each data set as weighting factors. In this way the partial derivative matrix is made "scale free". Ideally one should use the standard error of measurement of each data. In practice, the different noise levels can only be estimated from anomaly free profiles.

117

T : Dyke half-width

Z : depth

D : Dyke reference

X_o : Plate reference

Alt.: Flight altitude
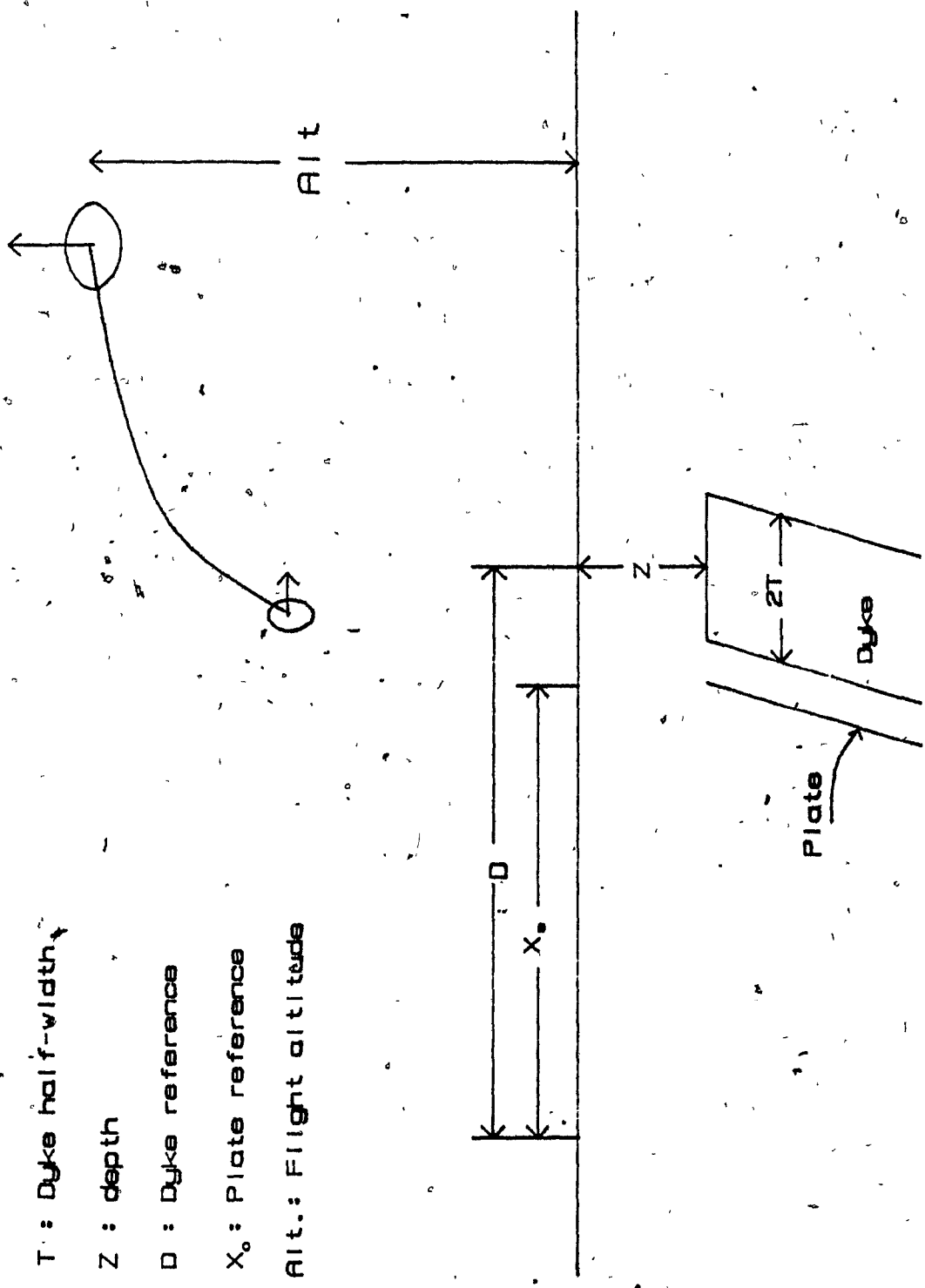
Figure 5.2 Model used for the joint inversion.

Plates of various dips, conductances and depths were used to test the joint inversion. The magnetic dike had a thickness of 100m and the conductor was located on its flank. Noise levels of 50ppm and 100ppm were added to the synthetic E.M. data and 2nT added to the magnetic data.

The first observation is that the initial model has to be closer to the true model than for the case of the E.M. inversion only. The second is that the rate of convergence is slower. This is associated with a much higher condition number, now of the order of 300 while it was about 10 for the E.M. inversion. On the positive side, the parameter variances are reduced for the parameters that are common to both data sets: depth and dip. We also note than the thickness of the dike and its center location are somewhat improved. Some cases will be presented in detail to illustrate this.

5.3   Inversion of Synthetic Data

5.3.1 Inversion of Synthetic Data With Noise.

It was noted in Section 4.3 than a plate with a conductance of 5S and a dip of 135° was a difficult case at the 50 and 100ppm noise level. Therefore, this model was used to test the joint inversion at the 100ppm noise level. A magnetic dike 100m thick with a susceptibility of .01 S.I. was modeled so that the conductor would be on its flank. The model and the E.M. and magnetic anomalies associated with it are illustrated

in Figure 5.3. The initial model and the results from the inversion are listed in Table 5.1. The joint inversion converged to the known solution in three iterations. The RMS residual error for the E.M. data was then 60ppm compared to 207ppm for the initial model. For the magnetic data the respective values are 0.5nT and 65nT.

The condition number (ratio of the largest to the smallest singular value) of the partial derivative matrix is 270. It should be recalled that the SVD is computed after scaling the matrix to reduce its condition number. The inversion of the E.M. anomaly alone results in a condition number of about 10, a much smaller number. The same phenomena has been observed for all the cases used to test the joint inversion. It should also be noted that at least one of the singular values is much smaller than the others. Two spectra are illustrated in Figure 5.4, both are from the last iteration of the inversions of synthetic profiles contaminated by a 100ppm noise; in one case the dip of the plate is 90° and in the other 135°. The conductance is 5S in both cases. The two spectra are remarkably similar and the singular values associated with the zero levels form a characteristic step in the spectra.

The singular values and the parameter singular vectors resulting from the joint inversion of the 135° dipping plate are shown Figure 5.5. The last parameter singular vector has two strong components: the susceptibility and the thickness of

Table 5.1 Joint inversion of 5S plate with a dip of 135°. The noise level is 100ppm for the INPUT data and 1nT for the magnetic data.

Parameter Iter.nb.	0	1	2	3	Std. error	Model
Conductance :	7.0	5.3	5.0	4.9	2.3	5.0
Depth :	125.0	145.6	153.0	149.4	1.0	150.0
Dip :	120.0	132.3	135.3	134.7	0.7	135.0
Ref. (plate) :	62.0	75.2	51.8	44.1	4.3	46.5
Zero levels						
Ch 1 :	0.0	25.6	19.8	4.6	26.8	0.0
Ch 2 :	0.0	18.4	24.0	19.3	24.5	0.0
Ch 3 :	0.0	7.2	15.0	14.3	13.2	0.0
Ch 4 :	0.0	2.1	6.2	6.4	12.3	0.0
Ch 5 :	0.0	0.8	1.1	1.1	7.9	0.0
Ch 6 :	0.0	7.6	6.9	6.9	7.7	0.0
Ref. (dike) :	107.0	97.8	96.3	96.8	0.7	96.5
Half-thickness:	45.0	40.6	46.3	51.9	2.9	50.0
Susceptibility:	.0090	.0096	.0105	.0095	.0005	.01
Base level (mag.):	0.0	-5.7	-3.2	-1.5	2.2	0.0
Base slope (mag.):	0.0	12.7	1.4	1.4	3.1	0.0
RMS Error INPUT :	206.9	158.6	76.1	60.0		
Mag. :	64.6	50.5	13.9	0.3		

Correlation matrix

```
1.00  0.73 -0.37  0.34 -0.17 -0.43 -0.32 -0.23 -0.08 -0.90    0.67  0.33 -0.65 -0.67  0.34  Conductance
      1.00  0.05  0.32 -0.02 -0.23 -0.20 -0.15 -0.05 -0.71    0.94 -0.08 -0.92 -0.46 -0.06  Depth
            1.00 -0.20 -0.03  0.08  0.09  0.07  0.03  0.26    0.09 -0.97 -0.10  0.80 -0.96  Dip
                  1.00  0.10  0.04 -0.01 -0.02 -0.01 -0.15    0.29  0.18 -0.28 -0.32  0.19  1
                        1.00  0.13  0.07  0.05  0.02  0.14   -0.02  0.03  0.02 -0.02  0.03  2
                              1.00  0.15  0.10  0.03  0.38   -0.21 -0.07  0.21  0.18 -0.07  3
                                    1.00  0.08  0.02  0.28   -0.19 -0.08  0.18  0.17 -0.08  4
                                          1.00  0.02  0.20   -0.14 -0.06  0.14  0.14 -0.07  5
                                                1.00  0.07   -0.05 -0.02  0.05  0.05 -0.02  6
                                                      1.00   -0.66 -0.23  0.64  0.57 -0.24  Plate reference
                                                             1.00 -0.11 -1.00 -0.34 -0.11  Susceptibility
                                                                  1.00  0.11 -0.72  0.89  Dyke reference
                                                                        1.00  0.30  0.12  Thickness
                                                                              1.00 -0.82  Base level
                                                                                    1.00  Base slope
```
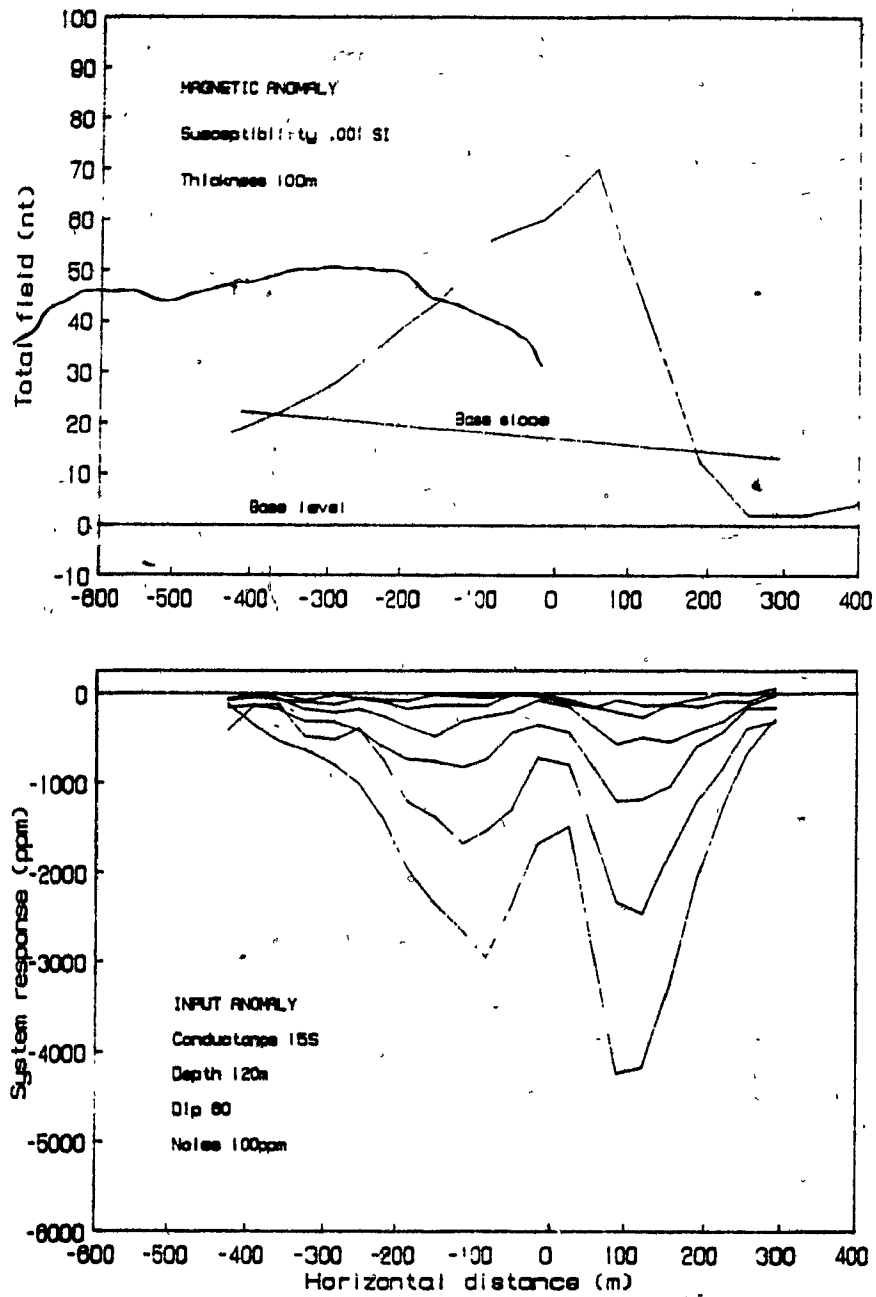
Figure 5.3 Exemple of Input and magnetic anomalies used to test the joint inversion.
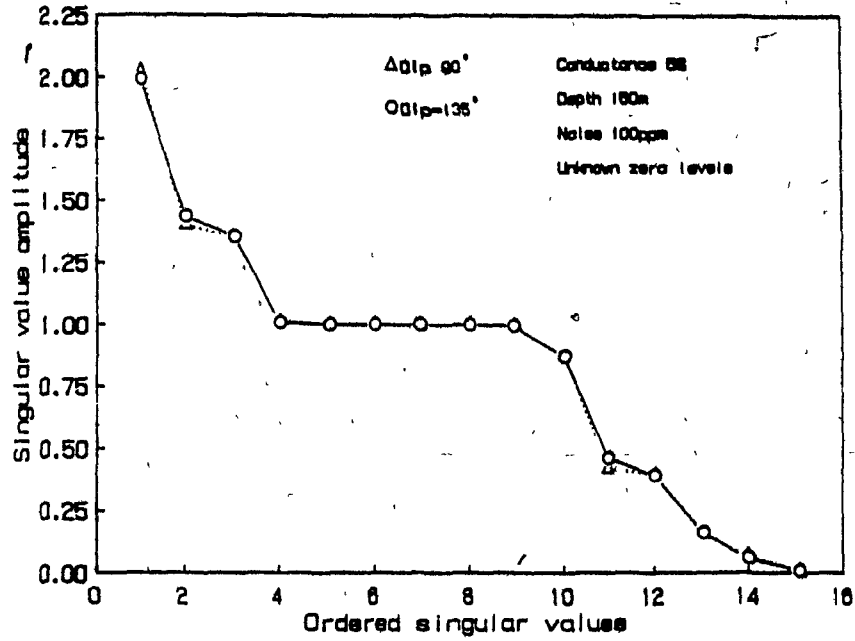
Figure 5.4 Singular value spectra for 5S plates dipping 90° and 135° and contaminated by a 100ppm noise. System integrators were simulated.
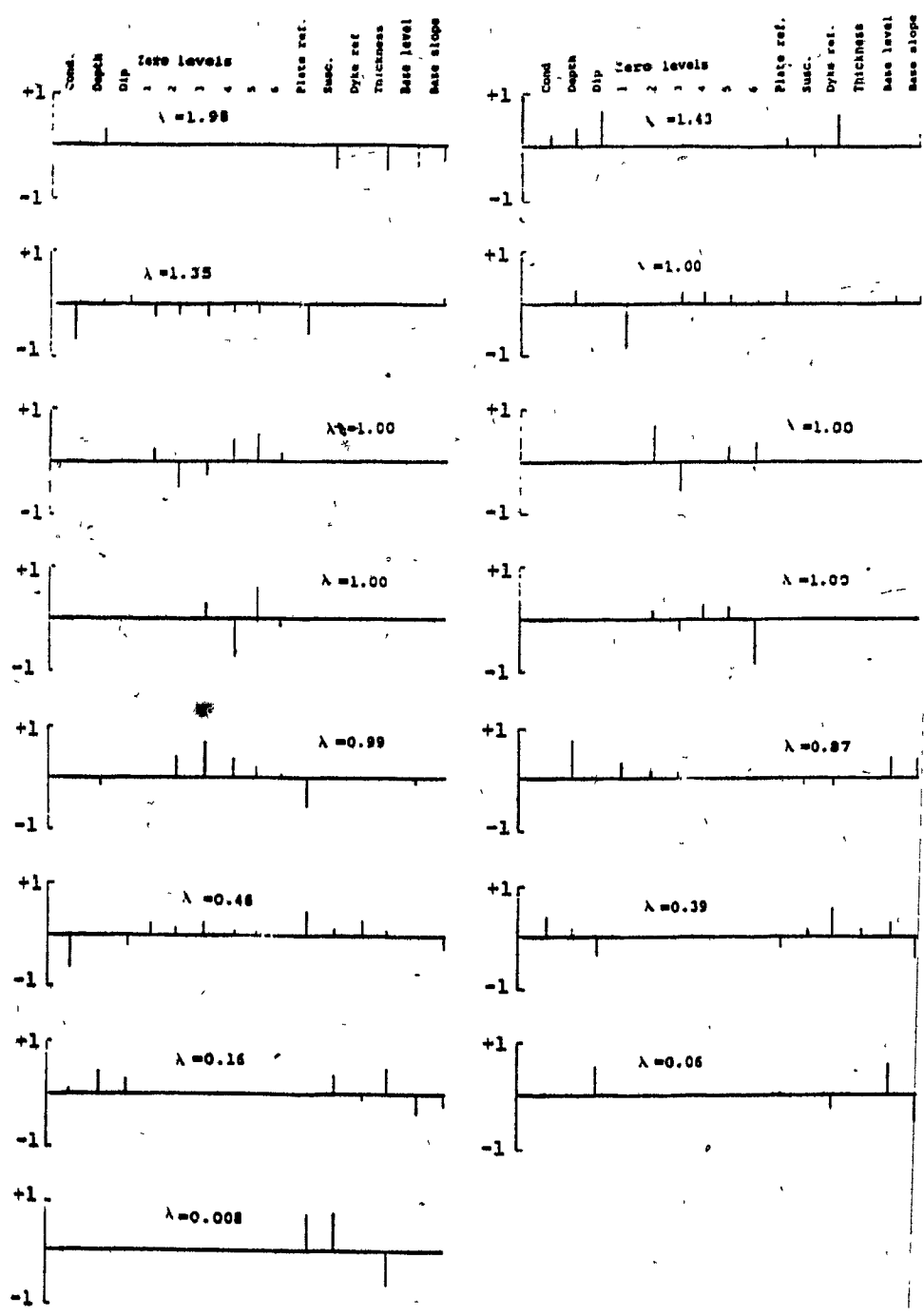
Figure 5.5 Parameter singular vectors from a joint inversion.

the dike. Both are highly correlated (1.00). The next to smallest singular value (0.06) is an order of magnitude smaller than the 13th singular value (0.16). It suggests that an increase of the dip and of the base level of the anomaly can offset a decrease of the reference of the dike and of the base slope of the anomaly. The reference and the dip have correlation of -0.97, the correlation of the dip and the base slope is -0.96. This relation is easier to understand if the parameter singular vectors are considered rather than only the correlation matrix.

Other high correlations are observed, especially between the conductance and the location of the plate along the profile (-0.92); the correlation matrix was listed in Table 5.1. The important conclusion is that the errors are reduced for most parameters, but the errors for the E.M. zero levels remain almost unchanged. An inversion of the magnetic anomaly was also done and the parameter errors for the separate inversion of magnetic and E.M. data are presented in Table 5.2.

In general the initial model has to be closer to the true model than for the inversion of E.M. data only. This corresponds to the observed increase of the partial derivatives condition number. This is not much of a problem if one carefully chooses the initial model. At worst, different initial models could be tested and the results examined to find the solution that best satisfied the data and the known

Table 5.2 Parameter standard errors for magnetic inversion, INPUT six channel inversion, joint inversion and constrained joint inversion.

Parameter		Mag.	Input	Joint	Constrained
Conductance		---	.29S	.23S	.31S
Depth		3.8m	3.65m	1.9m	1.81m
Dip		0.9°	2.5°	0.67°	0.68°
Zero levels	1	---	18.3	26.7	27.3
(E.M.)	2	---	16.4	24.5	24.8
	3	---	16.2	13.2	13.3
	4	---	15.2	12.3	12.7
	5	---	14.5	7.9	8.3
	6	---	14.3	7.8	7.9
Reference		---	2.2m	4.3m	4.8m
Thickness		7.6m	---	2.8m	21.8m
Susc.		$.124 \times 10^{-2}$	---	$.58 \times 10^{-3}$	$.39 \times 10^{-2}$
Base level		5.1	---	2.2	16.8
Base slope		5.4	---	3.1	25.5

or expected geology.

5.3.2 Joint Inversion With Known Zero Levels.

With the advent of digital receivers it is now possible to acquire data that is virtually drift free. This is why some tests were done assuming known zero levels for the six channels of the INPUT system. The main effect is mostly to reduce the condition number from 270 to about 50. Except for this difference one cannot conclude that the final results are better than previously. As an example we examine the results of the inversion of a synthetic profile contaminated by a 100ppm noise. The model is a 10S plate 120m below the transmitter with a dip of 60°. It is located on the flank of a magnetic dike 100m thick, of a susceptibility of .01 S.I.. The results are listed in Table 5.3.

The final model closely matches the true model except for the plate reference which is off by 7m. The correlation matrix is given in Table 5.4, there is a high correlation of -0.94 between the plate reference and its conductance. The parameter singular vectors are presented in Figure 5.6 and some groupings are observed. The second singular vector has two strong components along the conductance and the plate reference axis. For the sixth singular vector the component corresponding to the dip is offset by the depth and the reference of the dike. The last three singular vectors show groupings of pairs of components: the susceptibility and the

Table 5.3 Results of a joint inversion assuming known zero levels. The INPUT data is contaminated by a 100ppm white noise and the magnetic data by a 2nT noise.

Parameter		Model		Parameter
	Initial	Final	True	standard error
Conductance	15.0	10.2	10.0	0.27
Depth	150.0	120.8	120.0	0.46
Dip	50.0	60.6	60.0	0.48
Ref. plate	56.0	40.0	48.7	3.25
Ref. dike	111.0	96.7	98.7	1.01
Susceptibility	.0011	.0009	.001	.00009
Half-thickness	55.0	52.5	50.0	5.29
Base level	0.0	-0.2	0.0	0.57
Base slope	0.0	-0.3	0.0	0.82
RMS error INPUT	538.3	93.1		
mag.	5.6	0.5		

Table 5.4 Correlation matrix resulting from a joint inversion with known zero levels.

1.00	0.53	0.10	-0.94	0.03	-0.02	-0.03	-0.01	0.00	Cond.
	1.00	-0.24	-0.52	0.05	0.05	-0.04	-0.03	0.04	Depth
		1.00	-0.12	0.00	-0.21	-0.01	-0.04	-0.12	Dip
			1.00	-0.03	0.03	0.03	0.01	0.01	Ref.
				1.00	0.06	-1.00	0.43	-0.35	Susc.
					1.00	-0.07	0.19	-0.27	Ref. dike
						1.00	-0.49	0.40	Thick.
							1.00	-0.92	Base lev.
								1.00	Base slo.
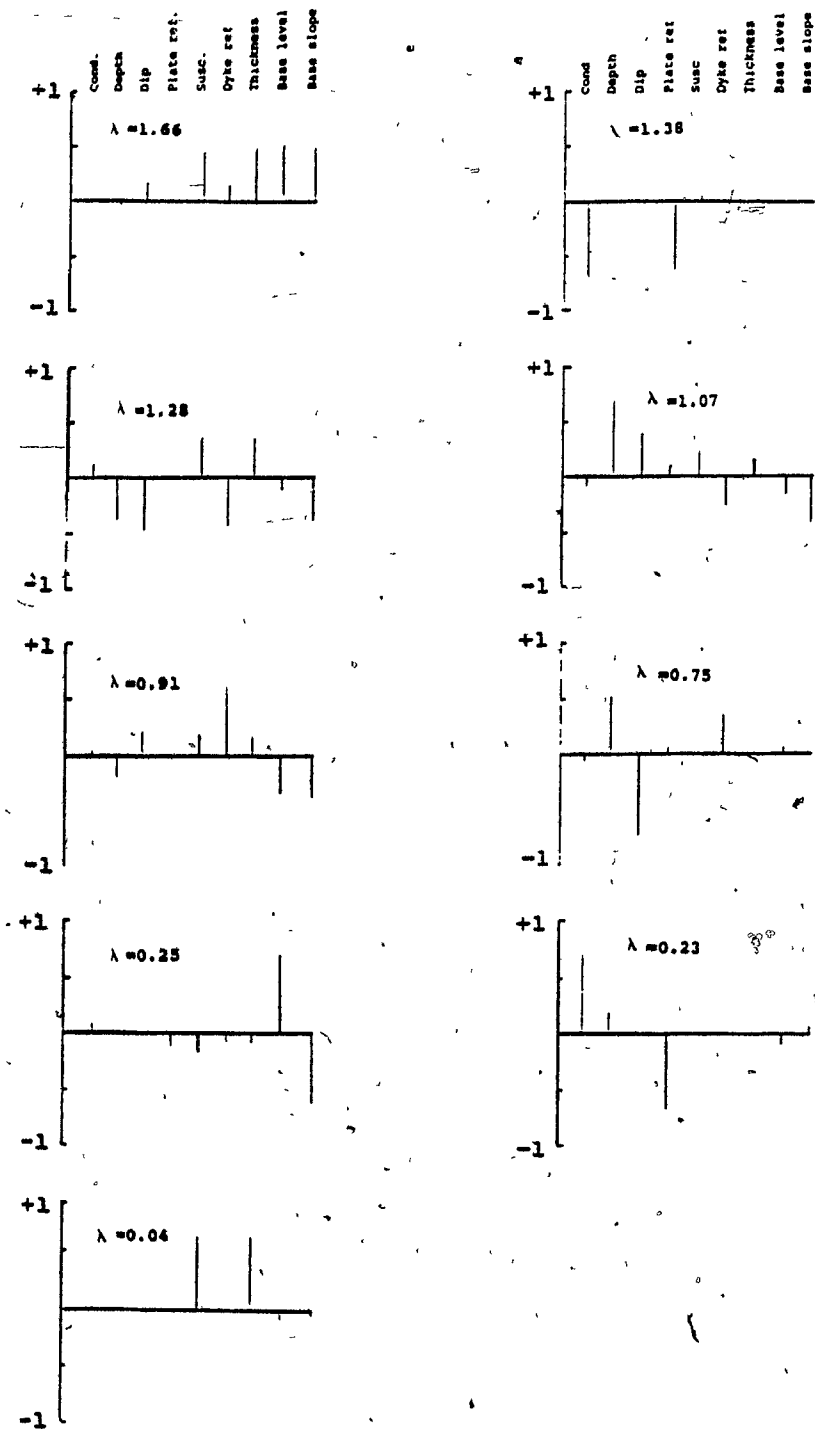
Figure 5.6 Parameter singular vectors from a joint inversion assuming known zero levels.

half-thickness, the conductance and the plate reference, the base level of the magnetic profile and its base slope. All these pairs correspond to high correlations.

The smallest singular value is an order of magnitude smaller than the next to smallest. It indicates that an increase or decrease of both the susceptibility and the thickness of the dike have little influence on the response. However, it is well known in magnetic interpretation that the thickness susceptibility product is easier to determine than both separately. The value of these parameters is very sensitive to the noise present in the data as indicated by the magnitude (0.039) of the singular value associated with them.

The spectrum of the singular values illustrated in Figure 5.7 shows a regular decrease of the singular value amplitude and we remark the absence of the step that is associated with the zero levels.

5.3.3 Constrained solution.

The model used in Section 5.4 was such that the conductor lies parallel to one of the flanks of the dike. The location of the plate, the center of the dike and its half-width are not explicitly related in the inversion. One can nevertheless force this relation by the use of constraints. The conducting plate will be located on the flank of the magnetic dike if at every iteration during the inversion the following equation is
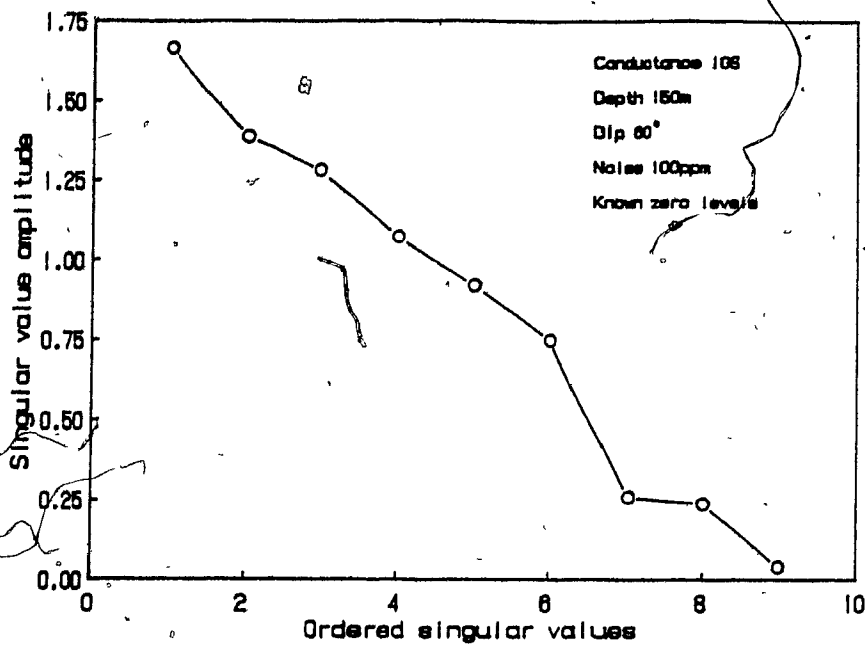
Figure 5.7 Singular value spectrum for a 10S plate, dipping 60° with known zero levels. System integrators were simulated.

respected:

$$X_0 \pm T = D. \text{ (The sign depends on which side of the dike}$$
$$\text{the plate is located)} \tag{5.1}$$

This is obvious if one looks at figure 5.1. This will be true if the variation of these parameters between each iteration obeys the same equation. We then have:

$$\Delta x_0 \pm \Delta T - \Delta D = 0. \tag{5.2}$$

Numerical aspects can be found in Lawson and Hanson (1974, Chapt. 20) and the development including the variance estimation is given by Crossley and Reid (1982) and we follow their development and notation.

Linear constraints can be written as:

$$B x = d , \tag{5.3}$$

where B is the matrix of constraints of dimension (r x m), in our case r the number of constraints is one and d is a null vector. They show that the least squares solution is then given by:

$$x = (A^t A)^{-1} [A^t c - B^t w], \tag{5.4}$$

where

$$w = (PB^t)^{-1} [PA^t c - d], \tag{5.5}$$

and

$$P = B(A^t A)^{-1}. \tag{5.6}$$

The inversion program was easily modified to introduce the constraint. The fact that d is zero simplifies the implementation.

respected:

$$X_0 \pm T - D.$$ (The sign depends on which side of the dike
the plate is located)   (5.1)

This is obvious if one looks at figure 5.1. This will be true if the variation of these parameters between each iteration obeys the same equation. We then have:

$$x_0 \pm \Delta T - \Delta D - 0.$$ (5.2)

Numerical aspects can be found in Lawson and Hanson (1974, Chapt. 20) and the development including the variance estimation is given by Crossley and Reid (1982) and we follow their development and notation.

Linear constraints can be written as:

$$B x - d ,$$ (5.3)

where B is the matrix of constraints of dimension (r x m), in our case r the number of constraints is one and d is a null vector. They show that the least squares solution is then given by:

$$x - (A^t A)^{-1}[A^t c - B^t w],$$ (5.4)

where

$$w - (PB^t)^{-1}[PA^t c - d],$$ (5.5)

and

$$P - B(A^t A)^{-1}.$$ (5.6)

The inversion program was easily modified to introduce the constraint. The fact that d is zero simplifies the implementation.

Crossley and Reid (1982) also note that the addition of constraints increases the magnitude of the parameter variance now given by:

$$var(x) = H_A H^t_A \ var(c); \qquad\qquad (5.7)$$

where

$$H_A = (A^t A)^{-1}[I_m - B^t(PB^t)^{-1}P]A^t. \qquad\qquad (5.8)$$

5.3.4 Constrained Inversion of Synthetic Data.

The constrained joint inversion was tested for different synthetic profiles at the 50 and 100ppm noise levels. The depths were 120 and 150m, dips were 60°, 90° and 135° and the conductances 5S, 10S and 20S. The constrained joint inversion converged to the correct parameter values for all the tested cases, provided that the initial model is not too far away from the true model as in Section 5.4. The convergence is slightly slower than for the joint inversion and one more iteration was usually required to attain the same residual error level.

Only one example will be studied in detail, since the conclusions are essentially the same for all cases. We again consider the case of a plate with a dip of 135° and a conductance of 5S located on the flank of a 100m thick dike. The noise level is 100ppm for the E.M. data and 1nT for the magnetic data. This corresponds to noise levels likely to be

present in actual data. The initial and final models are given in Table 5.5, the correlation matrix is also given. The results are not much different than for the unconstrained joint inversion and the main difference is, as expected, an increase in the parameters errors (see Table 5.2), especially for the magnetic parameters.

In our opinion the use of the constrained joint inversion should be restricted to the cases were one suspects from geological evidences that the conductor is very likely to be located on the flank of a magnetic formation.

5.4 Inversion of actual data.

Actual data from the Waconichi survey were used as a test case for the joint inversion algorithm. Anomaly E on flight line 4600 (see Figure 4.8) is associated with a weak magnetic anomaly that has an amplitude of 80nT (Figure 5.8). The INPUT anomaly was interpreted previously and the results of the inversion of the magnetic anomaly are given in Table 5.6. Both anomalies were used to test the inversion with the hope that the previous results could be improved.

The detailed results are given in Table 5.7. The depth is 133m, the conductance 9.7S and the dip 100°. These results are in better agreement with the known geology and the drilling results than the results obtained from the inversion of the INPUT data only (see Table 4.13). As predicted by the inversion of theoretical profiles, some parameter standard

Table 5.5 Results from a constrained joint inversion.

Parameter	Model Initial	Final	Parameter True	standard error
Conductance	7.0	5.6	5.0	0.31
Depth	125.0	149.7	150.0	1.81
Dip	120.0	130.9	135.0	0.68
Ref. plate	62.0	50.2	46.5	4.82
Ref. dike	107.0	103.2	96.5	5.94
Zero levels				
Ch.1	0.0	33.2	0.0	27.29
Ch.2	0.0	18.5	0.0	24.88
Ch.3	0.0	3.0	0.0	13.37
Ch.4	0.0	-3.8	0.0	12.72
Ch.5	0.0	-4.4	0.0	8.31
Ch.6	0.0	4.8	0.0	7.99
Half-thickness	45.0	52.9	50.0	21.84
Susceptibility	.009	.0087	.01	.0039
Base level	0.0	-16.4	0.0	16.85
Base slope	0.0	26.6	0.0	25.54
RMS error INPUT	206.9	63.1		
Mag.	64.6	4.3		

Correlation matrix

1.00	0.70	-0.32	0.10	-0.12	-0.39	-0.34	-0.29	-0.13	-0.92	0.63	0.29	-0.61	-0.62	0.31	Conductance
	1.00	0.11	0.36	0.05	-0.17	-0.20	-0.18	-0.08	-0.69	0.94	-0.13	-0.91	-0.42	-0.09	Depth
		1.00	-0.17	-0.05	0.04	0.07	0.07	0.03	0.24	0.15	-0.97	-0.16	0.78	-0.96	Dip
			1.00	0.10	0.03	-0.02	-0.03	-0.02	-0.20	0.33	0.16	-0.32	-0.33	0.17	1
				1.00	0.11	0.06	0.05	0.02	0.09	0.04	0.04	-0.04	-0.06	0.04	2
					1.00	0.16	0.13	0.05	0.35	-0.15	-0.04	0.15	0.12	-0.04	3
						1.00	0.10	0.04	0.31	-0.18	-0.07	0.17	0.16	-0.07	4
							1.00	0.04	0.27	-0.17	-0.07	0.16	0.16	-0.07	5
								1.00	0.11	-0.07	-0.03	0.07	0.07	-0.03	6
									1.00	-0.63	-0.21	0.60	0.55	-0.24	Plate reference
										1.00	-0.16	-1.00	-0.29	-0.15	Susceptibility
											1.00	0.17	-0.69	0.89	Dyke reference
												1.00	0.25	0.16	Thickness
													1.00	-0.82	Base level
														1.00	Base slope
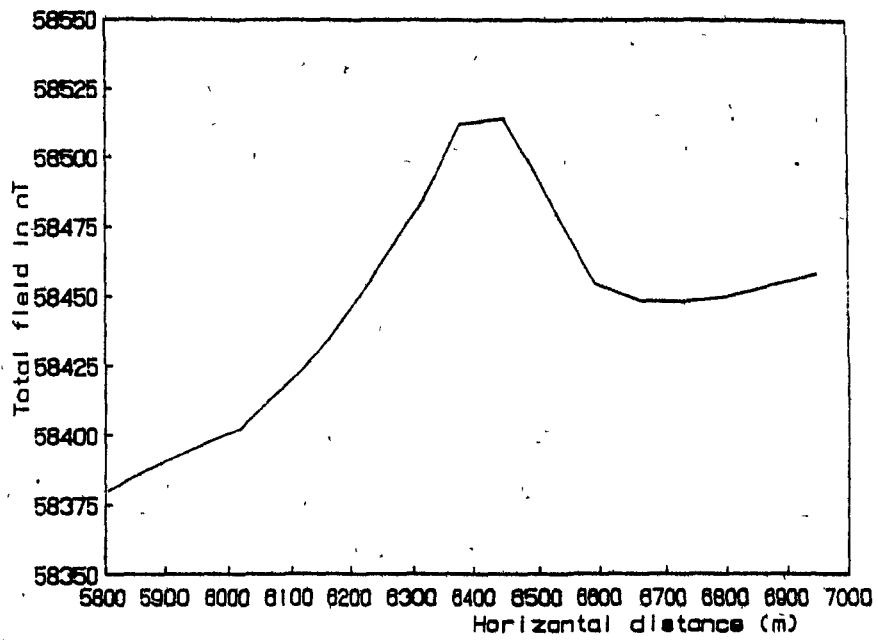
Figure 5.8 Magnetic anomaly associated with anomaly E, line 4600 of the Waconichi INPUT survey.

Table 5.6 Results from the inversion of the magnetic anomaly of line 4600.

Reference	:	6437m +/- 10.1m
Half-thickness	:	82m +/- 31.1m
Depth	:	128m +/- 19.9m
Dip	:	82.6° +/- 4.7°
Susceptibility	:	.00077 +/- .00035
Base level	:	58367nT +/- 3.6 nT
Base slope	:	95.1nT +/- 6.1nT
RMS error of fit:		2.2nT

Correlation matrix:

```
1.00 -0.02  0.04 -0.94  0.03 -0.53  0.79   Reference
      1.00 -0.92  0.02 -0.99  0.51 -0.12   Half-thickness
             1.00  0.04  0.96 -0.65  0.17   Depth
                   1.00 -0.03  0.61 -0.90   Dip
                         1.00 -0.57  0.15   Susceptibility
                               1.00 -0.79   Base level
                                     1.00   Base slope
```

Table 5.7 Detailed results of the joint inversion of anomaly E of line 4600.

             Conductance :   9.7S   +/- 1.2S

             Depth   : 132.4m   +/- 4.7m

             Dip   : 99.7°   +/- 3.2°

             Reference   : 6368.9m +/- 11.7m

             Zero levels : 277.5ppm +/- 39.8ppm

                    Ch 2 : 189.6ppm +/- 33.4ppm

                    Ch 3 : 151.2ppm +/- 17.2ppm

                    Ch 4 : 86.3ppm +/- 16.5ppm

                    Ch 5 : 51.3ppm +/- 11.2ppm

                    Ch 6 : 95.2ppm +/- 10.6ppm

          Susceptibility   : 0.001   +/- .0006

          Dike half-thickness : 57.5m   +/- 12.7m

          Mag. base level   : 58367nT   +/- 3.5nT

          Mag. base slope   : 94.5nT   +/- 7.2 nT

          Mag. reference   : 6430.9m   +/- 37.7m

          Mag. RMS error   :   5.2nT

          INPUT RMS error   : 103.5ppm

Correlation matrix

1.00	0.40	0.05	0.30	0.02	-0.23	-0.30	-0.37	-0.27	-0.97	0.22	-0.05	-0.20	-0.06	-0.03	Conductance
	1.00	0.87	0.59	0.33	0.23	0.03	-0.05	-0.06	-0.48	0.58	-0.75	-0.53	0.35	-0.69	Depth
		1.00	0.40	0.26	0.25	0.11	0.06	0.02	-0.15	0.52	-0.86	-0.47	0.46	-0.80	Dip
			1.00	0.22	0.15	0.01	-0.05	-0.05	-0.35	0.34	-0.35	-0.31	0.13	-0.31	1
				1.00	0.14	0.07	0.04	0.01	-0.06	0.19	-0.23	-0.17	0.10	-0.21	2
					1.00	0.14	0.13	0.08	0.18	0.13	-0.21	-0.12	0.11	-0.20	3
						1.00	0.14	0.09	0.27	0.02	-0.09	-0.02	0.06	-0.09	4
							1.00	0.11	0.35	-0.03	-0.05	0.02	0.05	-0.05	5
								1.00	0.25	-0.04	-0.02	0.03	0.03	-0.02	6
									1.00	-0.27	0.13	0.24	0.02	0.11	Plate reference
										1.00	-0.44	-1.00	0.43	-0.45	Susceptibility
											1.00	0.40	-0.30	0.58	Dyke reference
												1.00	-0.46	0.43	Thickness
													1.00	-0.79	Base level
														1.00	Base slope

errors have been reduced: the depth, the dip and the thickness of the magnetic dike. The interpreted width of the magnetic formation is 115m.

The singular values and the parameter singular vector are illustrated in Figure 5.9. The last parameter singular vector has two strong components: the susceptibility and the thickness of the dike, that are highly correlated (-1.00). The conductance and the plate reference have a correlation of -0.97, they are the two strongest components of the next to latest parameter singular vector.

Bands of magnetite have been observed over a distance of about 50m in drill hole #2 which is 200m west of the anomaly. The INPUT anomaly coincides with Line 52E of the ground survey grid. The HLEM anomaly has been interpreted as subvertical, its conductance as 55S and its width as 70m. A refraction seismic profile was also done along this line. The interpreted results are shown in Figure 5.10. Overburden thickness varies from 2m to 7m and it mostly consists of dry gravel and sand (Bazinet and Sabourin, op. cit.). The conductor is embedded in a 90m thick high velocity zone. Our interpretation is that the conductor is subvertical and that the magnetic anomaly is caused by thin bands of magnetite. The total width of the magnetic formation is about 100m. The different dips interpreted along the conductor suggest the possibility that the fault observed north east of Lake Sirois extends south and passes between drill hole #2 and the INPUT anomaly.
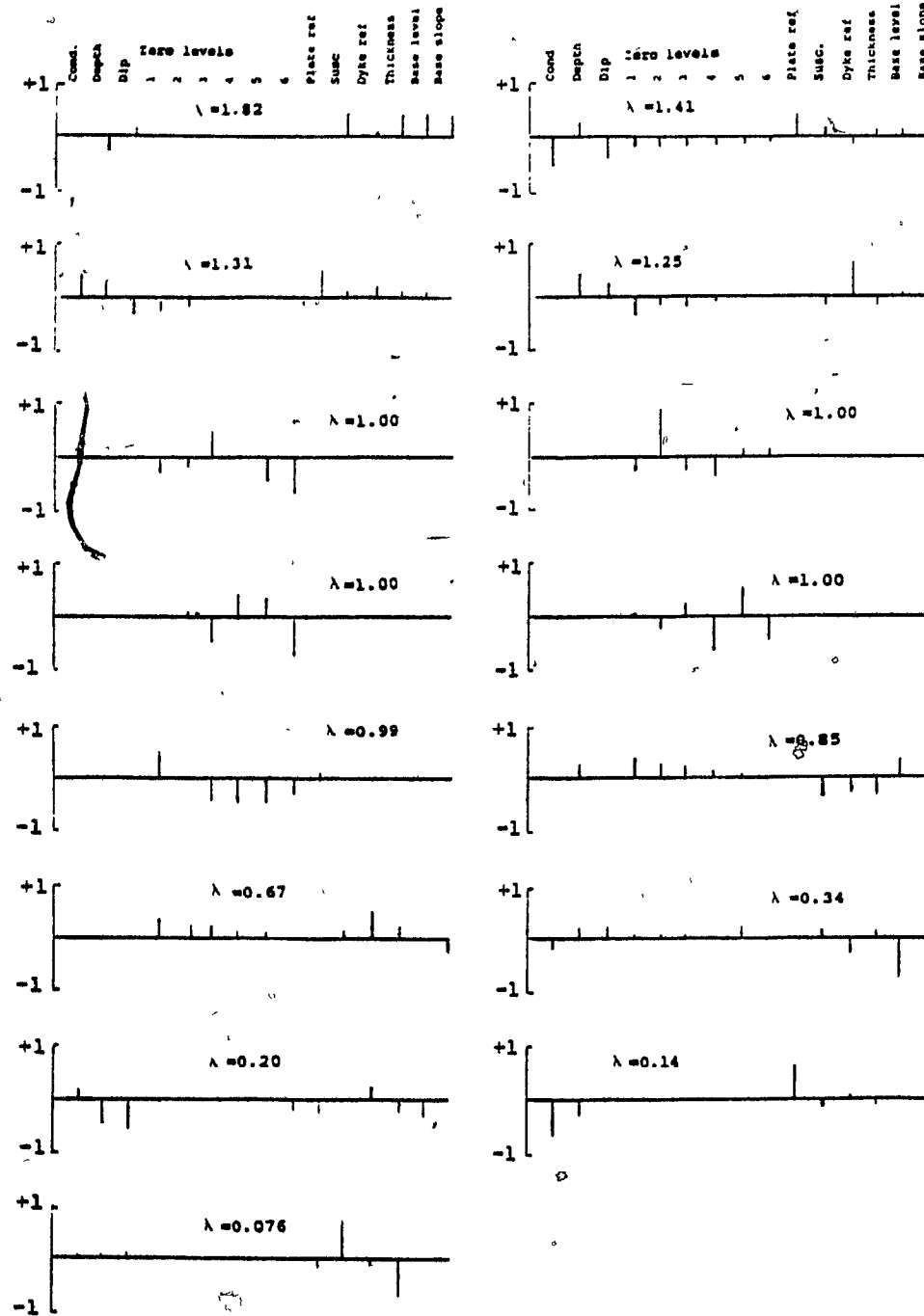
Figure 5.9 Singular values and parameter singular vectors for the joint inversion of anomaly E of line 4600.
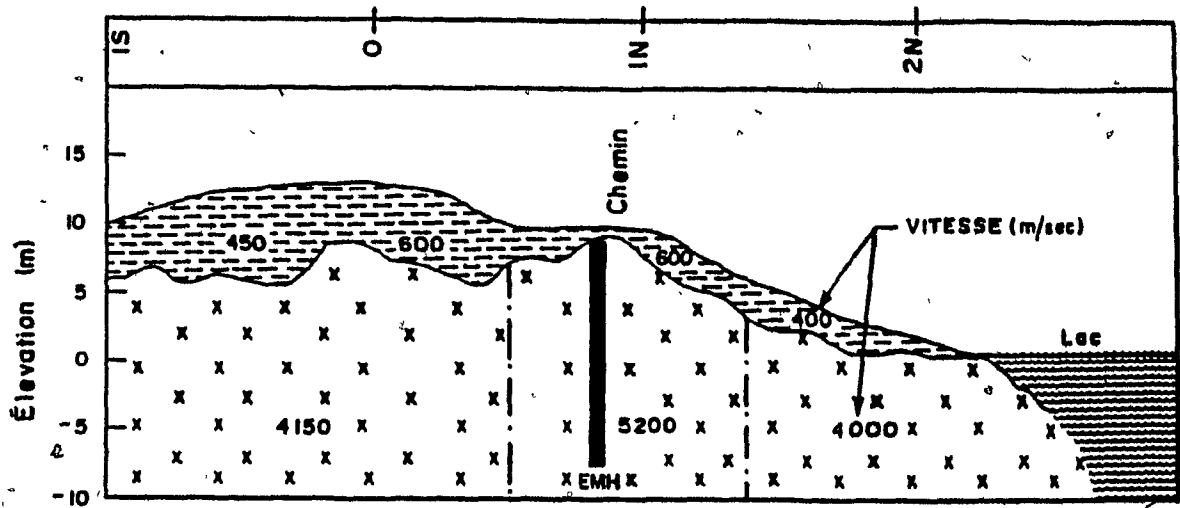
Figure 5.10 Interpreted overburden fom a seimic profile on line 52E (after Bazinet and Sabourin, 1987)

Chapter 6

LATE TIME INVERSION

6.1 Overburden Problems.

The interpretation of airborne E.M. anomaly is often complicated by the presence of conductive overburden. In the time domain the effect is easily observed as a strong response of the early channels. The interpretation of INPUT data in the presence of overburden was studied by Palacky (1975). Thin aluminum sheets were used to simulate thin sheets and overburden in a series of analog scale measurements. For vertical plates the presence of a conductive overburden raised the channel background levels and distorted the anomaly shape, particularly for channel one. This distortion is most severe for a dipping half-plane as it increases with the conductance both of the overburden and the conductor. These effects are mostly on the early time channels for the illustrated examples. The current interpretation practice is to subtract the background levels and then interpret the residual anomaly using nomograms and the late time channels only.

The problem was recently studied by Ferneyhough (1985) who used a quantitative approach. The conductive overburden is

approximated by a low pass filter as suggested by Lowrie and West (1965). The overburden is assumed to have infinite lateral extent and it is assumed that the total response can linearly be decomposed into an overburden response and a bedrock conductor response in the presence of overburden. The primary field is filtered (phase-shifted and attenuated) by the overburden and the secondary field is also filtered by the overburden. In the time domain the effect is to delay and smooth the free space response. As noted by Ferneyhough it is important to realise that the assumption is that the total response is the linear sum of the overburden response and the filtered target response. In practice the overburden and the target mutually interact and this effect is ignored by the filtering approach. Should the overburden and the target be in contact this interaction could be substantially enhanced. His suggestion for the interpretation of INPUT response is to subtract the overburden response to obtain the target response and then interpret the late time channels. Our inversion program was modified to use only the last three channels of the INPUT system.

Rather than subtract the overburden response it is assumed it will then show up as zero level shifts of the E.M. anomaly. This problem is easy to solve for the zero levels are considered as unknowns in the inversion program. As usual, the overburden is assumed to be flat and of infinite extent. It is nevertheless possible to invert time domain airborne

E.M. data for a one layer earth (Keating and Vallée, 1985), but this has to be done away from subvertical conductor anomalies to be valid, complicating the whole process.

6.2 Inversion of Synthetic Data.

Noise free synthetic profiles were used to test the algorithm and study the characteristics of the results. As expected, it is always possible to recover the original model for noise free data; recall that the signal to noise ratio is then infinite. All these tests were performed with the same starting models as those used for the inversion of six channel data in Chapter 4. Some singular value spectra resulting from the inversion of six and three channels are illustrated in Figure 6.1. The late time inversion has three less unknowns (the zero levels of the first three channels), this results in seven singular values rather than ten. The general shape of the spectrum remains unchanged, except for the second singular value that has a higher amplitude.

For noise free data, the rate of convergence of the inversion is the same when six or three channels are used. This is illustrated in Figure 6.2. For these particular inversions the same initial model was used in both cases and the RMS residual error was normalised by the RMS error of the initial model.
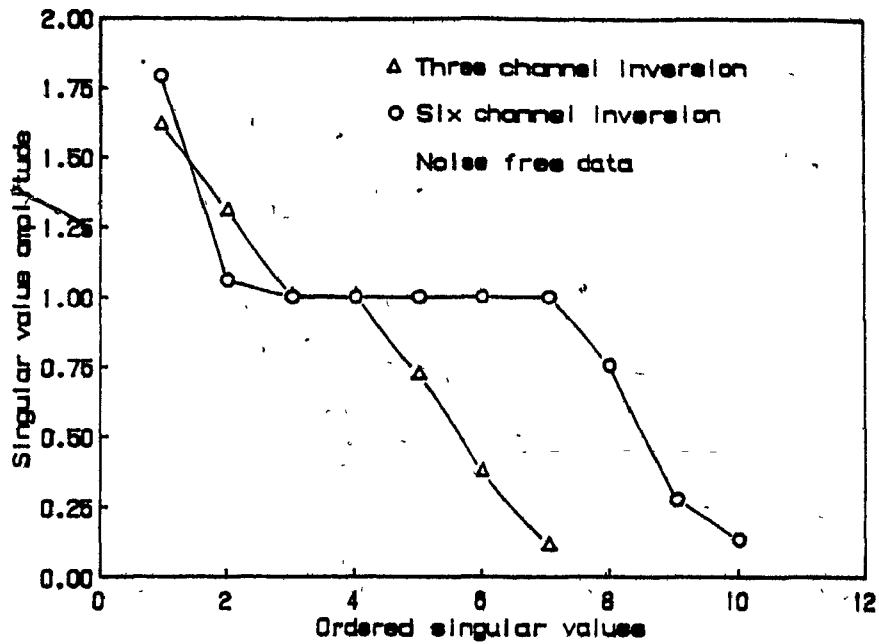
Figure 6.1 Singular value spectra from the inversion of six and three three channels INPUT anomalies. System integrators were not simulated.
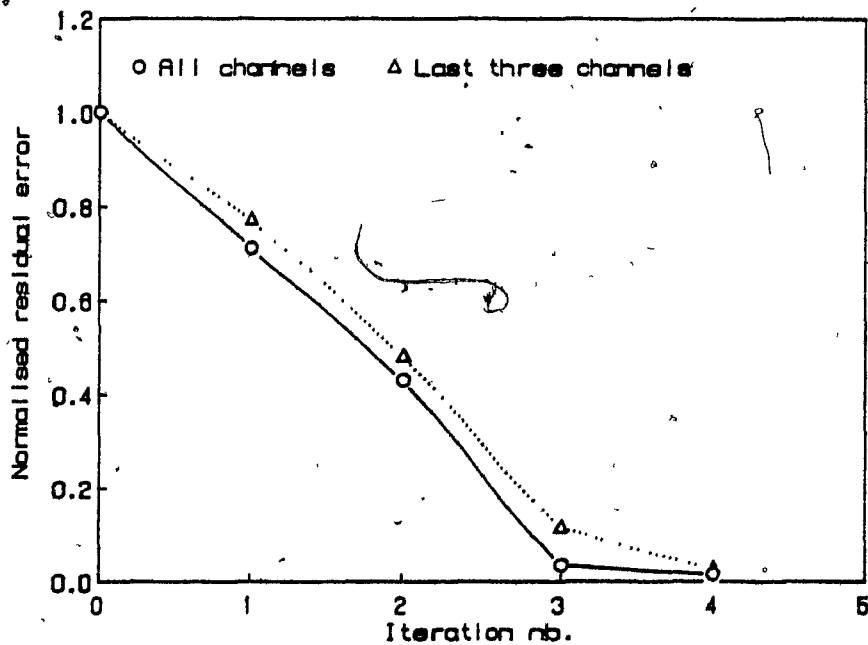

Figure 6.2 Convergence of the inversion for three and six channels inversion.

The influence of noise on the singular value spectra is illustrated in Figure 6.3. The effect of noise is mostly to alter the amplitude of the second and sixth singular value, the condition number remaining almost unchanged.

The late time inversion was tested for different dips, conductances and noise levels. The depth of the plate below the transmitter was kept constant at 150m. Consider first the inversion of a synthetic profile contaminated with a 100ppm noise level. This model has a dip of 135° and a conductance of 20S. The signal to noise ratios at peak amplitude, for the last three channels are respectively 12, 10 and 6. The anomaly was illustrated in Figure 4.6. The inversion was first tested without weighting and the initial model was the same as the one used to test the six channel inversion (see Table 4.3). The inversion was stopped after six iterations and the results are given in Table 6.1.

The rate of convergence was slow for the last four iterations without much improvement of the estimated parameters. For a second test the data were weighted by the inverse variances of each channel and using the same initial model the inversion diverged after the first iteration. The effect of the weighting is that each channel influences the inversion so a low signal to noise ratio channel has less influence than one with a high signal to noise ratio.

The second example is the inversion of a 20S plate with a dip of 60° and contaminated by a 100ppm noise. Although the
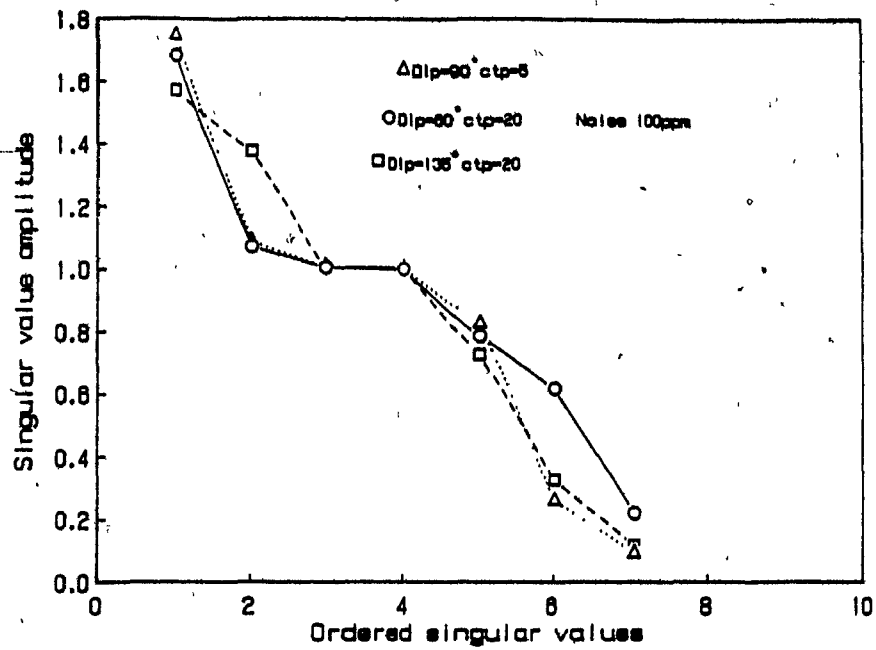
Figure 6.3 Singular value spectra from late time inversions of various INPUT anomalies.

Table 6.1 Results of the inversion of a synthetic profile contaminated with noise (Dip: 135°, Cond.: 20S)

Iter.	Cond. (S)	Depth (m)	Dip (deg.)	Zero levels (ppm)			Refer. (m)	RMS error (ppm)
0	10.0	125	90	10	3	0	65.0	116.0
1	24.6	171	136	24	2	5	18.7	91.9
2	9.8	170	149	1	-3	5	49.2	80.1
3	15.1	155	135	10	1	9	32.2	53.7
4	19.1	155	139	-2	-4	4	45.3	43.4
5	18.6	152	138	-3	-3	5	45.3	43.1
6	19.5	154	139	-3	-5	4	44.4	43.1
-	4.3	8.6	6.4	13	13	12	6.3	<-- parameter std. error
Model	20	150	135	0	0	0	49.25	

signal to noise ratios for the last three channels are respectively 3.1, 2.6 and 1.5, impressive results were nevertheless obtained. The anomaly is illustrated in Figure 6.4 and it is obvious that it cannot be interpreted with nomograms. The final results from the inversion are listed in Table 6.2. The calculated anomaly that would results from the interpreted model is shown in Figure 6.5. The information density profiles are illustrated in Figure 6.6. Their shape is similar to the calculated anomaly, the maxima corresponding to those observed on the E.M. anomaly. The information density of the last channel is less than the minimum information density of the other two channels indicating a weak contribution of this channel to the inversion. This is easy to understand since the signal to noise ratio of this channel at peak amplitude is 1.5 and less than one on the average.

6.3 Inversion of Actual Data.

Although there is not much conductive overburden present in the Waconichi test site area, in order to have an excellent geological control, the same three anomalies interpreted in Section 4.4 were used to test the late time inversion. Detailed results are listed in Table 6.3. The average depth is about 150m below the transmitter or 30m below the ground surface. Conductances range from moderate (13S) to high (34S). The dip of the conductor at line 4600 is 106° a result that is

Table 6.2 Results of the inversion of a 60° dipping plate.

Parameter		Initial value	Final value	Std. error	Model
Conductance	:	15.0	20.6	2.6	20.0
Depth	:	125.0	145.2	4.7	150.0
Dip	:	45.0°	60.7°	1.4°	60.0
Zero level 4:		0.0	-17.5	11.9	0.0
5:		3.0	0.6	5.8	0.0
6:		0.0	-16.2	4.8	0.0
Reference	:	62.0	56.1	6.23	46:5
RMS error	:	99.2	36.2		
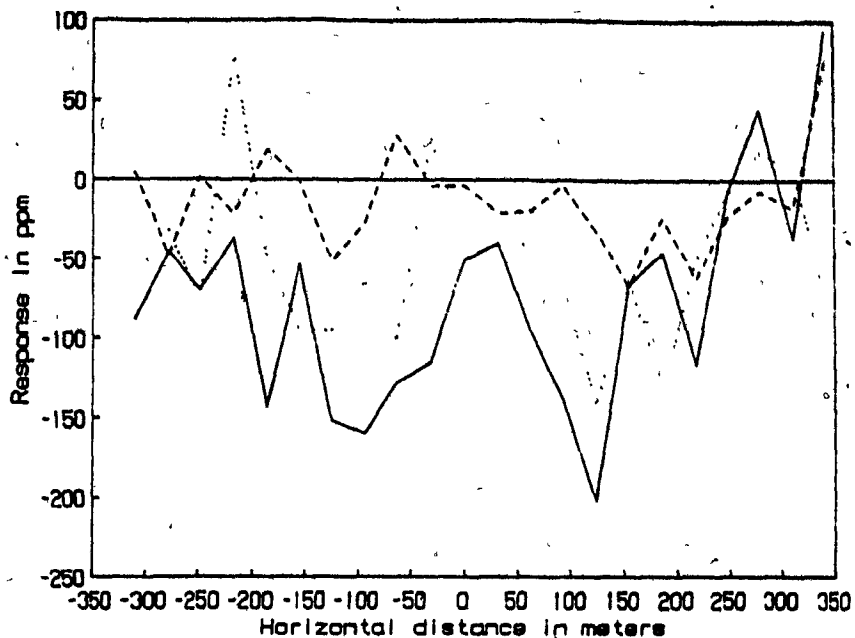
Figure 6.4 Three last channels of an INPUT anomaly caused by a 60° dipping plate. The conductance is 20S and the noise level 100ppm
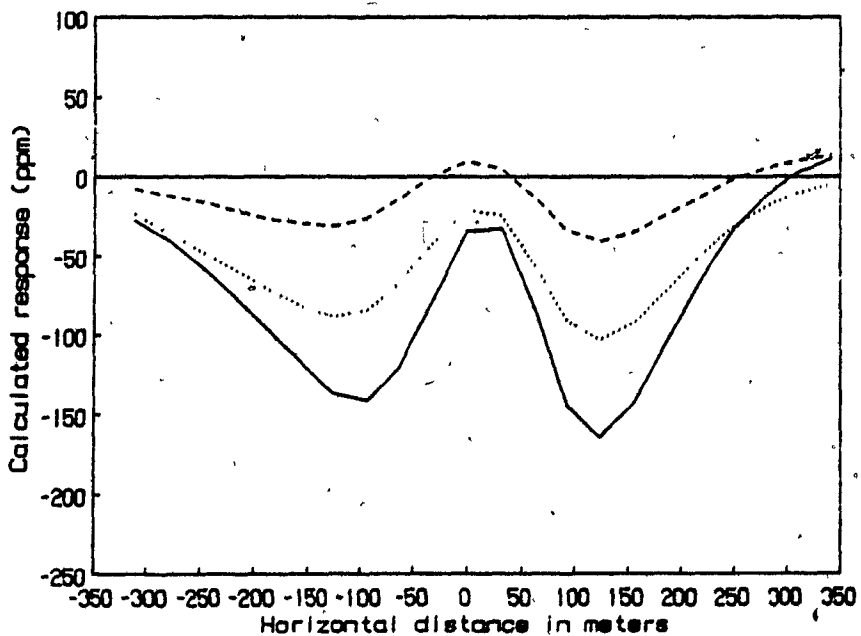

Figure 6.5 Calculated anomaly from the interpreted model of Table 6.2
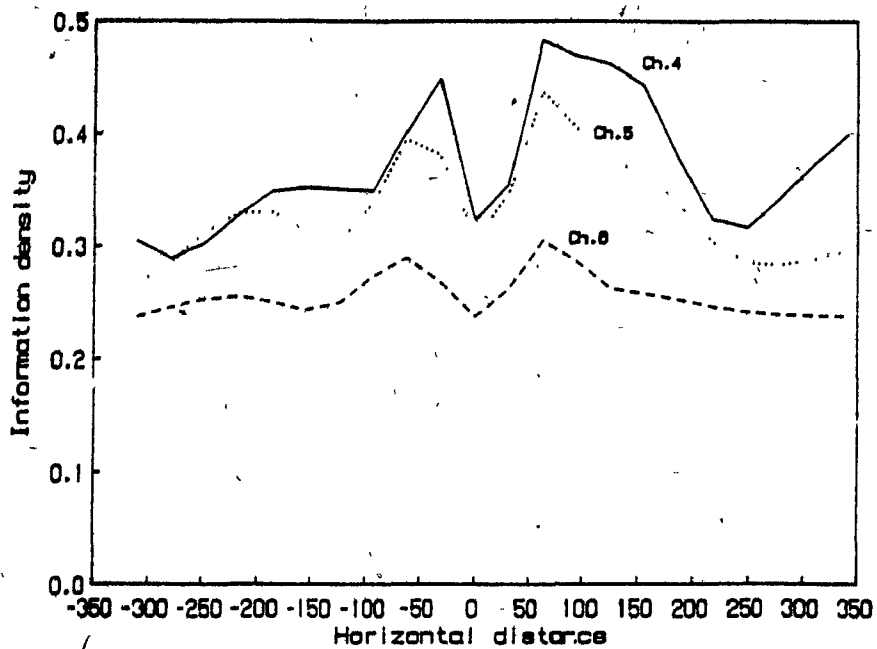
Figure 6.6 Information density profile from the inversion of the anomaly presented in Figure 6.4.

Table 6.3 Results of the inversion of actual anomalies when the late channels are used.

A- The data were weighted by their noise level.

Flight line		4550	4600	4615
Conductance (S)	:	52.9 (5.1)	14.8 (1.6)	21.8 (0.8)
Depth (m)	:	154.1 (6.2)	159.0 (8.3)	143.6 (1.8)
Dip (South)	:	50.3°(2.4)	106.2°(5.1)	134.2°(1.3)
Reference	:	6299.5 (9.4)	6340.6 (4.2)	665.8 (0.9)
Zero levels (ppm)				
Channel 4	:	-31.8 (10.1)	90.6 (7.7)	-35.1 (3.0)
Channel 5	:	-29.8 (5.7)	45.3 (4.8)	-11.4 (2.0)
Channel 6	:	-42.4 (4.4)	87.9 (4.5)	-6.0 (2.0)
RMS error (ppm)	:	28.6	28.6	13.9

B- The data are not weighted with their noise level

Conductance	:	33.5 (6.9)	13.6 (4.3)	21.9 (2.0)
Depth (m)	:	143.1 (2.9)	156.1 (1.9)	142.3 (4.1)
Dip (South)	:	49.8 (1.8)	105.8 (1.2)	133.0 (3.4)
Reference (m)	:	6314.5 (7.6)	6344.9 (9.8)	665.4 (2.1)
Zero levels (ppm)				
Channel 4	:	-56.2 (7.6)	88.4 (16.2)	-36.2 (6.0)
Channel 5	:	-39.5 (7.4)	42.1 (13.9)	-11.7 (5.8)
Channel 6	:	-44.9 (6.1)	90.5 (13.2)	-6.0 (5.9)
RMS error (ppm)	:	15.7	28.8	13.7

in agreement with the dip of 103° obtained from the joint inversion.

Because weighting can influence the solution, the three anomalies were first interpreted after weighting the E.M. channels by their assumed noise levels. They were interpreted again without any weighting. The results of these inversions are listed in Tables 6.3.

Some of these results have been obtained after damping the singular values to reduce the effect of noise sensitive small singular values. For the INPUT anomaly of line 4550, best results were obtained without weighting the data in the inversion. Channel six of that particular anomaly has a low signal to noise ratio compared to the last channel of the other two interpreted anomalies. The anomaly peak amplitude of the last channel is about 60ppm, while it is more than 150ppm in the other two cases.

The interpreted depths are greater than those obtained when the six channels are used in the inversion. Physically the response of the last channels is mostly due to deeply circulating currents. This also results in an increase of the apparent conductance. The dips interpreted with six or three channels are essentially the same. The interpreted dip (106°) of anomaly E of line 4600 is close to the dip (100°) interpreted from the joint inversion of magnetic and INPUT data.

In that case the erroneous dip of 37/North obtained from the inversion of six channel data was probably caused by the early channels. Two hypothesis could explain this: first, as interpreted from the HLEM survey the conductor is inductively thick (70m) at early times; second, the overburden is conductive. The last hypothesis is unlikely since, as noted previously, a nearby seismic survey line indicates a relatively thin and dry overburden.

According to these interpretations, the conductor is at a depth of about 30m below the surface, and its conductance ranges from 15S to 30S. The interpreted dips are virtually the same as when using the six channels in the inversion.

6.4 Conclusion.

As anticipated, as the signal to noise ratio is decreased a point is reached where the inversion breaks down. A low signal to noise ratio renders the inversion unstable. For example the signal to noise ratio of a 5S plate dipping 60° and located 150m below the transmitter has signal to noise ratios smaller than 1 for the last three channels if the noise level is 100ppm. The same plate with a dip of 90° has signal to noise ratios of 1, 0.5 and 0.12, and the inversion then converges to a local minimum. When the dip is 135° and the noise level 50ppm the signal to noise ratios are then 6.6, 3.0 and 0.6. The true model can then be recovered. Results improve

with higher conductances since it implies better signal to noise ratios. Other factors influencing the signal to noise ratio are the dip and the depth of the plate. For a given plate of fixed depth and conductance the minimum anomaly amplitude is for a near vertical plate. It can be expected that the late time inversion will give good results for moderate and high conductance targets. If the inversion results indicate a low conductance, then they should only be accepted with caution.

CHAPTER 7

DISCUSSION OF RESULTS

7.1 Summary.

The objective of this work was the development of a quantitative interpretation method, based on inverse theory, of airborne time-domain anomalies caused by plate like conductors. The method has been successfully used to interpret synthetic and actual data. To obtain reasonable computing time it was necessary to modify the order of the quadrature of the numerical integration routines used in the forward problem solution. The numerical errors introduced by these modifications is less than the noise level of the different airborne time-domain E.M. now in commercial use.

The method was extended to the joint inversion of E.M. and magnetic anomalies. It has been observed that the parameter variances are then reduced, thereby improving the inversion results. It has been found that the introduction of constraints is not of great help since it tends to increase the parameter variance at each iteration.

In Chapter 6, it was shown that plate like conductors can be interpreted in the presence of a conductive overburden if it is not too conductive. In this case, the late time

channels, which are less affected by the overburden, are used, for the inversion. Excellent results were obtained when the signal to noise ratio is sufficient (>2); low ratios (<2) generally correspond to low target conductances (<10S) although the dip and the depth affect the anomaly amplitude.

7.2 Numerical Advantages Derived From This Study.

This is the first time that inverse theory has been used to interpret airborne E.M. anomalies caused by plate like conductors. The high cost associated with the solution of the forward problem was probably the factor that prevented others from solving the problem before. This is why much effort was spent to reduce the computing time.

During the first stages of the development, the plate location was found by using the maximum of the anomaly after deconvolution of the spatial phase shift introduced by the system integrators. Perfect results for noise free anomalies could only be obtained by the inclusion of this parameter as an unknown in the inversion. The problem was that the maximum could not be located with enough precision because of a data sampling interval of about 30m at ground scale. The inclusion of the zero levels as unknowns was necessary since actual data are not drift free (the system calibrations are sometimes unavailable).

The joint inversion of magnetic and E.M. anomalies and the inversion of E.M. anomalies in the presence of overburden are natural extensions of the inversion algorithm that we have developed.

The inversion program is easy to use and now runs in less than 15 minutes on a micro-computer equipped with a 32 bit coprocessor card. The first development runs, on a Univac 80 mini-computer, lasted for two or three hours...Although it would not be practical to interpret all the anomalies of a survey, it is now feasible to select and process the most interesting targets in a relatively short time at a reasonable cost.

7.3 Recommendations for Future Work.

The next logical step after this work would be the inversion of frequency domain E.M. data. Because of a different and smaller system geometry it would be necessary to check the effect of the reduction of the order of quadrature of the integration routines. Smaller plate sizes would probably be necessary to approximate a half plane. Overburden effects in the frequency domain are more complex than in the time domain. The phase and the amplitude are modified as a function of frequency and the solution may not be as easy as in the time-domain.

Other forward models should also be used. The sphere has been used by Dyck (1981) for the interpretation of borehole E.M. data. Another useful model would be a conductive thick plate. The most useful improvements would undoubtably be a more realistic treatment of overburden and host rock effects. These are essentially forward problems and they are receiving appropriate attention.

REFERENCES

Abramowitz, M. and Stegun I. A., 1965, Handbook of mathematical functions with formulas, graphs and mathematical tables: Dover, New York.

Annan, A. P., 1974, The equivalent source method for electromagnetic scattering analysis and its geophysical application: Ph.D. Thesis, Memorial University of Newfoundland.

Avramtchev, L. and LeBel-Drolet S., 1980, Catalogue des gîtes minéraux du Québec: Ministère de l'Enèrgie et des Ressources, DPV-744.

Backus, G. and Gilbert, F. ,1967, Numerical application of a formalism for geophysical inverse problems: Geophys. J. Roy. Astr. Soc. v. 13,pp. 247-276.

Backus, G. and Gilbert, F., 1968, The resolving power of gross earth data: Geophys. J. Roy. Astr. Soc., v. 16, pp.169-205

Barringer, A. R., 1962, New approach to exploration: the INPUT airborne electrical pulse prospecting system: Mining Congress Journal, October.

Best M. E. and Bremmer T.G.T., 1986, The Sweepem airborne electromagnetic system in Airborne Resistivity Mapping

ed. G.J. Palacky; Geological Survey of Canada Paper 86-22, pp.71-77.

Chan, T. F., 1982, An improved algorythm for computing the singular value decomposition: A.C.M. Transactions on Mathematical Software, v. 8, pp. 72-83.

Crossley, D. J. and Reid, A. B., 1982, Inversion of gamma-ray data for elements abundances: Geophysics, v.47, pp. 117-126.

De Moully, G. T. and Becker, A., 1984, Automated interpretation of airborne electromagnetic data: Geophysics, v. 49, pp. 1301-1312.

Dhatt, G. and Touzot, G, 1981, Une présentation de la méthode des éléments finis : Presses de l'Université Laval.

Dyck, A. V., Bloore, M., Vallée M.A., 1980, User manual for program Plate and Sphere: Research in Applied Geophysics, v. 14, Departement of Physics, University of Toronto.

Dyck, A. V., 1981, A method for quantitative interpretation of wideband, drill-hole EM surveys in mineral explora tion: Ph.D. Theseis, University of Toronto.

Ferneyhough A. B., 1985, The quantitative interpretation of airborne electromagnetic data: M.Sc Thesis, University of Toronto.

Forsythe, G., Malcom, M., Moler, C., 1977, Computer methods for mathematical computation: Prentice-Hall, Englewood Cliffs.

Fullagar, P. K., 1984, A uniqueness theorem for horizontal loop electromagnetic frequency sounding: Geophys. J. Roy. Astr. Soc., v. 17, pp. 559-566.

Golub, G. H. and Reinsch, C., 1970, Singular value decomposition and least squares solutions: Numer. Math., v. 14, pp. 403-420.

Ghosh, M. K., 1972, Interpretation of airborne E.M. measurements based on thin sheets models: Ph.D. Thesis, University of Toronto.

Hanneson, J. E. and West, G. F., 1984, The horizontal loop electromagnetic response of a thin plate in a conductive earth: Part I- Computational method: Geophysics, v. 49, pp. 411-420.

Inman, J. R., 1972, Resistivity inversion with ridge regression: Geophysics, v. 40, pp. 798-817.

Jackson, D. D., 1972, Interpretation of innacurate, insufficient and inconsistent data: Geophys. J. Roy. Astr. Soc., v. 28, pp. 97-109.

Jackson, D. D., 1979, The use of "a priori" data to resolve non-uniqueness in linear inversion: Geophys. J. Roy. Astr. Soc., v. 57, pp. 137-157.

Jupp, D. L. B. and Vozoff, K., 1975, Stable iterative methods for the inversion of geophysical data: Geophys. J. Roy. Astr. Soc., v. 42, pp. 957-976.

Keating, P. and Vallée, M.A., 1986, One layer inversion of

airborne transient EM data: 46th Annual International SEG meeting.

Kolumzine, T., Lamontagne, Y., Nadeau, A., 1970, New methods for the direct interpretation of magnetic anomalies caused by dikes of infinite lenght: Geophysics, v. 35, pp. 812-830.

Konings, M., Lazenby, P.G. and Becker, A., Helicopter INPUT, two years of survey experience, Paper presented at the annual EAEG meeting, London, England, June 1984.

Lamontagne, Y. and West, G., 1971, Electromagnetic response of a rectangular thick plate: Geophysics, v. 36, pp. 1204-1222.

Lamontagne Y., 1970, Model studies of the Turam electromagnetic method: M.Sc Thesis, University of Toronto.

Lanczos, C., 1961, Linear differential operators, D. Van Nostrand Co., London.

Lawson, C. L. and Hanson, R. J., 1974, Solving least squares problems: Englewood Cliffs, Prentice-Hall.

Lee, T. J., 1984, Inversion of transient electromagnetic data from a spherical conductor: IEEE Transactions on Geoscience and Remote Sensing, v. GE-22, pp. 14-20.

Lowrie, W. and West, G. F., 1965, The effect of a conductive overburden on electromagnetic measurements: Geophysics, v. 30, pp. 624-632.

Menke, W., 1984, Geophysical data analysis: Discrete inverse theory: Academic Press.

M.E.R., 1980, Levé EM (INPUT): Région de Waconichi, 13 maps.

Palacky, G. J., 1972, Computer assisted interpretation of airborne electromagnetic measurements: Ph.D. Thesis, University of Toronto.

Palacky, G. J., 1975, Interpretatin of INPUT airborne electromagnetic measurements in areas of conductive overburden: Geophysics, v. 40, pp. 490-502.

Penrose, R., 1955, A generalised inverse for matrices, Proc. Camb. Phil. Soc., v. 51, pp. 406-413.

Pilkington M. and Crosley D. J., 1986, Determination of crustal interface topography from potential fields: Geophysics, v. 51, pp. 1277-1284.

Paterson, N. R., Edwards, R. N., Reford, S. W., 1982, Continuous two-layer inversion of multi-coil EM data: 9th Annual Meeting of CGU, York University.

Rao, Murthy, Rao, 1973, Two methods for computer interpretation of magnetic anomalies of dikes: Geophysics, v. 38, pp. 710-728.

Stroud, A. H., 1971, Approximate calculation of multiple integrals: Prentice-Hall, Englewood Cliffs.

Telford W.M., Geldart, L. P., Sheriff R. E., Keys, D. A., 1976, Applied Geophysics : Cambridge University Press, Cambridge.

Thomson S., 1986, personnal communication.

Ward, S., Ryu, Gleen, Hohmann, Dey, Smith, 1974, Electromagne-

tic methods in conductive terranes: Geoexploration, v.12,
pp.121-183.

Weidelt, P., 1983, The harmonic and transient response of a
thin dipping dike: Geophysics, v. 48, pp. 934-952.

Wiggins, R. A., 1972, The general linear inverse problem, im-
plications of surface waves and free oscillation for
Earth structure: Rev. Geophys. Space Phys., v. 10, pp.
251-285.

APPENDIX

Mathematical formulation of the plate problem.

Annan (1974) uses the equivalent source method to compute the secondary field of a thin rectangular plate excited by a time varying E.M. field. Other descriptions of the method have been given by Walker (1981) and Ferneyhough (1985). Here we follow Ferneyhough notation and description.

The total electric field in the anomalous conductivity zone is:

$$E(r) = E_i(r) + E_s(r), \tag{A1}$$

where E_i is the incident, or primary field. It is the field that would normaly exist if there were no anomalous zone. E_s, is the field due to the scatered currents (J_s), it is also called the secondary field. For the case of an inductively thin rectangular sheet, the equation of the surface current is:

$$\frac{K_s(r)}{\sigma_t s} - j \omega_o \mu \int_s K_s(r') \, g(r,r') \, d^2r' = E_i(r) \tag{A2}$$

Where: $K_s = J_s$, the surface current density,

   ω_o : the angular frequency of the source,

   μ : magnetic permeability of the plate, assumed to be that of free space,

   $g(r,r') = 1/ 4\pi (r-r')$,

$\sigma_t s$ is the conductivity thickness product,

$E(r)$ is the electric field at r caused by a unit dipole at r'.

Since the current is confined to the surface of the plate, it is represented in term of a scalar current potential.

$$K_s = \nabla \times U\ e_3 = -e_3 \times \nabla U, \qquad (A3)$$

where e_3 is the unit vector normal to the plate. By taking the curl and using Faraday's law ($\nabla \times E = -i\omega\mu_o H$), equation A2 becomes:

$$\frac{\nabla^2 U(r)}{\sigma_t s} - i\omega\mu \int \nabla' g(r,r')\ \nabla' U(r')\ d^2 r' = i\omega\ \mu_o H_3(r). \qquad (A4)$$

H_3 is the magnetic field normal to the plate.

Annan (1974) uses the Galerkin method to solve this integral equation. It is assumed that the potential U can be represented by a set of basis functions ϕ such that:

$$U = \Sigma\ \phi_i C_i. \qquad (A6)$$

The function choosen by Annan are:

$$\phi_{m,n} = [1 \cdot (x_1/a_1)^2][1 \cdot (x_2/a_2)^2]\ T_n(x_1/a_1)\ T_m(x_2/a_2),$$

where the T_i are Chebychev polynomial of the first kind. Their order is such that: $n+m < N$, where N is the maximum polynomial degree.

In the Galerkin method the inner product of the basis function and equation A4 is set to zero. The resulting set of linear equations is expressed in matrix form as:

$$\left(\frac{F}{\sigma_t s} + i\omega\mu_o L \right) C = -i\omega\mu_o H \qquad (A7)$$

Where:

$$F_{ij} = \int_s \frac{\partial \phi_i(x_1,x_2)}{\partial x_1} \frac{\partial \phi_j(x_1,x_2)}{\partial x_1} +$$

$$\frac{\partial \phi_j(x_1,x_2)}{\partial x_2} \frac{\partial \phi(x_1,x_2)}{\partial x_2} \cdot dx_1 dx_2$$

$$L_{ij} = \iint_{s\,s} g(x_1,x_2\,x'_1,x'_2) \frac{\partial \varphi_j(x_1,x_2)}{\partial x_1} \frac{\partial \varphi_i(x'_1,x'_2)}{\partial x'_1} +$$

$$\frac{\partial \phi_j(x_1,x_2)}{\partial x_2} \frac{\partial \phi_i(x'_1,x'_2)}{\partial x'_2} \quad dx'_1 dx'_2 dx_1 dx_2$$

$$H_j = \int_s \phi_j(x_1,x_2) \, H_3(x_1,x_2) \, dx_1 dx_2.$$

This can be rewriten as:

$$Z \, C = -i \omega \mu_0 H, \tag{A8}$$

where $Z = (1/\sigma_t s) F + i \omega \mu_0 L$ is the general impedance matrix,
F, the internal resistance matrix and L, the general
inductance matrix. Equation A8 could be solved by standard
inversion techniques; however, Annan (1974) choose the
weighted eigenvalue method. The geometry and the electrical
parameters are then decoupled. The eigencurrents coefficients
C depends only on the geometry of the plate, i.e. the ratio of
its strike length to its width. The eigenvectors and
eigenvalues are computed for a whole range of aspect ratios
and stored for future use.

In the time domain, the impulse response is:

$$I(t) = \Sigma \, a_n(x,y,z) \, b_n(x,y,z) \, [\, \delta(t) - (1/\tau_n) \exp(t/\tau_n)] \tag{A9}$$

for $t \geqslant 0$.

The a_ns are called the exitation coefficients and represent the coupling between the primary magnetic field and the nth eigencurrent. The b_ns, the secondary field coefficients, represent the coupling between the secondary field at the receiver and the nth eigencurrent. The time constants τ_n are inversely proportional to the eigenvalues.